Modulation of Materials Properties of Thin Surface Layers by Means of UV-Light

PhD Thesis

(Dissertation)

by

Matthias Edler

Chair of Chemistry of Polymeric Materials

University of Leoben

Thesis Supervisor: Univ.-Prof. Mag.rer.nat. Dr.techn. Wolfgang Kern

AFFIDAVIT

I declare in lieu of oath, that I wrote this thesis and performed the associated research myself, using only literature cited in this volume.

EIDESSTATTLICHE ERKLÄRUNG

Ich erkläre an Eides statt, dass ich diese Arbeit selbständig verfasst, andere als die angegebenen Quellen und Hilfsmittel nicht benutzt und mich auch sonst keiner unerlaubten Hilfsmittel bedient habe.

_____ _____

Datum Unterschrift

ABSTRACT

The present work deals with photoreactive thin films and describes processes to tune both surface and material properties by means of UV-irradiation. Selected applications of these materials as UV-tunable interfaces in organic electronics are demonstrated. Examples of photoreactive poly(norbornenes) together with the underlying synthesis and photochemistry are presented. Upon exposure to UV-light polymers bearing ortho-nitrobenzyl ester units in their side chains undergo the scission of the ester unit and polar carboxylic acids are generated. Employing these photosensitive polymers as interfacial layers between an organic semiconductor and the gate dielectric, characteristics of organic thin film transistors (OTFTs) such as carrier mobility and threshold voltage could be varied over a wide range. Moreover, the epitaxial growth of organic semiconductors (para-sexiphenyl and pentacene) on these surfaces was influenced by the photochemical adjustment of surface polarity. The photo induced modulation of surface polarity was accompanied by a significant change in the refractive index (Δn up to 0.047). Copolymers bearing ortho-nitrobenzyl ester moieties and aryl ester units (photo-Fries rearrangement) in their side chains allowed wavelength-selective tuning, patterning and even inverting of the refractive index. Proceeding from thin polymer layers to molecular layers silane based bifunctional molecules forming photoreactive mono- and oligolayers on metals and oxidic surfaces are presented. These layers, containing ortho-nitrobenzyl ester units, were modified by UV-illumination and post-exposure derivatization. Lithographic patterns in molecular layers were characterized with friction force microscopy (FFM). Furthermore, a novel polyaniline derivative bearing photosensitive N-formamide groups is demonstrated. Via UV-illumination a decarbonylation reaction resulting in polyaniline was introduced that was subsequently protonated to yield the conductive emeraldine salt. These photoinduced conductivity changes were corroborated in thin films by conductive AFM (CAFM) measurements. In addition, the application as photopatternable charge injection layer for structured OLEDs is demonstrated.

KURZFASSUNG

Die vorliegende Arbeit beschäftigt sich mit dünnen photoreaktiven Schichten und beschreibt Prozesse, um Oberflächen- und Materialeigenschaften durch UV-Strahlung exakt einstellen zu können. Auch werden potentielle Anwendungen in organisch elektronischen Bauteilen präsentiert. Die photoreaktiven Polymere auf Norbornenbasis, die mittels ringöffnender Metathese-Polymerisation (ROMP) hergestellt worden sind, verfügen über ortho-Nitrobenzylesterseitengruppen. Diese Seitengruppen sind in der Lage unter Einwirkung von UV-Licht funktionelle Carbonsäuregruppen auszubilden. Mit diesen photoreaktiven, dünnen Polymerschichten, die in organischen Dünnfilmtransistoren zwischen der organischen Halbleiterschicht und dem Gate-Dielektrikum positioniert werden, konnten Transistoreigenschaften wie die Mobilität der Ladungsträger als auch die Schwellenspannung gezielt gesteuert werden. Zusätzlich konnte das epitaktische Wachstum organischer Halbleiter (Pentacen, Parasexiphenylen PSP) auf den Polymerfilmen eingestellt werden.

Neben einer Steigerung der Polarität wurde durch ellipsometrische Messungen gezeigt, dass die Photoreaktion eine signifikante Änderung des Brechungsindex im Polymerfilm verursacht. Mit der Synthese von Copolymeren, die sowohl ortho-Nitrobenzylesterseitengruppen als auch Phenylestereinheiten tragen (Photo-Fries-Umlagerung), wurde eine mehrstufige Variation des Brechungsindex, abhängig von der Wellenlänge des UV-Lichtes, realisiert. Das Konzept der Änderung von Oberflächeneigenschaften - basierend auf der ortho-Nitrobenzylesterseitengruppe - wurde in einem weiteren Schritt auf bifunktionelle Moleküle übertragen. Diese mit Silan-Ankergruppen ausgestatteten Moleküle sind imstande auf oxidierten Oberflächen (Metalle) Mono- bzw. Oligolagen zu bilden. Neben Strukturierungen im Mikro- und Nanometerbereich konnten die Oberflächeneigenschaften dieser organischen Monoschichten zusätzlich durch geeignete Derivatisierungsreaktionen eingestellt werden. Des Weiteren wurde ein neues photoreaktives mit N-Formamid-Gruppen ausgestattetes Polyanilinderivat hergestellt. Unter Bestrahlung mit UV-Licht wurde eine Decarbonylierungsreaktion initiiert und Polyanilin gebildet. Eine nachfolgende Protonierung ermöglichte die Bildung des leitfähigen Emeraldinsalzes.

Die lichtinduzierte Modifikation der Leitfähigkeit, welche durch CAFM-Messungen charakterisiert wurde, ermöglichte die Anwendung dieser Polymerfilme als UV-strukturierbare Ladungsinjektionsschichten in organischen LEDs.

ACKNOWLEDGEMENT

This thesis was performed at the Chair of Chemistry of Polymeric Materials (University of Leoben in the period from 02/2009 to 06/2012). First of all I would like to thank my supervisor *Univ.-Prof. Dr. Wolfgang Kern* for giving me the opportunity to carry out this PhD thesis, for his helpful suggestions and his pleasant guidance.

Special thanks I want to pronounce to my colleague and co-supervisor *Ass.Prof. Dr. Thomas Grießer* for his scientific advices, helpful discussions and great support as friend over the last years.

I also want to express my thanks to all members of my working group and the whole institute for the good working conditions during my PhD time. Especially, I want to mention my students *Judith Niklas*, *Stefan Mayrbrugger* and *Dietmar Haba*.

Furthermore, I want to thank my numerous collaboration partners from the Institute of Chemistry and Technology of Materials (TU Graz), Institute of Solid State Physics (TU Graz), Institute of Physics (University of Leoben), Institute for Semiconductor and Solid State Physics (JKU Linz) and Joanneum Research (NMP, Weiz).

Thanks go in particular to:
Marco Marchl and *Egbert Zojer* for the setup and characterization of the OTFTs
Quan Shen, *Andreas Pavitschitz* and *Christian Teichert* for the SPM measurements
Alfred Neuhold, *Jiri Novak*, *Roland Resel* for XRR measurements
Alexander Fian for the ellipsometric measurements of polymers
Clemens Simbrunner and *Helmut Sitter* for the setup of the OLED
Simone Radl for cooperation at the polyaniline topic

Financial support by the FWF – Austrian Science Fond project: „Design and application of tuneable surfaces based upon photoreactive molecules" (S9702-N20) is gratefully acknowledged.

Finally, I want to gratefully thank *Julia, Lisa, Michael* and my parents *Peter* and *Margarita*, for always being a great support and to be solidely behind me in good times as in not so good times.

Thanks are given to all friends!

TABLE OF CONTENTS

1 MOTIVATION AND OUTLINE

The technological interest in the application of photosensitive materials for the fabrication of organic opto-electronic devices has seen a strong increase during the last decades and is today an active area of science.

In particular, materials that operate at deep UV-wavelengths and simultaneously offer the advantage of a well-defined photochemistry are of substantial interest for optical data storage, optical elements and modern organic electronic devices such as organic thin film transistors (OTFT) and organic light emitting devices (OLED).[1]

The capability of adjusting the surface as well as the bulk properties, e.g. the surface polarity[2] and the refractive index[3] of thin organic films by means of photochemistry is the main advantage of photoresponsive materials. Besides the realization of novel optical devices via photoinduced patterning of the refractive index[4] in thin polymer films, this approach also offers the possibility of a selective modulation of the performance of organic devices using photosensitive interfacial layers.[5,6]

Depending on the application and technology, different types of photoinduced processes and reactions are used in such photosensitive materials. These include radiation induced cross-linking, photopolymerization of styrene or (meth)acrylate monomers[7,8], and photoreactions such as photo dimerization[9], photorearrangement[10] and photocleavage reactions.[11] Such well defined photoreactions are capable of undergoing structural changes in the chemical composition by means of UV-illumination and cause significant changes in the surface- and bulk properties, respectively. One particular class of photoresponsible materials is based on photoreactions which offer the possibility of reversible changes in their molecular conformation upon irradiation with light in the UV- and visible range, respectively. These materials contain photochromic molecules such as azobenzene[12], spiropyrane[13], anthracene[14], fulgides[15], diarylethenes[16] and cumarine groups.[17] Although reversibility enables the realization of novel optical elements or a reversible modulation of the performance of organic devices, the formed photoproducts are often thermally instable and even room temperature can cause a revision of the photoreaction which limits the practical applicability of such photosensitive materials.

In the present thesis the main focus is set on new photoreactive materials whose surface as well as bulk properties can be tuned when exposed to UV-light. For this purpose, polymers bearing photocleavable o-nitrobenzyl ester groups, or aryl ester units have been synthesized. Thus, upon irradiation with UV-light surface properties such as chemical

reactivity and surface energy shall be modified and furthermore, optical parameters, e.g. the refractive index shall be exactly adjusted.

Another goal of the present work has been the synthesis of a polyaniline derivative bearing photosensitive N-formamide groups. When exposed to UV-light the polymer is capable of undergoing a photodecarbonylation reaction yielding in polyaniline. Due to the fact that the conductivity depends on the conversion of the photoreaction, a selective adjustment of the conductivity by means of UV-light is feasible.

In a second step it has been assessed to transfer the concept of photopatterning from polymer surfaces to very thin surface layers of bifunctional molecules, or better still self-assembled monolayers (SAMs).

Self-assembled monolayers (SAMs) are highly ordered and oriented monomolecular layers of bifunctional organic molecules that assemble spontaneously on suitable solid surfaces. These ultra-thin layers should allow a better resolution down to the nanometer regime, as diffuse scattering within the polymer layer can almost be neglected. Using experimental methods such as scanning near field lithography, even a lateral resolution below 10 nm has already been achieved using SAMs on gold surfaces in special material combinations.[18,19]

Besides the possibility of adjusting the surface properties, the conductivity and the optical parameters such photoreactive thin films shall be applied as UV-patternable interfacial layers in organic devices to improve the performance of the device characteristics. A schematic overview of the potential applications is shown in Figure 1.1.

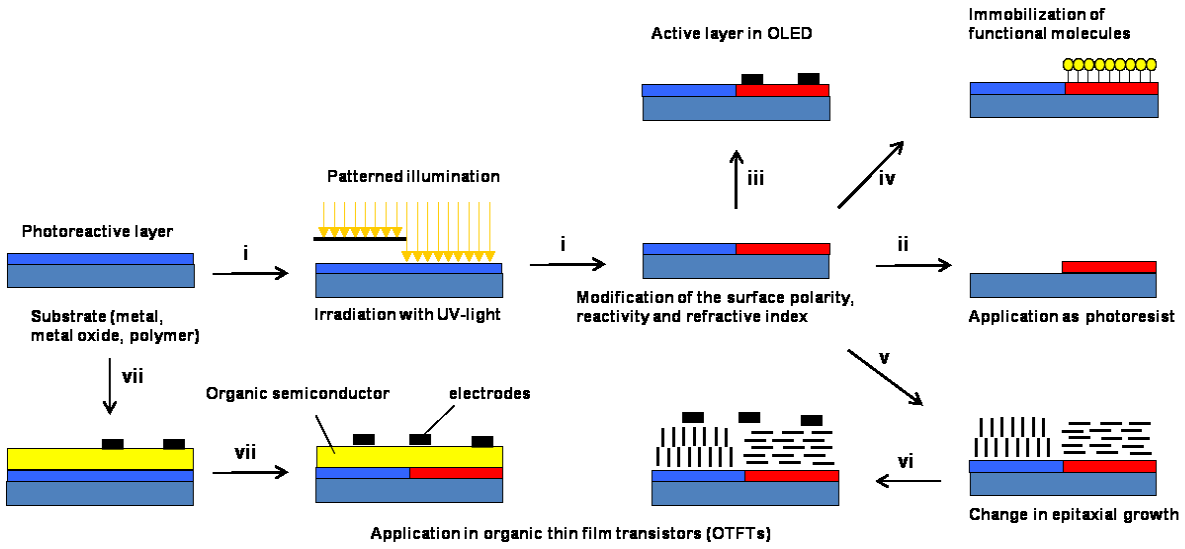

Figure 1.1: Field of application for photoreactive organic thin films

Starting from a homogeneous photoreactive polymer film, illumination with UV or visible light changes the molecular structure of the photoreactive groups and thus the properties of the material (i). The most interesting properties include the refractive index, surface polarity and chemical reactivity, as well as conductivity. Changes in the refractive index are of substantial interest in optical data storage or the field of waveguides and are discussed in chapter 3.1.4. In the case of suitable photoreactive conductive polymers, such materials can be directly used for patterned organic devices, i.e. for organic light emitting devices (OLEDs) (iii, see section 3.3.3). Applying photolithographic techniques a patterned modulation of material properties can be achieved. In the current examples presented the reactivity of the surface is always enhanced and therefore activated, e.g. for the immobilization of functional molecules, including dyes, nanoparticles and biomolecules (iv).

The change in surface polarity can be used to influence the growth of small organic molecules (e.g. para-sexiphenyl (PSP), pentacene) by vapour deposition (PVD).[20,21] Differences in the wetting behaviour of these molecules induce changes of the growth conditions leading to differences in the crystal morphology and/or crystal size (v). Based on the influence of the crystal structure and morphology on the electrical and optical bulk parameters, a tuning of organic light emitting diodes (OLED) and organic thin film transistors (OTFTs) (vi) is possible.

Potential applications are the use of such layers as dielectric layer or additional interfacial layers in OTFTs.[22] In this case, the performance of the OTFT is strongly dependent on the doping situation at the interface between the gate oxide and the organic semiconductor.[19] A modification of the electronic properties at this interface therefore has an enormous influence on the transistor characteristics. However, to exclude other effects stemming from different growing behaviour (vide supra), it may be necessary to illuminate the assembled device (vii, section 3.1.5).

2 INTRODUCTION

2.1 BASICS AND THEORY

Photochemistry is the science discipline in chemistry, which deals with the interaction between matter and light and treats physical and chemical processes based on electronically excited states formed by the absorption of photons. A photochemical reaction occurs when a molecule is excited from its lowest electronic ground state (S_0) to one of various vibrational levels of the electronically excited singlet state (S_1) by incoming light. Usually, molecules are excited by suitable electromagnetic radiation in the range of 100 – 1000 nm.

This range of wavelengths is subdivided into ultraviolet (UV-irradiation, 100 – 380 nm), visible light (380 – 780 nm) and infrared (780 – 1000 nm) wavelengths. In Figure 2.1 the electromagnetic spectrum is depicted.

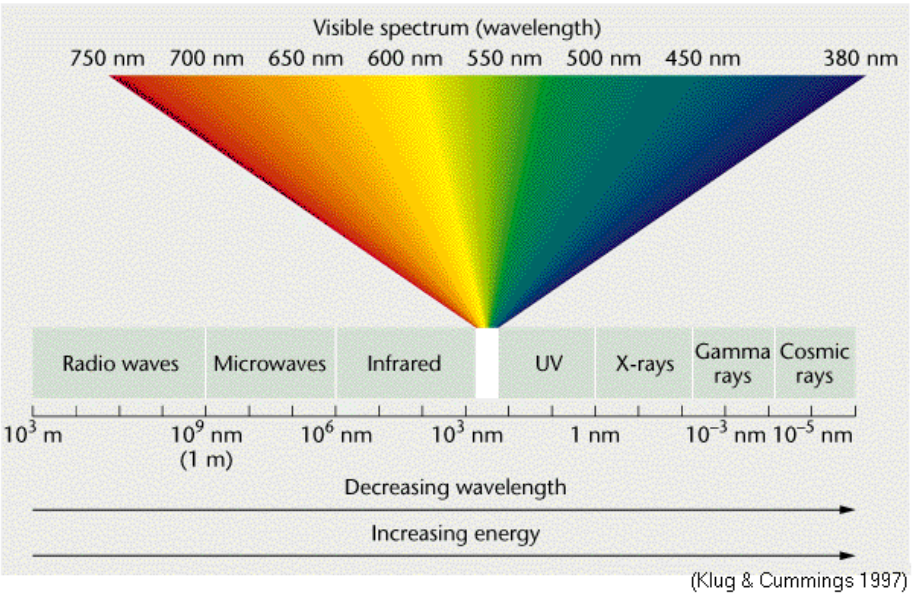

Figure 2.1: Depiction of the electromagnetic spectrum[23]

The absorption or emission of light itself is regarded as transfer of energy. In absorption of light an excitation of a species is obtained by a photon. This photon contains the energy equal to the difference of ground state E_0 to excited state E_1. A photon exhibits properties of both waves and particles and is defined as product of the frequency of oscillation (ν) and the Planck's constant (h).

$$E_1 - E_0 = h \cdot \nu \tag{1}$$

During the absorption process the photon is completely destroyed and the energy becomes part of the total energy of the absorbing species.

Related to the absorption of light two fundamental principles are the laws of Grotthus-Draper and Einstein:

- The Grotthus-Draper law specifies that only the light absorbed by a chemical entity leads to a photochemical change- neither the reflected nor the light passed through.
- The second law of photochemistry, the Stark-Einstein law states that the light absorbed by a molecule is a one quantum process. For one photon absorbed only one molecule is excited. Exceptions are known for very intense light sources, e.g. lasers, where two-photon absorption processes can take place.

The efficiency of the ratio radiation to intended photoprocess is defined as the term of the overall quantum yield. It is calculated out of the number of molecules reacting (n_A) per number of photons (n_Q) absorbed at a specific wavelength.

$$\phi = \frac{n_A}{n_Q} \tag{2}$$

According to the Stark-Einstein law, ϕ should be equal to 1. However, if secondary reactions occur, ϕ can be greater than 1.[24]

A detailed graphical overview of absorption and emission processes accompanied with radiative and non-radiative transitions is the so called Jablonski diagram. The typical Jablonski diagram, as shown in Figure 2.2, illustrates a singlet ground electronic state prior to the excitation process; the electronic configuration of the species is described as ground state (S_0). Upon absorbing a photon of excitation light, the electrons are raised to a higher energy and consequently higher vibrational excited states. These states are energetically unstable and thus relaxation occurs, which can be divided into radiative or non-radiative decay processes. Internal conversion (IC) or vibrational relaxation represents a non-radiative decay where the transition from upper to lower state is obtained by the release of energy. Fluorescence is typically slower than the vibrational relaxation. Hence, the molecules have sufficient time to achieve the thermally equilibrated lowest-energy excited state prior to the photon emission. Phosphorescence decay is similar to that of fluorescence. However, the electron has to undergo a spin conversion into a "forbidden" triplet state (T_1) instead of the lowest singlet excited state (S_1). This process is known as intersystem crossing (ISC). Triplett states are very long lasting states (10^{-4} s). The emission from the lowest triplet state occurs with lower energy relative to fluorescence; consequently the emitted photons have longer wavelengths.

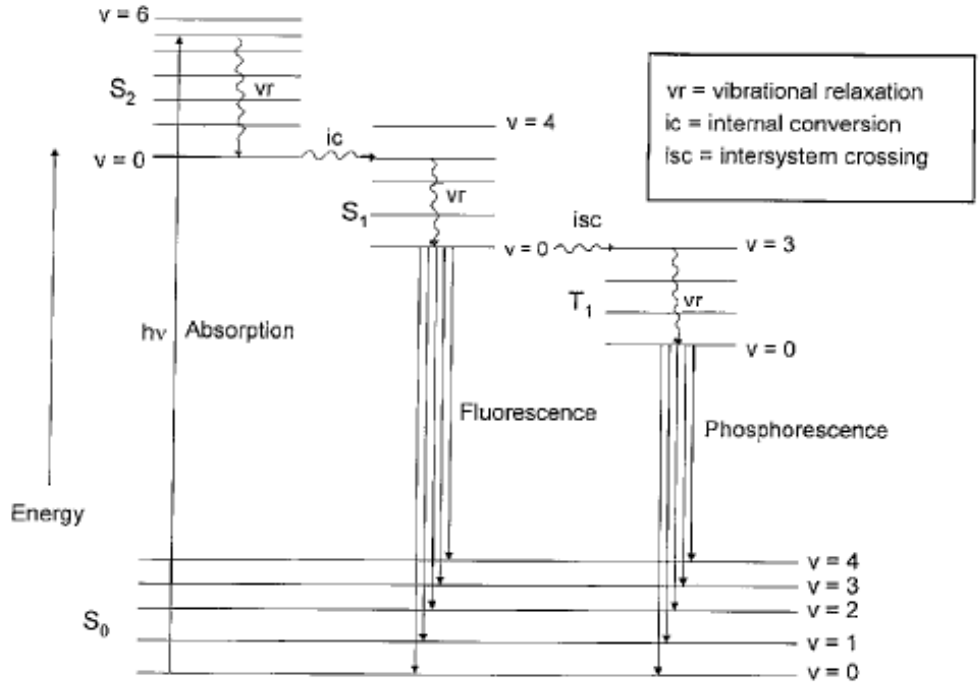

Figure 2.2: Depiction of absorption and emission processes illustrating radiative and non-radiative transitions[24]

2.2 STATE OF THE ART AND LITERATURE REVIEW

2.2.1 EXAMPLES OF PHOTOREACTIONS

Among the variety of photoreactions which are known to proceed in organic polymers and/ or self-assembled monolayers, it is focused on two photoreactions which have been the center of our interest over the last years. Firstly, the photoreaction of aromatic esters, the photo-Fries rearrangement is presented, followed by the photocleavage of ortho-nitrobenzyl esters. Both of these reactions cause a high change in surface polarity as well as in the chemical reactivity being induced by the photoreaction. Furthermore, it is reported on a novel polyaniline derivative bearing photosensitive N-formamide groups. UV-illumination of this polymeric material leads to a decarbonylation resulting in polyaniline.

2.2.1.1 PHOTO-FRIES REARRANGEMENT OF AROMATIC ESTERS

The thermal Fries reaction was discovered by Fries and Fink in 1908.[25] In the presence of aluminium chloride as Lewis acid a rearrangement of aromatic ester groups occurs and consequently ortho- and para-hydroxyketones are formed. The light induced Fries reaction was first mentioned in the 1960s. Anderson and Reese[26] discovered that upon irradiation with UV-light aryl esters can be transformed into hydroxyketones. In contrast to the chemical Fries reaction the photo-Fries rearrangement is based on a radical mechanism (cf. Figure 2.3).[27] Besides aromatic esters, aromatic amides also show this photoisomerization reaction leading to ortho- and para-aminoketones as photoproducts.

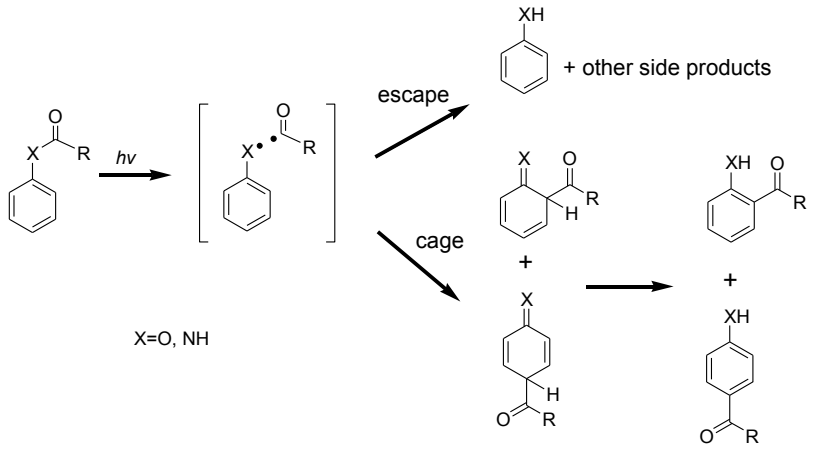

Figure 2.3: Reaction scheme of the photo-Fries rearrangement

The accepted mechanism for the photo-Fries reaction of phenyl esters, introduced by Lochbrunner et al., is shown in Figure 2.3. The photolysis reaction mainly proceeds from an exited singlet (S1) state (π - π* transition). Via crossing with the π -σ* state, the C-O bond in the ester group is elongated. Consequently, the C-O bond cleaves and free radicals are formed. In the solvent cage the photogenerated radicals can recombine to the starting compound or ortho- and/or para-isomers of cyclohexadienone are generated as “cage product” via an acyl shift. Tautomerism then gives hydroxyketones. The “escape product” of the geminate radical pair is mainly phenol, which is formed by H abstraction from the solvent.

Compared to the photoreaction of low-molecular weight esters, the yield of photoproduct in polymeric layers is significantly lower. This is caused by stronger absorption behaviour of the generated hydroxyketones, forming a blocking layer for the UV-light. Consequently, this kind of filter effect inhibits a further photoconversion of ester groups and degradation of the product.

The formation of the ortho product is favoured in highly viscous solvents or solid matrices. The reaction mechanism shows that the limited mobility of the acyl radicals hinders high yields of the para product and the attachment on the ortho position is preferred. In addition phenol as side product is formed.[10]

2.2.1.2 PHOTOREACTION OF ORTHO-NITROBENZYL ESTER UNITS

The o-nitrobenzyl group is well known to provide a photocleavable protection for hydroxyl compounds, such as alcohols and carboxylic acids.[28] In 1901 Ciamician and Silber discovered that upon irradiation with UV-light 2-nitrobenzylaldehyde undergoes an intramolecular conversion to nitrosobenzoic acid.[29] In 1966, Barltrop et al.[30] introduced o-nitrobenzyl moieties as photolabile protecting groups, which can be cleaved upon UV irradiation and consequently release the functional group. The deprotection of the ester groups and formation of the carboxylic acid is a photoacid generating (PAG) process. Therefore, nitrobenzyl ester groups are applied as PAG groups.

An accepted mechanism for the photochemical deprotection is based on a Norrish-type II reaction.[31] Upon irradiation with UV-light an n- π* transition occurs. The excited singlet state is transferred into a triplet state and the nitro group abstracts a proton from the methylene carbon in the γ-H position. An aci-nitro intermediate is formed and resonance stabilized by a five-membered ring intermediate, which rapidly decomposes to an aldehyde and a carboxylic acid.[11] The reaction of these photolabile compounds is shown in Figure 2.4.

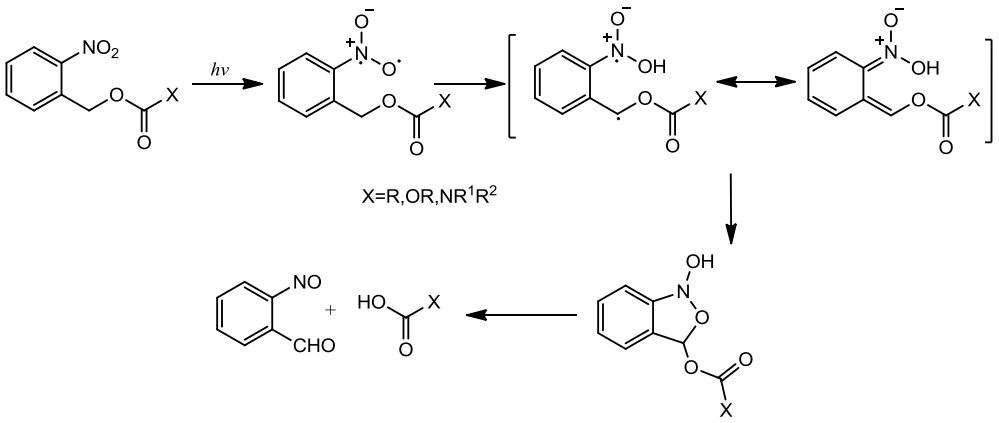

Figure 2.4: Reaction scheme of the ortho-nitrobenzyl ester cleavage upon irradiation with UV-light

2.2.2 TUNING OF MATERIAL PARAMETERS

Photolithographic patterning of polymers selectively induces changes of material properties in the irradiated area and is useful in a variety of applications: e.g. a difference in solubility for photoresists, refractive index modulation for optical data storage, waveguides, grating or distributed feedback lasers, the chemical reactivity for site-selective immobilization and electroless plating of metals. In the following, examples of photoinduced changes of the properties and post-modification reactions as well as applications are shown for polymers investigated during the last years in our group.[2–4, 32–35]

2.2.2.1 REFRACTIVE INDEX CHANGES INDUCED BY THE PHOTO-FRIES REARRANGEMENT AND RELATED PHOTOREACTIONS

Polymeric materials with tunable refractive index are of interest for applications related to optical communication (e.g. polymeric waveguides, optical switches)[36] and data storage devices.[37] Besides well-established data storage devices (e.g. CD, DVD, and blue-ray discs) holographic and two-photon recording processes offer incomparably high storage densities.[38]

A large number of photoreactive polymers with tuneable refractive index have therefore been developed and introduced over the last few years. A commonly used technology is based on the photobleaching process of dye-doped polymers, which results in required refractive index changes Δn for optical devices in the order of 10^{-3}. Photochromic dyes, which bleach upon UV-irradiation are dispersed in thermoplastic polymeric matrices, e.g. polymethylmethacrylate (PMMA), polystyrene and polyethylene.[39] Alternatively, photoinduced refractive index modification can also be achieved with photosensitive polymers, in which the dye units are covalently attached to the polymer backbone. These polymers have the advantage that a high chromophore concentration can be incorporated into the polymer system without crystallization, phase separation, or the formation of concentration gradients. In addition, these systems are expected to be more stable over time than the dye-doped systems due to the covalent immobilization of the chromophores.[40] Besides these photochromic materials, other approaches are based on photopolymerisable acrylate resins and polymers with photoreactive side groups, e.g. cinnamate units which undergo a [2 + 2] cyclodimerization.[41]

Recently, it has been shown that the photo-Fries reaction of phenyl esters and N-aryl amides in polymeric materials induces very high refractive index changes compared to other

polymer based systems.[2] The observed large increase in refractive index stems from the difference in the chemical structure of the phenyl ester (before illumination) and the hydroxyketone (after illumination). Furthermore, the change in refractive index is proportional to the conversion of the starting compound, which allows a selective adjustment of the refractive index by the irradiation dose. Figure 2.5 provides examples of photoreactive polymers exhibiting high refractive index changes. The polymers have been either prepared using ring opening metathesis polymerization or radical polymerization, with the polymer backbone consisting of a polynorbornene main chain or a polyvinyl chain. This has, however, only a minor effect on the photochemistry, whereas the photoreactions used are based on functional groups. Hence, the conversion efficiency, the wavelength of illumination and the photochemistry itself can be influenced. The basic motif for polymers that undergo the photo-Fries rearrangement is shown in p-1 and p-2. Both polymers are easily accessible and possess a suitable aryl ester unit, which can be excited with UV-light up to 270 nm. Using the naphthyl ester chromophor instead, the photo-Fries reaction can be induced with UV-light up to 320 nm (p-3). However, in these polymers, the yield of the photo-Fries reaction is rather low. By using fully aromatic esters, as realized in the structures p-7, p-9 and p-10, the yield of the ortho- and para-hydroxyketone can be increased. Furthermore, photoreactive aryl amides (p-4 and p-5) are an alternative material with high refractive index changes, but with a difference in the reaction products (aromatic amines instead of phenols). Instead of a photo-Fries reaction, the formic acid amide (p-6) shows a photodecarbonylation with almost 100 % yield, (extrusion of C≡O).

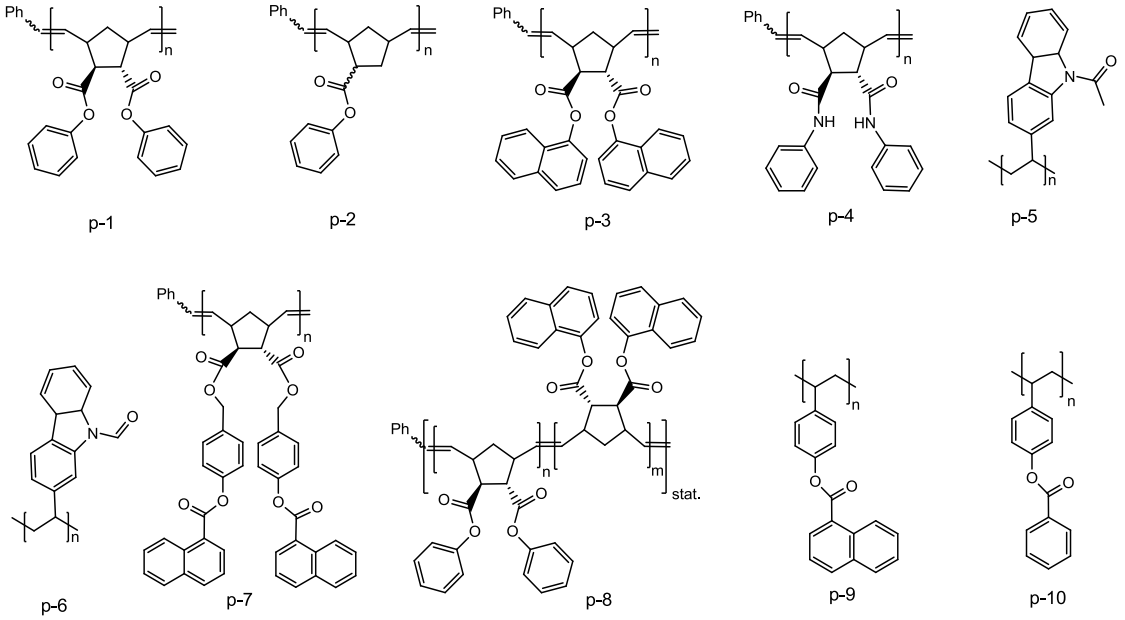

Figure 2.5: Overview of various photoreactive polymers applied for refractive index modulation

The main features of the photo-Fries reaction are exemplarily illustrated using poly(endo,exo-diphenyl bicyclo[2.2.1]hept-5-ene-2,3-dicarboxylate)[35] (p-1) in Figure 2.6. To avoid photooxidative side reactions, illumination with UV-light of 254 nm was carried out under inert atmosphere. The change of the chemical structure in p-1 causes a significant change in the UV-Vis spectrum. As depicted in Figure 2.6, the phenyl groups absorb UV-light at a wavelength λ~ 280 nm (π-π* transitions). The ester shows characteristic absorption near λ~ 190 nm (C=O group, π-π* transitions) and 270 nm (n-π* transitions). Illumination with monochromatic UV-light (254 nm, energy density E= 0.5 J cm^{-2}) causes the formation of two new absorbance maxima at λ~ 260 nm and λ~ 330 nm, which reveal the generation of aromatic hydroxyketone units. The FTIR spectra display the depletion of the ester peaks at 1745 cm^{-1} (C=O stretch) and 1197 cm^{-1} (asym. C-O-C stretch) accompanied by the formation of bands at 3400 cm^{-1} for the O-H stretching of the hydroxyl group and 1632 cm^{-1}, which can be attributed to the formation of an ortho-hydroxyketone. Furthermore, a weak signal emerges at 1670 cm^{-1}. This signal describes the formation of para-hydroxyketone groups. In addition, the evaluation of the FTIR spectra provided an estimate of the yield of the photo-Fries products. A comparison of the intensity of the ester carbonyl peak (1763 cm^{-1}) in non-irradiated p-1 and the ortho-hydroxyketone carbonyl peak (1641 cm^{-1}) showed that the yield of o-hydroxyketone in p-1 is approximately 25 % after 10 min of irradiation (E= 0.5 J cm^{-2}), while approximately 45 % of the ester units remain unchanged. Ellipsometric measurements

were performed for the determination of refractive index modulation. For p-1 a significant change of the refractive index by up to Δn= 0.05 was obtained.

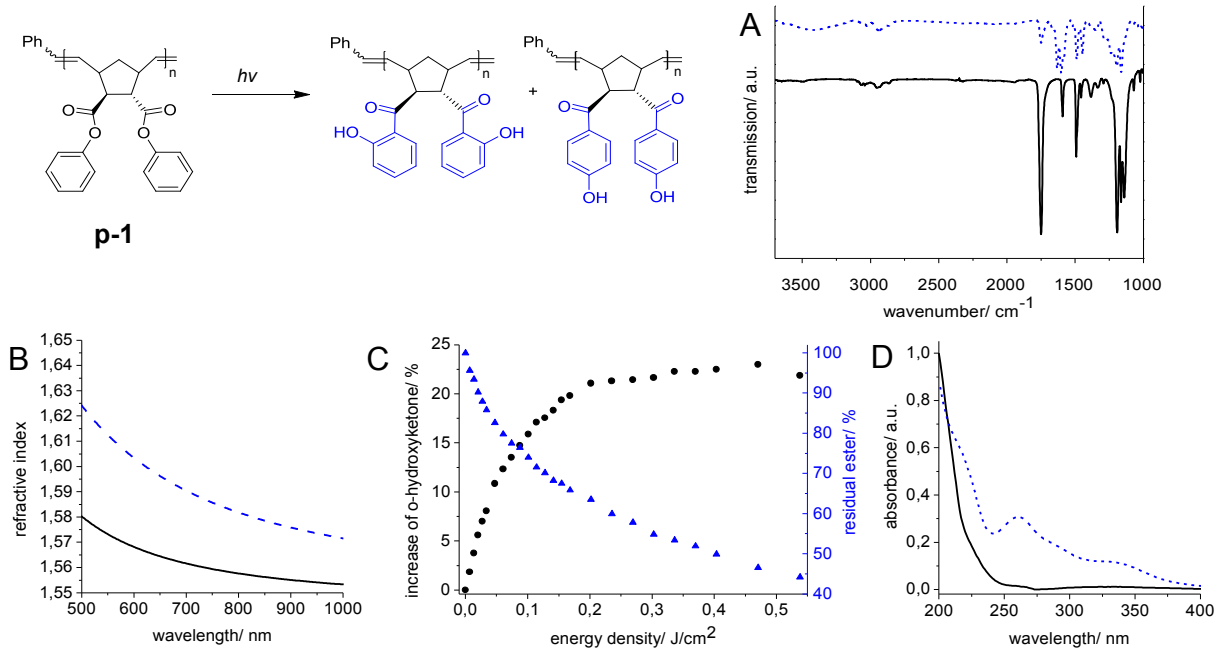

Figure 2.6: FTIR spectra (A), Cauchy Fit of the dispersion of the refractive index (B), progress in photo-Fries rearrangement (C) and UV-Vis spectra (D) of a film of p-1 before (solid line, black) and after (dotted line, blue) illumination with UV-light of 254 nm (energy density E= 0.5 J cm^{-2})

The observed difference in refractive index is directly proportional to the yield of photoproduct and can significantly be attributed to the progress of photoreactions. Figure 2.6 shows the optimal illumination time and thus the refractive index modulation can be exactly tuned. In Table 1 the refractive index changes, which can be obtained for the polymers presented in Figure 2.5 are summarized.

Table 1: Refractive index changes (Δn) and photoconversion upon UV-irradiation in polymers bearing aryl ester and amide units.

Polymer		Change in Refractive index ($\Delta n_{(x)}$)	Formation of hydroxyketone / %	Literature
Poly(endo,exo-diphenyl bicyclo[2.2.1]hept-5-ene-2,3-dicarboxylate)	p-1	$+0.049_{(450)}$	24	[35]
Poly(endo,exo-phenyl bicyclo[2.2.1]hept-5-ene-2-carboxylate)	p-2	$+0.042_{(450)}$	21	[35]
Poly(endo,exo-dinaphthyl bicyclo[2.2.1]hept-5-ene-2,3-dicarboxylate)	p-3	$+0.048_{(589)}$	27	[3]
Poly(endo,exo-N,N´-diphenyl bicyclo[2.2.1]hept-5-ene-2,3-dicarboxamide)	p-4	$+0.100_{(450)}$	n.d.	[2]
Poly(1-(2-vinyl-9H-carbazol-9-yl)ethanone)	p-5	$+0.010_{(650)}$	n.d.	[4]
Poly(2-vinyl-9H-carbazole-9-carbaldehyde)	p-6	$+0.038_{(650)}$	n.d.	[4]
Poly(endo,exo-di(benzyl-4-oxycarbonyl-naphthalen-1-yl) bicyclo-[2.2.1]-hept-5-ene-2,3-dicarboxylate)	p-7	$+0.043_{(370)}$	37	[33]
Poly(endo,exo- diphenyl bicyclo[2.2.1]hept-5-ene-2,3-dicarboxylate-co- endo,exo-di(1-naphthyl) bicyclo[2.2.1]hept-5-ene-2,3-dicarboxylate)]	p-8	$+0.036_{(589)}$	n.d.	[3]
Poly(4-vinylphenyl 1-naphthoate)	p-9	$+0.010_{(600)}$	45	[32]
Poly(4-vinylphenyl benzoate)	p-10	$+0.036_{(600)}$	45	[32]

n.d.: Formation of photoproduct not determined

$\Delta n_{(x)}$: refractive index change determined at defined wavelengths

All investigated polymers show high refractive index changes in the range of Δn= +0.01 (for p-5 and p-9) up to an astonishing value of Δn= +0.10 in p-4. Usually, the refractive index variations in the range from 0.003 to 0.03 are already considered to be high and a refractive index change of approx. 0.005 is sufficient for many optical applications such as waveguiding.[42]

The change of the refractive index is based on the difference in the chemical structure before and after illumination. Comparing polymers p-1, p-2 and p-3, all of them convert an aliphatic carboxylic acid aryl ester into a hydroxy-arylketone. In all cases a similar and relatively high refractive index change (Δn between 0.042 and 0.049) could be observed. It has to be noted that a slight contribution to the increase in refractive index can stem from

photocrosslinking, which is observed as a side reaction in these polymers and is expected to cause a slight reduction in volume.[43]

Changing from phenyl esters in p-1 and p-2 to naphthyl ester units in p-3 allows the use of wavelengths above 300 nm for the photoreactions with similar results for the refractive index change. In this context, copolymers bearing both chromophores phenyl and naphthyl esters are interesting materials as realized with p-8. A selective excitation of the naphthyl ester is achieved with UV-light > 300 nm whilst both phenyl and naphthyl ester units are converted by using UV-light < 270 nm. This allows a finer tuning of the refractive index and a double writing methodology.

The conversion of the ester units in the fully aromatic ester systems in p-9 bearing naphthyl ester groups and in p-10 bearing phenyl ester is comparably high for polymeric materials resulting in up to 45 % hydroxyketone formation (see Table 1). However, the refractive index change for p-9 is relatively low (Δn= 0.011), while p-10 yielded in Δn= 0.036 compared to the aliphatic carboxylic acid aryl esters (p-1, p-2 and p-3).

The highest refractive index changes - Δn= +0.10 at 450 nm - obtained in polymers have been realized in p-4, the aryl amide based system.

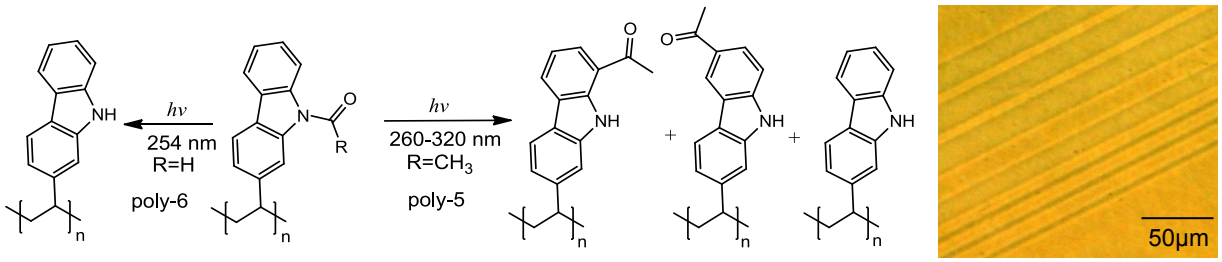

Figure 2.7: Photodecarbonylation of p-6 and photo-Fries rearrangement of p-5[4]; pattern in p-5

P-5 and p-6 are a special class of materials based on carbazole polymers.[4] The photochemical reaction in p-5 is a partial photo-Fries reaction analogous to the reaction in aryl amides (p-4). Photodecarbonylations occur to a lesser extent than common side reactions of the photo-Fries reaction (escape product). A refractive index modulation of Δn= 0.01 was obtained in p-5. However, the higher refractive index change in p-6 (Δn= 0.03) is based on the quantitative photodecarbonylation to poly(2-vinyl-9H-carbazole). This can be attributed to the low-stability of the formyl radical, which is formed upon UV-exposure. Moreover, an optical phase contrast image can be achieved via mask aligner illumination as shown in Figure 2.7. Well separated lines have been realized.

2.2.2.2 TUNING THE CHEMICAL REACTIVITY

In addition to the change of the refractive index UV-irradiation leads to a significant change in chemical reactivity. The enhancement is caused by the formation of aromatic o- and p-hydroxyketones. By combination of photolithographic techniques and selective immobilization, patterned functionalized surfaces can be obtained. Using p-1 as an example several possibilities of post-modification reactions are shown in Figure 2.8.

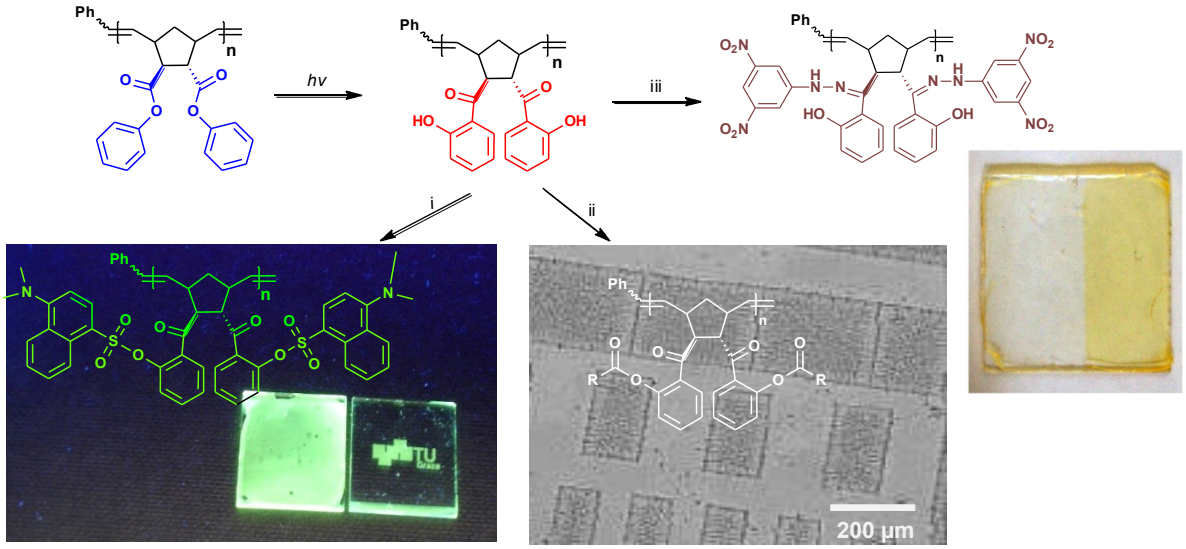

Figure 2.8: Subsequent post-exposure reactions with dansyl chloride (i), acetyl chloride (ii) and 2,4-dinitrophenylhydrazine hydrochloride (iii)[44]

The hydroxyl groups can react with acid chlorides to give the corresponding esters. For the immobilization of fluorescent dyes, the illuminated films were immersed in a solution of dansyl chloride (i) and both flood and patterned functionalization of the thin polymer film were realized. Another approach for the immobilization of molecules on the irradiated areas of the p-1 surface is the reaction of hydroxyl groups with acetyl chloride and the presence of CH_2Cl_2 (ii). The latter reagent is added to cause a swelling of the polymer film, enabling a derivatization throughout the whole layer. Another functionalization is based on the reaction of the ortho-, para photoproduct with hydrazine derivatives such as 2,4-dinitrophenylhydrazine hydrochloride resulting in the corresponding hydrazones (iii). A selective change in colour to yellow indicated the effective post-exposure reaction of the layer of p-1.[44]

A further functionalization using p-10[32] is shown in Figure 2.9. The post-modification reaction was performed in a solution of $Ru(bpy)_2(phen\text{-}5\text{-}NCS)(PF6)_2$ in acetonitrile. The

photogenerated hydroxyl groups react readily with the isothiocyanate groups of the red fluorescent dye. Confocal fluorescence micrographs indicate that the immobilization of the fluorescence dyes proceeds through the whole polymeric layer, as depicted in Figure 2.9. The immobilized dye was excited with light of 488 nm wavelength.

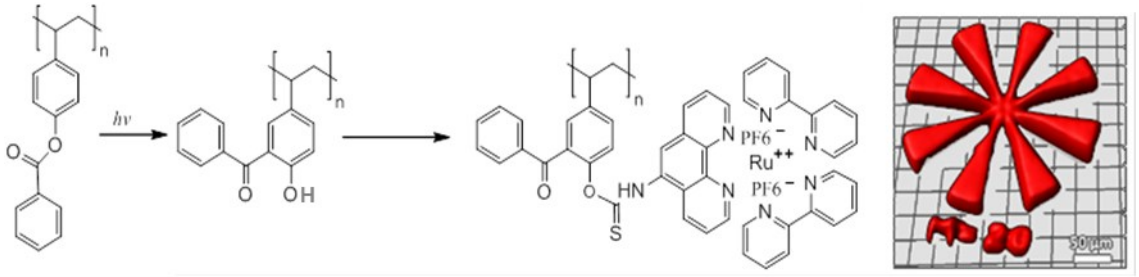

Figure 2.9: Derivatization reactions of p-10 and postmodification of patterned polymeric layer with $Ru(bpy)_2(phen\text{-}5\text{-}NCS)(PF6)_2$ (red)[32]

2.2.3 INFLUENCE ON EPITAXIAL GROWTH OF SMALL MOLECULES

Electroluminescence and charge carrier mobility, crucial electrical and optical characteristics of organic semiconducting layers largely depend on crystal structure, crystallite size and morphology. This can be strongly influenced by the interaction of the molecules with the substrate and the surface energy of the substrate plays a major role.

Again, using the photochemistry of p-1, the growth of para-sexiphenyl (PSP, $C_{36}H_{26}$) on the pristine polymer substrates has been compared to the growth on an illuminated polymer surface at different temperatures. PSP is an interesting semiconductor for electroactive layer in OLED displays. The photoluminescence of PSP is thereby dependent on the morphology and crystal structure.[45] The concept is depicted in Figure 2.10. The change in surface polarity induced by the photo-Fries reaction is expected to influence the growth morphology of PSP. Hot wall epitaxy as deposition method was chosen, because it enables organic molecules to adjust in the most suitable arrangement before fitting in the crystal lattice.[46] Prior to each growth experiment, one half of the substrate was illuminated (the other half covered) allowing the comparison of the growth conditions on the different surfaces, keeping all other parameters constant.

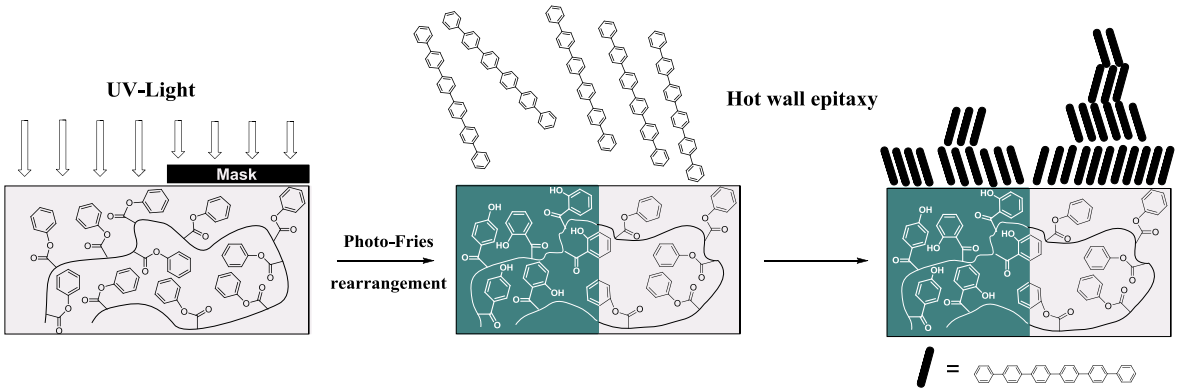

Figure 2.10: UV-illumination of a film of p-1 through a mask and subsequent growth of PSP performed by hot wall epitaxy[21]

The change in surface energy was first studied by contact angle measurements. Due to the illumination of the p-1 the surface tension decreases from 43.4 mJ m^{-2} to 40.6 mJ m^{-2}. However, this slight difference already has an enormous influence on the obtained crystal morphology. In Figure 2.11, the AFM images of samples prepared at two different temperatures and with different deposition times prove in all cases a significant difference in the crystal size and shape of PSP. In the non-illuminated region the film seems to be more homogeneous. Increasing the deposition time, a lateral expansion of single islands can be observed. This behaviour is based on the change in surface polarity via UV-irradiation. An additional increase in temperature coincides with the increase in structure size. A change in polarity of amorphous polymer films of p-1 significantly influences the growth of PSP film deposited by hot wall epitaxy. Treating substrates with UV-light as a prestructuring process therefore enables new perspectives for the fabrication of devices.

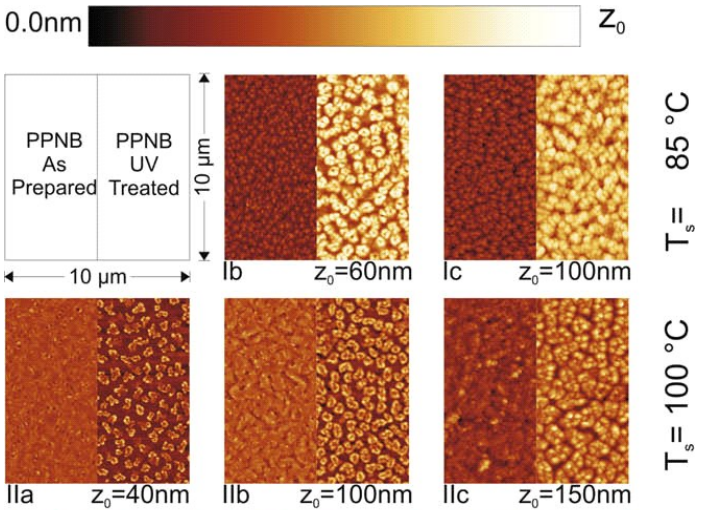

Figure 2.11: AFM images of PSP deposited via different substrate temperatures and deposition times on variably illuminated p-1[21]

2.3 MODIFICATION OF INORGANIC SURFACES WITH PHOTOREACTIVE ORGANOSILANES

2.3.1 HISTORY AND BACKGROUND

Although the thickness of thin molecular films is composed of only a few nanometers, these thin films are able to open the opportunity to completely modify and adjust the chemical and physical surface properties of different substrates. Next to Langmuir-Blodgett technique[47,48] the application of chemisorbed self-assembled monolayers (SAMs) have attracted much attention for the preparation of thin films in the last decades. The incredible popularity and potential of self-assembled monolayer can be derived by the number of publications related to this topic. The versatility of application ranges from nanotechnology, biotechnology to molecular electronics. Potential applications are the selective immobilization of several functional molecules, such as catalysts nano particles and biomolecules, passivation coatings and the area of operation in organic electronic devices. Beyond that, the extremely thin films are able to completely modify the surface properties, e.g. wetting, adhesion, conductivity, and friction.

In 1946 Zisman[49] et al. for the first time reported on the formation of oleophobic monolayers on polar solid substrates. With the application of molecules based on long-chain hydrocarbons and polar groups the formation of hydrophobic surfaces on the polar substrates as a consequence of densely packed hydrocarbons is enabled.

In the 1980s the topic of self-assembled monolayers started to attract attention with the introduction of two of the most common and investigated anchor group/ substrate combinations. It was Sagiv[50,51], who reported on the formation of silane monolayers by adsorption on SiOx surfaces from solution. Nuzzo[52] was the first who presented thiol monolayers on gold surfaces by adsorption of bifunctional organic disulfides from solution. In 1989 Whitesides et al.[53] reported about the chemisorption of alkanethiols on gold. Thiols on gold and silane coupling agents with chloro- or alkoxysilyl groups reactive to various oxidic surfaces show different characteristics. Considerable advantages of the thiol based system are the convenient handling and the compatibility of thiols with functional groups and the inertness of the gold substrate. However, fast and thermal bonding stability on oxidic surfaces evince the interest in the application of trichlorosilane anchor groups.

Next to thiols on gold[47,54,55] and organosilanes on oxide surfaces such as silicon oxide or glass[56–59], there exists a broad variety of additional molecule/substrate combinations ranging from phosphonic acids on oxidic surfaces (ITO[60], Al_2O_3,[61] TiO_2,[62]), to selenols on gold[63] and silver.[64]

2.3.2 CONCEPT OF SELF-ASSEMBLY

In this thesis the focus is set on different organosilane molecules, which have been used for the modification of silicon oxide substrates. Consequently, the characteristics of monolayer formation based on chlorosilanes are discussed.

The concept of self-assembled monolayers (SAMs) is based on the formation of a monolayer of highly ordered and vertically oriented bifunctional organic molecules that assemble spontaneously on suitable substrates. In Figure 2.12 the setup and layer formation is depicted. The molecules, which form the self-assembled monolayer consist of a head group capable of binding to a defined substrate, an alkyl or aryl spacer and a tail group. The alkyl or aryl spacer is responsible for the orientation of the bifunctional molecules forming highly ordered and dense layers through van der Waals force interactions. The tail group, however, determines the essential surface properties.

These surface properties can be tailored over a wide range by the choice of the tail group that spans from apolar to polar, from non-reactive to reactive, and from acidic to basic groups.[65]

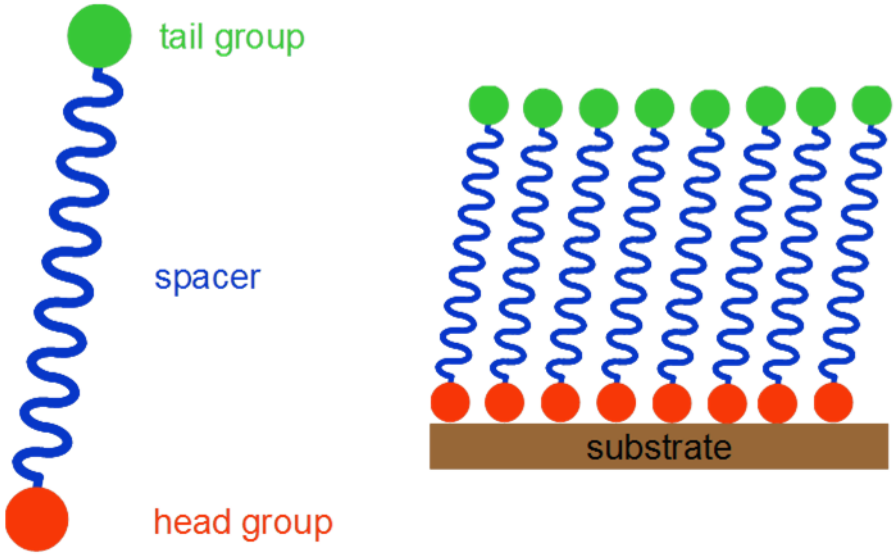

Figure 2.12 Scheme of a SAM forming molecule and a monolayer of the molecule assembled on a substrate[66]

Furthermore, by varying the head group the application of different substrate materials becomes possible. Thus, the combination of several tail and head groups enables nearly indefinite opportunities in the area of organic thin film coatings. Additionally, defined surface properties can be adjusted. The preparation of self-assembled monolayers is performed by either vapor-phase or solution deposition. Using vapor-phase deposition a substrate is exposed to the vapor of a reactive molecule in a closed chamber for a certain period of time. For solution deposition a substrate is exposed to a solution of the bifunctional molecules in a suitable organic solvent.

2.3.3 FORMATION OF A SILANE BASED SELF-ASSEMBLED MONOLAYER ON SILICON OXIDE

Today the most frequently applied molecule within the field of organosilane based SAMs is octadecyltrichlorosilane (OTS, $CH_3(CH_2)_{17}SiCl_3$). That bifunctional molecule equipped with a trichlorosilane anchor group is able to form monolayers on a variety of oxidized substrates such as aluminum, oxidized silicon, mica and glass. It was Sagiv[50] in 1980 who argued that the mechanism of monolayer formation scenario in solution by using OTS molecules consists of three main steps. The first step includes the hydrolysis of the trichlorosilane groups, caused by trace amounts of water. As a consequence silanol intermediates are formed. The second step involves the formation of hydrogen bonds between hydroxy groups of the silicon oxide surface and the silanols. Followed by the third step, where a planar polymerization of the remaining -OH groups of the molecules by condensation takes place and a two dimensional polysiloxane network is developed, in which each OTS molecule is covalently anchored to the surface. However, multiple factors of influence, in combination with inconsistent results obtained by the investigation of the exact binding mechanism still give rise to a lot of discussion.[67]

Thus, Finklea et al.[68] as well as Allara et al.[69] figured out that mainly a thin film of water absorbed on a substrate causes self-assembly and even gold, a surface without hydroxy groups represents a suitable substrate. They conclude that self-formation takes place on the water film, where silane head groups develop a two-dimensional cross-linked network of Si-O-Si bonds only connected by a few bonds to the surface (about 5 OH/nm^2). X-ray reflectivity (XRR) measurements of Silberzan et al.[70] and IR studies of Tripp and Hair[71,72] using silicon oxide as substrate, confirmed that the cross-polymerized molecules are only linked by a low number of Si-O-Si bonds. In addition, Rye et al.[73] argued that the competition between the reaction of the silane with surface hydroxyl groups and surface water plays a decisive role.

Crucial parameters influencing the deposition process of the organic molecules and the subsequent monolayer formation are the water content, the application of an appropriate solvent temperature and deposition time.

2.3.3.1 WATER CONTENT

Definitely, the amount of water is one of the most important facts in the formation of high quality monolayers based on trichlorosilanes. While trace amounts of water on the substrate are regarded as essential for the formation of smooth and densely packed monolayers, a large amount of water in the silane solution leads to condensed aggregates, which subsequently adsorb onto the substrate. Since the aggregates are already formed in solution a fast coverage of the surface is observed, but not able to form smooth monolayers.[67] Using anhydrous solvents, the formation of a water layer exclusively on the substrate surface is ensured. Thus, hydrolysis of the trichlorosilane moities is limited to the surface and true monolayers could be grown. Furthermore, the formation of three dimensional condensates is prevented.

2.3.3.2 SOLVENT

Silane deposition on glass was investigated by McGovern et al.[74], who reported that the most dense monolayer films can be achieved by using aromatic solvents such as benzene or toluene. While solvents with a high capacity of dissolving water, e.g. dioxane, cause polymerization in solution aromatic solvents are appropriate to extract sufficient amounts of water from the substrate to the bulk phase so that enough alkyltrisilanol is generated. Wang et al found that hydrophobic solvents such as Isopar-G (isoparaffin fluid), where the water films can stay in close vicinity to the substrate support the development of ultra-smooth layers. As drawback the long deposition time can be regarded.[75] Widely used solvents for the monolayer formation are toluene and mixtures of dicyclohexane and tetrachloromethane.

2.3.3.3 DEPOSITION TIME

The published data for the optimal deposition time for OTS molecules forming a complete layer differ significantly. Small variations in the content of water, the selection of the solvent and temperature may lead to several deposition times. Furthermore, the application of trichlorosilane or trialkoxysilane molecules are the cause of differences.[58] Silberzan et al. reported on the complete formation of OTS monolayers after 2 min of immersion time, while

Wang claimed that the layer formation was completed after 48h under dry conditions using a mixture of Isopar G and CCl_4.

2.3.3.4 INTERACTION OF PARAMETERS

In 1947 Zisman et al.[76] stated the temperature dependency of monolayer formation. A critical temperature is mentioned, where complete monolayers are no longer formed. With the application of time-resolved AFM studies Carraro et al.[77] observed three distinct mechanisms depending on deposition temperature. While at low temperatures island growth is predominant, at high temperatures a homogenous assembly occurs. Furthermore, the combined impact of water and temperature on the formation OTS monolayer showed that higher water content and low temperature favour the formation of aggregate growth in solution.

2.4 PHOTOPATTERNABLE CONDUCTIVE POLYANILINE FILMS

2.4.1 INTRINSICALLY CONDUCTIVE POLYMERS

In the 1970s the investigation of conjugated polymers exhibiting special electronic, optical and magnetical properties was intensified. A doping of these special polymers led to conductive polymers. Chiang et al. introduced the concept of synthetic metals. These metals consist of organic polymeric materials that show similar electrical and optical characteristics like a metal, while the mechanical and processing properties of a conventional polymer are still retained. These polymers are termed to be “intrinsically conducting polymers” (ICPs).[78]

In the IUPAC Compendium of Chemical Terminology intrinsically conducting polymers are defined as electrically conducting polymers composed of macromolecules having fully conjugated sequences of double bonds along the chains.[79]

In contrast to standard insulating polymers consisting of saturated (sp^3 hybridized) carbons in the chain backbone, conjugated polymers are based on sp^2 hybridized carbons. As consequence the electron configuration results in three σ-bonding electrons, the 2s, $2p_x$ and $2p_y$ electrons and a remaining $2p_z$ electron. A characteristic π-bond is comprised of two adjacent $2p_z$ orbitals. The orbitals overlap along the backbone and augment the delocalisation of the π electron system. Thus, the basis of a conductive polymer is provided. In contrast to conductors conjugated polymers only show conductivity till in the semiconductor regime. As explanation the Peierls theorem postulates that the distortion of the lattice based on an alternate interatomaric distance leads to the formation of an energy gap. Thus, only semiconductive conditions are accomplished.

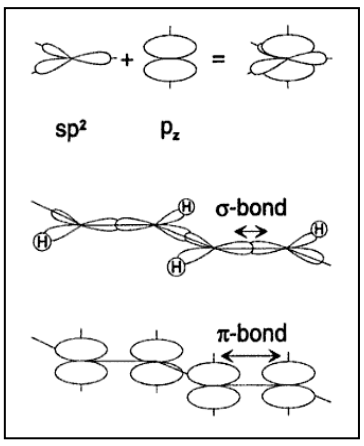

Figure 2.13: Simple depiction of σ-bonds and π-bonds[80]

However, the properties of these polymeric materials are intrinsic to a “doped” form of the polymer. The concept of “doping” is the decisive point that distinguishes conductive polymers from all other types of polymers. Based on the doped form, the polymer consists of a conjugated backbone in which the π-system is delocalised. Due to a doping process, via removing of electrons (p-doping) or adding electrons (n-doping) charged bipolarons are generated that move in the π-system of the polymer chain and consequently enhance conductivity. Thus, a weakly conducting organic polymer is converted to a polymer, which is in the “metallic” conducting regime (up to 10^4 Siemens per centimetre [S/cm]). The raise of conductivity in the range of 10 orders of magnitude can be simply achieved by doping. Doped polyacetylene approaches the conductivity of copper on a weight basis at room temperature. With the exact adjustment of the doping level, a conductivity anywhere between that of the undoped (insulating or semiconducting) and that of the fully doped (metallic) form of the polymer may be obtained. Furthermore, doping is reversible: that means that a recovery of the original polymer is obtained with little or no damage to the backbone chain. Therefore, the dopant counter ions responsible for the doping and undoping processes- the doped states are stabilized- can be chemically or electrochemically removed.

P- and/or n-redox doping are performed by chemical and/or electrochemical processes. Using p-doping a partial oxidation of the π-system takes place, whereas n-doping involves partial reduction of the π-system. Polyaniline, the best known and most fully investigated example, also undergoes doping by a large number of protonic acids, during which the number of electrons associated with the polymer backbone remains unchanged. Thermal, hydrolytic and oxidative stability of doped forms of pure conducting polymers varies enormously. The n-doped form of polyacetylene undergoes instant decomposition in air, while polyaniline shows sufficient stability in air even heated up to 240 °C.

Moreover, the oxidative and hydrolytic stability can be significantly increased by using the conductive polymers in form of blends with conventional polymeric material. In this area research is essential for the future use in commercial applications.

2.4.2 POLYANILINE (PANI)

Polyaniline one of the oldest polymers was first synthesized 150 years ago[81] and especially today attracts great scientific and industrial attention for research and technological applications in electrical devices.

The monomer aniline was obtained via pyrolytic distillation of indigo and was called “Krystallin” because of the generation of well-formed crystalline salts in the presence of sulfuric and phosphoric acidic media. The oxidation of aniline led to the formation of polyaniline. However, the ultimate breakthrough of polyaniline accomplished in the mid-1980s as MacDiarmid et al. published the sensational discovery of the electrical conductivity of emeraldine salt.[82]

2.4.2.1 SYNTHESIS OF POLYANILINE

In general polyanilines are produced by chemical and electrochemical oxidative polymerization in acidic solution. Polyaniline exhibits predominantly head-to-tail polymerization with essentially linear chains and in solution either tight coils or expanded chains appear, depending on the used solvent. The standard synthesis of the emeraldine salt is performed using ammonium persulfate [$(NH_4)_2S_2O_8$] oxidation of aniline in aqueous HCl, most advantageously at -25 °C.[83,84]

Polyaniline occurs in three accessible oxidation conditions showing various electrical properties. Different states are depicted in Figure 2.14.

- The insulating, fully reduced colorless polybenzenoid leucoemeraldine (LES, LEB) which is composed of phenylene diamine repeating units.
- The partially oxidized (half-oxidized and half-reduced) blue emeraldine base form (EB). In acidic media (emeraldine salt, ES, in green) conductivity is realized. The repeat units consist of alternating quinone imine and phenylene diamine structures.
- Complete oxidation leads to the insulating blue-black polyquinoid pernigraniline. This form is on repeating quinone imine units (PB, PS).[85,86]

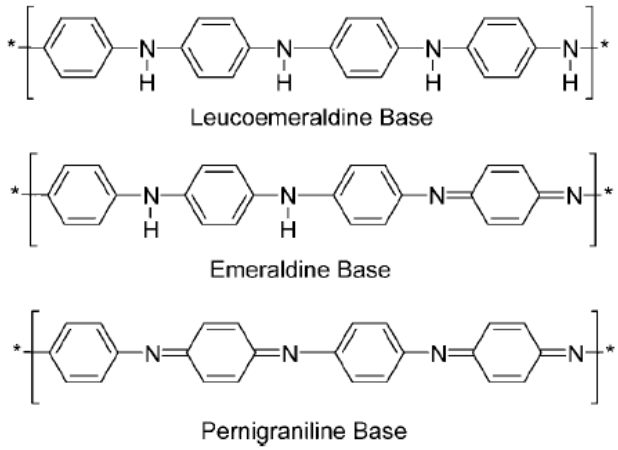

Figure 2.14: Representation of various oxidation states in base form

2.4.2.2 ELECTRICAL PROPERTIES

As mentioned above next to the oxidation level, the degree of doping of the polyemeraldine base is a crucial parameter influencing and controlling the conductivity of polyaniline. Usual methods are the application of electron acceptors, e.g. Lewis acids and metal complexes. Using Brönsted acids, such as HCl, HNO_3 and carboxylic acids respectively, the imine sequences are protonated by acids to the bipolaron (dication salt) form. A further rearrangement leads to the delocalized polaron lattice (polysemiquinone radical-cation salt) as shown in Figure 2.15. Conductivity is ensured as soon as the electrons are thermally brought up to the unfilled bands.

Furthermore, additional parameters such as temperature, humidity as well as polymer morphology and the choice of solvent the polymer is cast from massively influence the conductivity of polyaniline.[87]

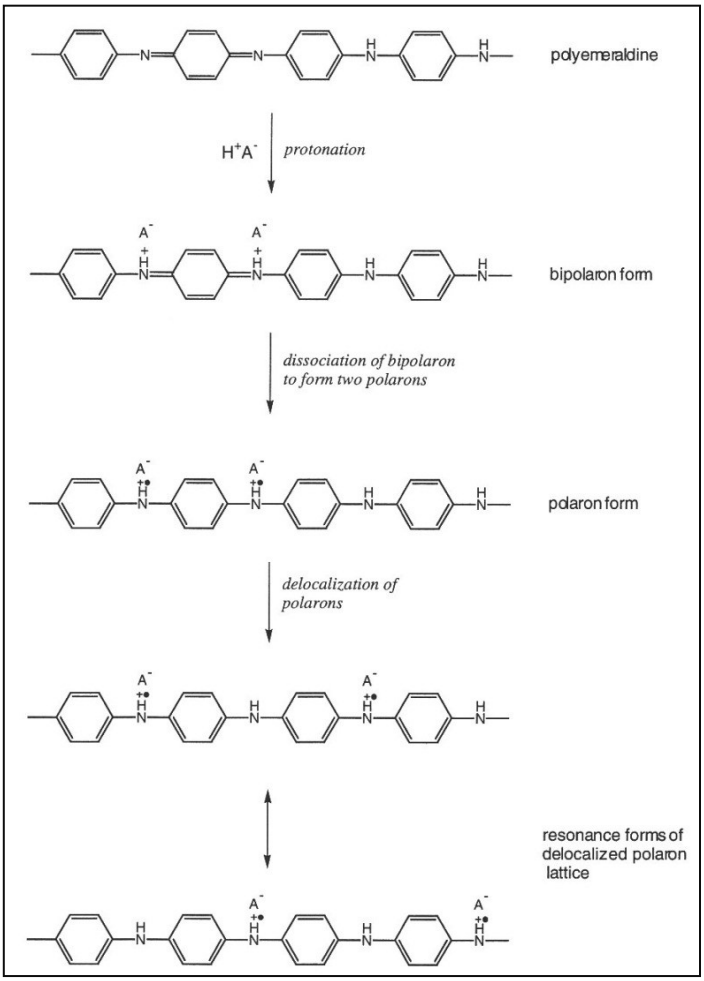

Figure 2.15: Depiction of the detailed protonation process[88]

In general PANI is moderately soluble in polar organic solvents such as *N,N*-dimethylformamide (DMF), dimethyl sulfoxide (DMSO), and *N*-methylpyrrolidone (NMP). The solubility of the base form is much better than that of the salt form.[89]

2.5 TUNING OF POLYANILINE FILMS BY PHOTOCHEMICAL TECHNIQUES

In the past years the interest in the characterization and modification of electrically conductive polymers has grown steadily and today is one of the most important research areas in the field of polymers and materials. Especially, polyaniline (PANI), first mentioned in the literature in the 19th century, has become the focus of attention in modern science.[81] Characteristics of polyaniline (PANI) and its derivatives, such as the relatively high electric conductivity, stability against environmental impacts and attractive redox properties makes

PANI a suitable candidate for the application in modern electronic devices.[90–93] Typical applications are polymeric electrodes and interconnects in organic thin film transistors[94], organic light emitting diodes[95], batteries, electrochromic devices[96], as well as chemical sensors.[97]

In the literature various contributions focus on the direct photolithographic patterning of PANI. Most of them refer to photodoping of thin PANI films using photoacid generators (PAG).[89] The acid, formed in the irradiated regions protonates the PANI and thus, electrical conductivities up to 0.1 S/cm dependent on PAG concentrations (10 to 50 mol%) can be accomplished. Furthermore, the different solubility behaviour of doped PANI that is typically insoluble in organic solvents and pristine PANI that is soluble enable the opportunity of direct photopatterning. Another interesting approach is the application of spin cast PANI in its protonated, conductive form in the presence of an aliphatic phenylketone.[98] Here, the ketone, if illuminated, forms radicals that reduce PANI to its non-conductive leucoemeraldine form. After removal of the photoinitiator by postbaking a sheet resistance of 1kΩ/square in the unexposed areas has been ascertained, while in the exposed region an increase of 1 kΩ/square to 10^{11} kΩ/square has been obtained. Consequently, the fabrication of electrodes and interconnects in all-polymer OTFTs is ensured.[99] In addition, conductive patterns of PANI have also been achieved by radiation induced crosslinking.[100]

All of these methods, however, are dependent on photosensitive polymer additives for the patterning process. Also the polyaniline layers obtained do not reach the conductivity of pristine doped polyaniline (3-5 S/cm).

3 RESULTS AND DISCUSSION

3.1 SYNTHESIS AND CHARACTERIZATION OF NORBORNENE BASED POLYMERS BEARING PHOTOREACTIVE UNITS

3.1.1 SYNTHESIS OF THE MONOMERS

Two photoreactive norbornene based monomers endo,exo-di(2-nitrobenzyl) bicyclo[2.2.1] hept-5-ene-2,3-dicarboxylate (M-1) and endo,exo-diphenyl bicyclo[2.2.1]hept-5-ene-2,3-dicarboxylate (M-2) were synthesized via esterification reaction. A third monomer of endo,exo-dimethyl bicyclo[2.2.1]hept-5-ene-2,3-dicarboxylate (M-3) also based on endo,exo-bicyclo[2.2.1]hept-5-ene-2,3-dicarboxylic acid ester equipped with photostable methyl moieties was acquired from commercial sources. The molecules synthesized correspond well with the characteristic spectroscopic data presented in chapter 4.2.

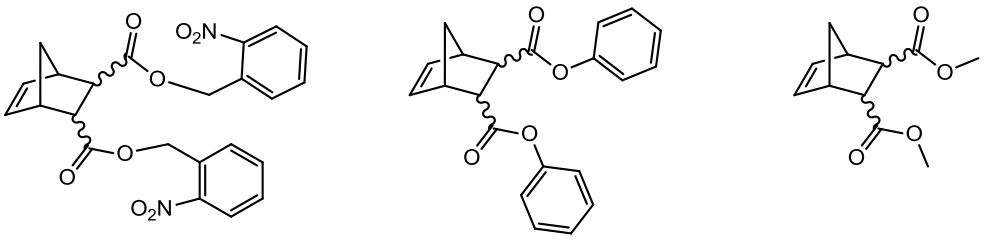

M-1 **M-2** **M-3**

Figure 3.1: Depiction of the monomers used for polymer synthesis

3.1.1.1 SYNTHESIS OF ENDO,EXO-DI(2-NITROBENZYL) BICYCLO[2.2.1] HEPT-5-ENE-2,3-DICARBOXYLATE (M-1)

The photosensitive monomer M-1 was synthesized in a one-step reaction. Therefore, (2-nitrophenyl)methanol was added to a solution of endo,exo-bicyclo[2.2.1]hept-5-ene-2,3-dicarbonyl dichloride and dichloromethane in the presence of pyridine. The reaction scheme is depicted in Figure 3.2.

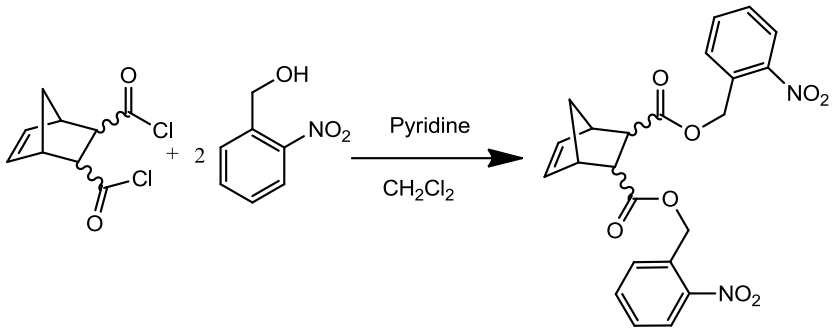

M-1

Figure 3.2: Synthesis route of endo,exo-di(2-nitrobenzyl) bicyclo[2.2.1]hept-5-ene-2,3-dicarboxylate

3.1.1.2 SYNTHESIS OF ENDO,EXO-DIPHENYL BICYCLO[2.2.1]HEPT-5-ENE-2,3-DICARBOXYLATE (M-2)

The photosensitive monomer M-2 was synthesized in a similar way. Here, phenol was added to a solution of endo,exo-bicyclo[2.2.1]hept-5-ene-2,3-dicarbonyl dichloride and dichloromethane in the presence of pyridine. The reaction scheme is depicted in Figure 3.3.

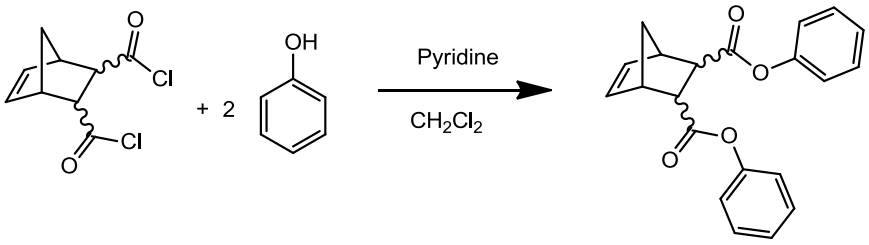

M-2

Figure 3.3: Synthesis route of endo,exo-diphenyl bicyclo[2.2.1]hept-5-ene-2,3-dicarboxylate

3.1.2 SYNTHESIS OF THE PHOTOREACTIVE POLYMERS

In Figure 3.4 the homopolymer (poly-1) and the two statistical copolymers poly(1-co-2) and poly(1-co-3) synthesized are depicted. All polymers were synthesized in an analogous manner using ring opening metathesis polymerization (ROMP), which proceeded in high yields.

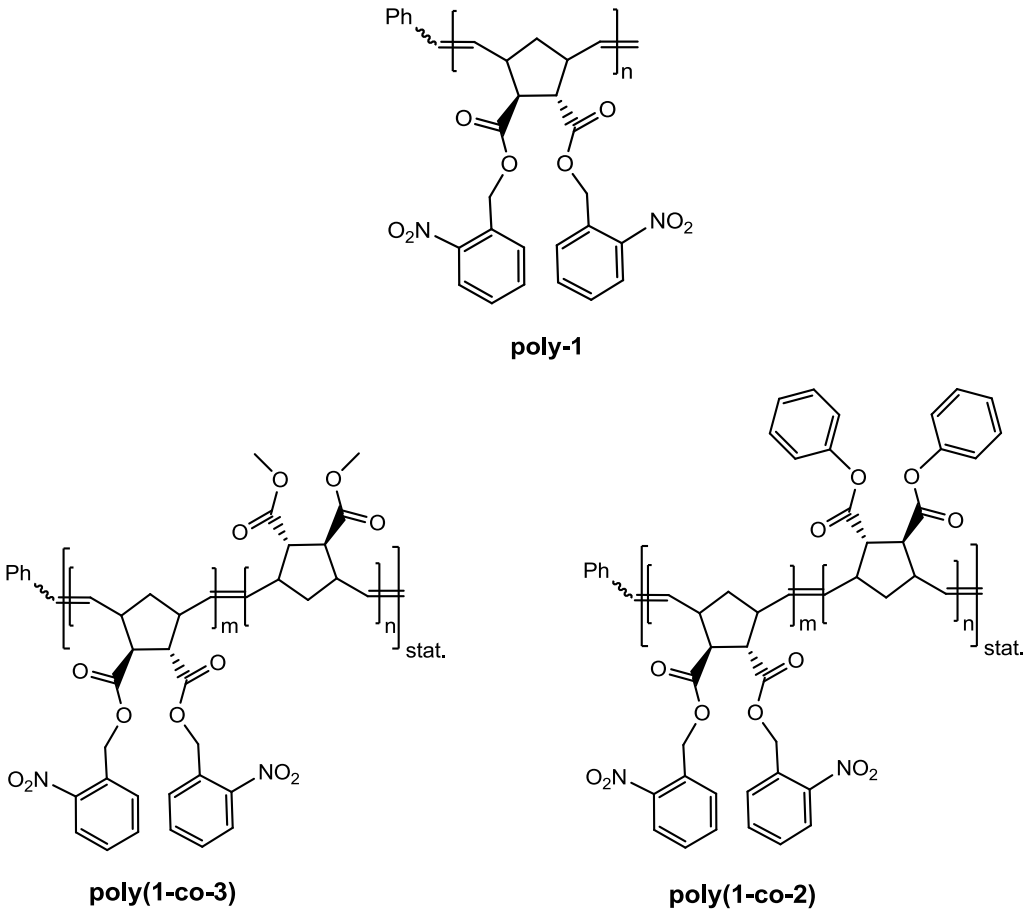

Figure 3.4: Overview of the photoreactive polymers synthesized

For the subsequent synthesis of the photosensitive polymers, two different polymerization initiators, Grubbs 1st generation (G-1) and 3rd generation Grubbs-type (G-3) catalysts were used.[101] Both catalysts are depicted in Figure 3.5. The synthesis of the G-3 was performed by adding (H_2IMes)-$(PCy_3)(Cl)_2Ru$=CHPh (Grubbs 2nd generation catalyst) to a solution of pyridine in toluene.

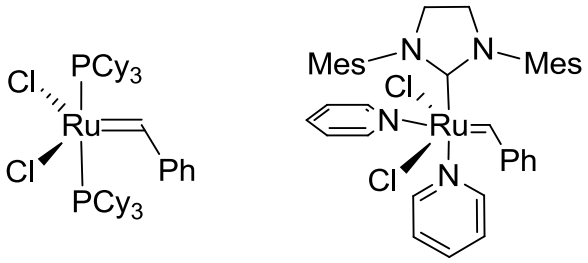

G-1 **G-3**

Figure 3.5: Representation of Grubbs 1st (G-1) and Grubbs-type 3rd (G-3) generation catalyst

3.1.2.1 SYNTHESIS OF POLY(ENDO,EXO-DI(2-NITROBENZYL) BICYCLO[2.2.1] HEPT-5-ENE-2,3-DICARBOXYLATE) (POLY-1)

Poly-1 was obtained by the polymerization of M-1 using G-3 catalyst (s. Figure 3.6). The simple ring opening metathesis polymerization proceeded in high yields. Using a ratio catalyst-monomer (1:120) a narrow molecular weight distribution with a PDI of 1.04 was achieved. The glass transition temperature measured amounted to 58 °C.

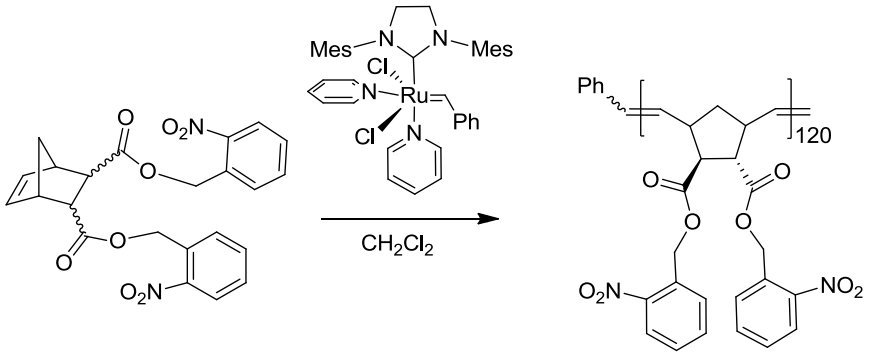

poly-1

Figure 3.6: Polymerization route of poly(endo,exo-di(2-nitrobenzyl) bicyclo[2.2.1]hept-5-ene-2,3-dicarboxylate)

3.1.2.2 SYNTHESIS OF POLY(ENDO,EXO-DI(2-NITROBENZYL) BICYCLO[2.2.1] HEPT-5-ENE-2,3-DICARBOXYLATE-CO- ENDO,EXO-DIMETHYL BICYCLO[2.2.1]HEPT-5-ENE-2,3-DICARBOXYLATE) (POLY(1-CO-3))

This statistical copolymer also was synthesized in high yields by using Grubbs-type 3rd generation catalyst (G-3). Here, ROMP also resulted in a narrow weight distribution and a PDI of 1.05. The ratio of catalyst-monomer amounted to 1:120.

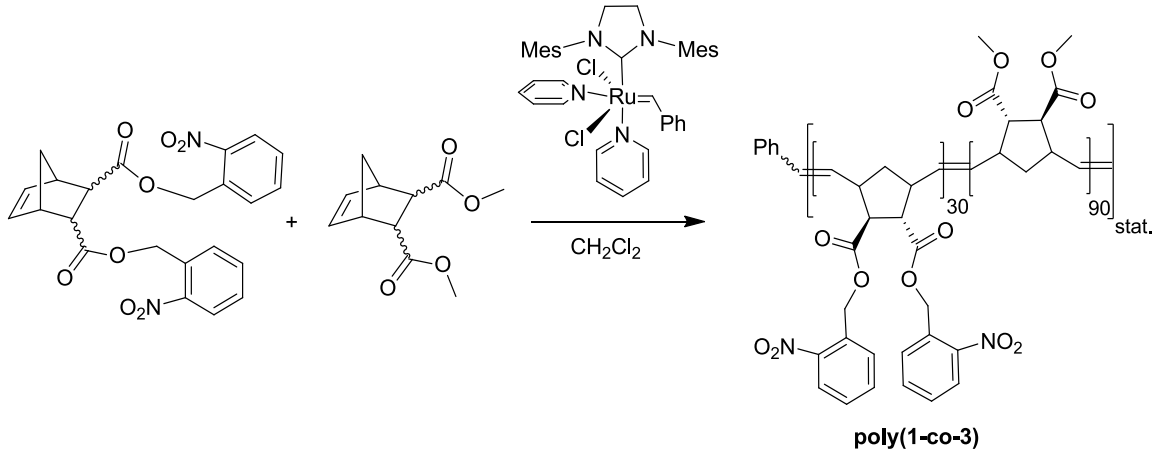

Figure 3.7: Polymerization route of poly(endo,exo-di(2-nitrobenzyl) bicyclo[2.2.1] hept-5-ene-2,3-dicarboxylate-co-endo,exo-dimethyl bicyclo[2.2.1]hept-5-ene-2,3-dicarboxylate) (poly(1-co-3))

3.1.2.3 SYNTHESIS OF POLY(ENDO,EXO-DI(2-NITROBENZYL) BICYCLO[2.2.1] HEPT-5-ENE-2,3-DICARBOXYLATE-CO- ENDO,EXO-DIPHENYL BICYCLO[2.2.1]HEPT-5-ENE-2,3-DICARBOXYLATE) (POLY(1-CO-2))

The polymerization of poly(1-co-2) was performed by adding G-1 or G-3 catalyst. The ratio (catalyst:monomer, 1:120) resulted in a PDI of 1.08.

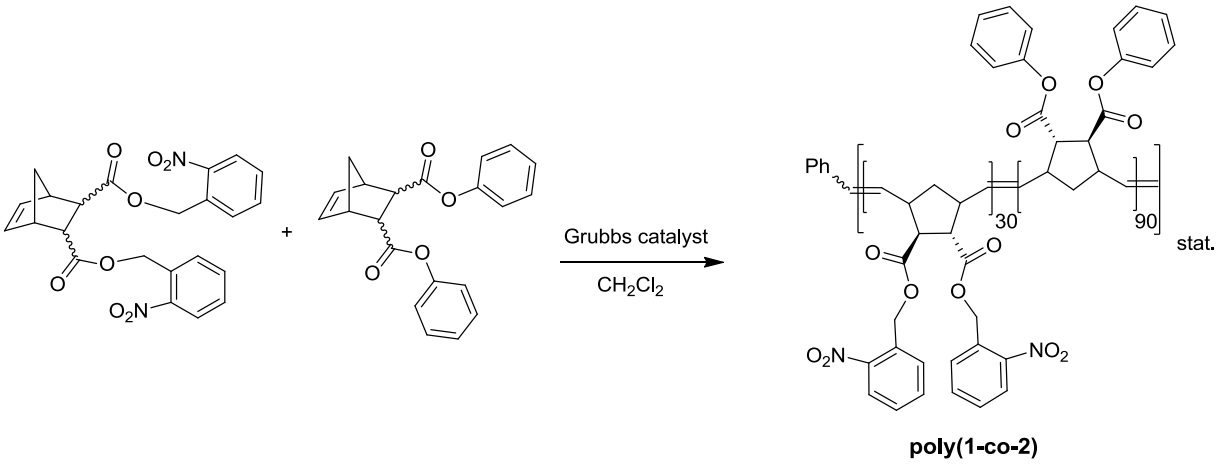

Figure 3.8: Polymerization route of poly(endo,exo-di(2-nitrobenzyl) bicyclo[2.2.1] hept-5-ene-2,3-dicarboxylate-co-endo,exo-diphenyl bicyclo[2.2.1]hept-5-ene-2,3-dicarboxylate) (poly(1-co-2))

In conclusion, the ROM polymerizations proceeded in high yields. The glass transition temperatures (T_g) of the polymers poly(1-co-2) and poly(1-co-3) were well above room temperature (poly(1-co-2) 80 °C and poly(1-co-3) 71 °C). All polymers showed excellent film forming properties when spin-cast from tetrahydrofurane solutions. Fully transparent and colourless optical films were obtained from all three polymers.

3.1.3 PHOTOREACTION OF THE POLYMERS

The formation of the carboxylic acid upon the irradiation of 2-nitrobenzyl esters is generally understood as intra- rather than intermolecular rearrangement process.[102,103] Detailed information is provided in chapter 2.2.1.2. The investigation of the photo-Fries reaction and the application of the photoinduced rearrangement for preparative synthetic chemistry has been shown by Bellus and Hrdlovic.[104] For instance, polymeric phenyl esters such as poly(4-acetoxystyrene) and poly(4-formyloxystyrene)[105] have been investigated as positive resist materials for photolithography.

In contrast to the investigation of photoreactive low molecular compounds in solution, the characterization of photoreactive units upon irradiation with UV-light in polymeric matrices is even more challenging. Reasons are concurrent photocrosslinking and photoscission of the polymeric material, which only allow a simple measurement of the photoreactive changes when spincast as a thin film on a suitable substrate, e.g. CaF_2, KBr etc. Thus, an easy determination of the photoreaction and quantitative conversion of the photosensitive moieties, when exposed to UV-light is accomplished. Spectroscopic methods such as FTIR and UV-Vis spectroscopy enable a simple characterization.

3.1.3.1 POLY(ENDO,EXO-DI(2-NITROBENZYL) BICYCLO[2.2.1] HEPT-5-ENE-2,3-DICARBOXYLATE) (POLY-1)

Upon irradiation with UV-light (>300 nm) the functional o-nitrobenzylester groups cleavage and carboxylic acid groups are formed. As side product o-nitrosobenzylaldehyde is produced.

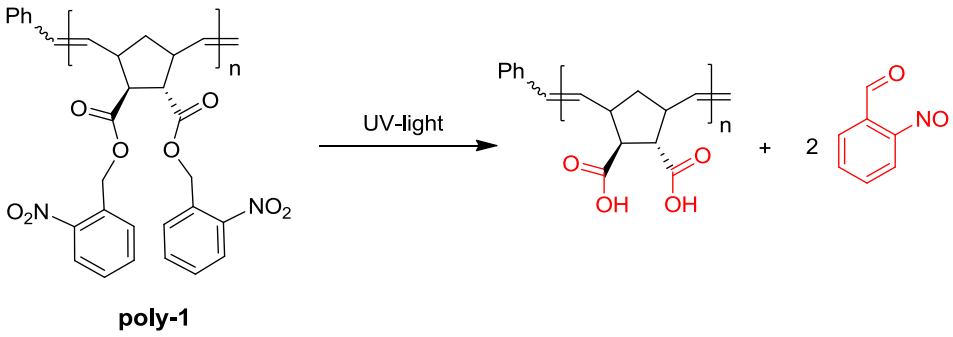

Figure 3.9: Photoreaction of poly-1 resulting in the formation of carboxylic acid groups

3.1.3.1.1 INVESTIGATION OF THE PHOTOREACTION BY MEANS OF UV-VIS SPECTROSCOPY

In Figure 3.10 the UV-Vis spectra of a film of poly-1 prior to and after flood UV-illumination (E= 19.8 J cm^{-2}, λ> 300 nm) under nitrogen atmosphere is presented. It is shown that poly-1 absorbs UV-light up to a wavelength λ~ 320 nm (peak maximum at λ~ 270 nm). The UV absorption behaviour in this range of the spectrum can be attributed to aryl chromophores with their π- π* transitions.

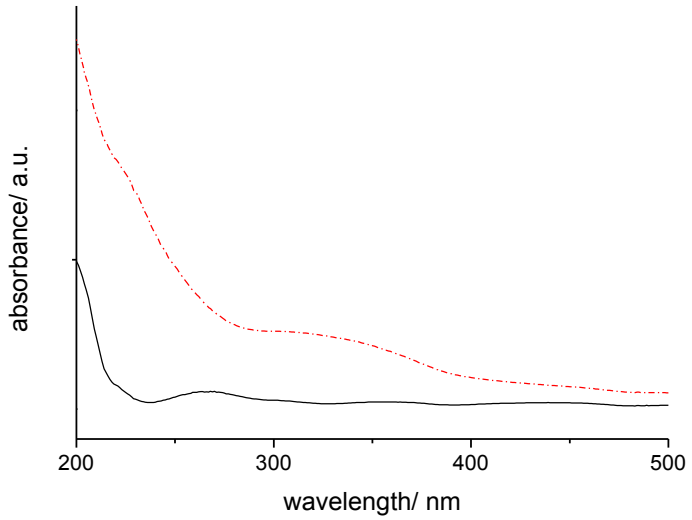

Figure 3.10: UV-Vis spectra of a film of poly-1 on CaF_2. prior to (solid black line) and after (dotted red line) UV-illumination (E= 19.8 J cm^{-2}, λ> 300 nm)

Prior to flood illumination the ester C=O groups itself absorb around 190 nm (π- π*) and with extremely low absorbance near 270 nm (n- π*). After flood UV-illumination performed under nitrogen atmosphere with an energy density E= 19.8 J cm^{-2} a bathochromic shift of absorption (>300 nm) based on the UV-induced generation of nitroso moieties and the subsequent formation of azobenzenes could be detected. These behavior was assigned to the π- π* and n- π* orbital transitions, respectively. The formation of azobenzenes led to a discoloration of the polymeric film from transparent to a yellow brownish shade.[28]

3.1.3.1.2 INVESTIGATION OF THE PHOTOREACTION BY MEANS OF FTIR SPECTROSCOPY

Since UV-Vis spectroscopy provides only limited information on the photoproducts in the polymers, silmultaneously, FTIR spectra of the polymers were recorded.

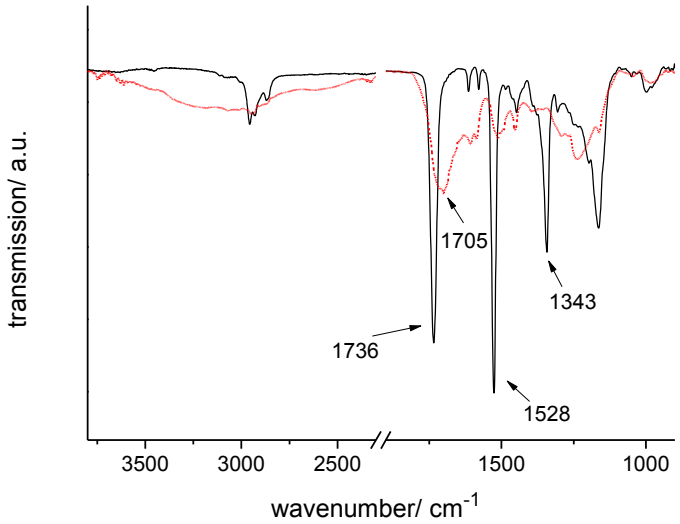

Figure 3.11: FTIR spectra of a film of poly-1 prior to (black solid line) and after irradiation (red dotted line) with an energy E= 19.8 J cm^{-2} (λ> 300 nm)

The FTIR spectra of a transparent film of poly-1 before illumination revealed strong signals at 1736 cm^{-1} (C=O stretch) and at 1165 cm^{-1} (asym. C-O-C stretch) that were attributed to the ester units. The strong signals at 1528 cm^{-1} and 1343 cm^{-1} are typical signals characterizing the nitro group. Exposure to UV-light formed a broad band emerging at 3400 cm^{-1} (OH stretching vibration of hydroxyl groups.) The signals of the ester group and the nitro group almost disappeared and new signals at 1705 cm^{-1} and 1239 cm^{-1} are characterizing the formed carboxylic acid group. Low absorption peaks at >1740 cm^{-1} and 1502 cm^{-1} indicated the minor formation of nitrosobenzaldehyde as side product.

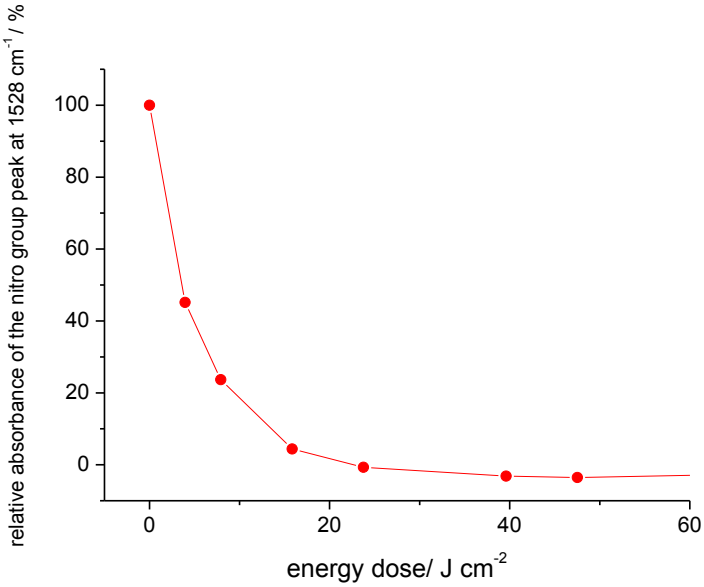

Figure 3.12: FTIR spectra of a film of poly-1 on CaF_2 after prolonged UV-irradiation times: Spectra were taken after irradiation with energy densities E= 0, 4.0, 8.0, 15.8, 23.7, 40.0, 47.6, J cm^{-2} (λ> 300 nm)

Furthermore, kinetic studies investigating the conversion of the functional groups have been performed. As a consequence of the overlap of the decreasing ester peak and the peak arisen at 1705 cm^{-1}, which can be assigned to the formation of the carboxylic acid the conversion of the first nitro group (representative signal at 1528 cm^{-1}) was used for kinetic investigation. In Figure 3.12 all spectra achieved after prolonged irradiation times are depicted. The collected FTIR data prove that the photoconversion proceeds in a 1st order exponential decrease.

In addition, UV-irradiation achieved a significant change in chemical reactivity. The enhancement was caused by the formation of aromatic photogenerated carboxylic acids. By combination of photolithographic techniques and selective immobilization, patterned functionalized surfaces could be obtained. In this thesis the illustration of selective post illumination reaction was demonstrated by using methylene blue.

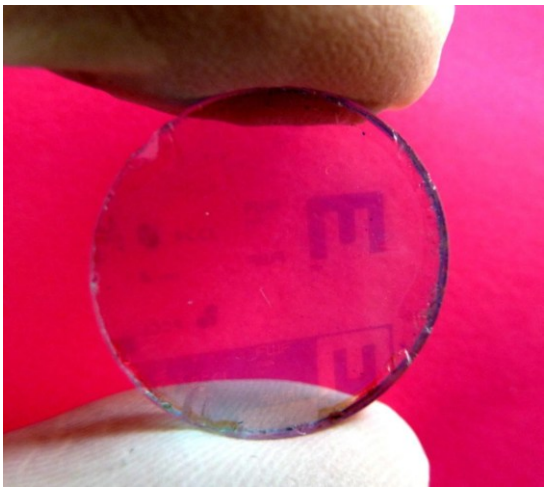

Figure 3.13: Depiction of a patterned film of poly-1: The pattern was visualized using methylene blue as derivatization reagent

A structured illumination was achieved by the application of a mask aligner (MJB4, Suess). Thus, a pattern even in the one-digit micron range could be accomplished. For visualization Figure 3.13 depicts a structured illuminated polymeric film subsequently derivatized with methylene blue.

3.1.3.2 POLY(ENDO,EXO-DI(2-NITROBENZYL) BICYCLO[2.2.1] HEPT-5-ENE-2,3-DICARBOXYLATE-CO- ENDO,EXO-DIMETHYL BICYCLO [2.2.1] HEPT-5-ENE-2,3-DICARBOXYLATE) (POLY(1-CO-3))

With the application of poly(1-co-3) similar results were obtained by FTIR and UV-Vis investigation. Both characterization methods again show the photoreactive cleavage of the ester group accompanied with the formation of the carboxylic acid groups. The residual methyl ester groups of the non-photoreactive norbornene methyl ester units remained unaffected during exposure to UV-light.

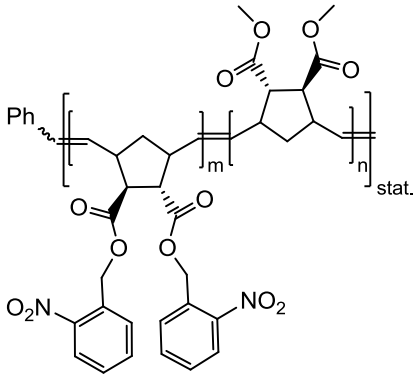

poly(1-co-3)

Figure 3.14: Structural representation of poly(1-co-3)

3.1.3.2.1 INVESTIGATION OF THE PHOTOREACTION BY MEANS OF UV-VIS SPECTROSCOPY

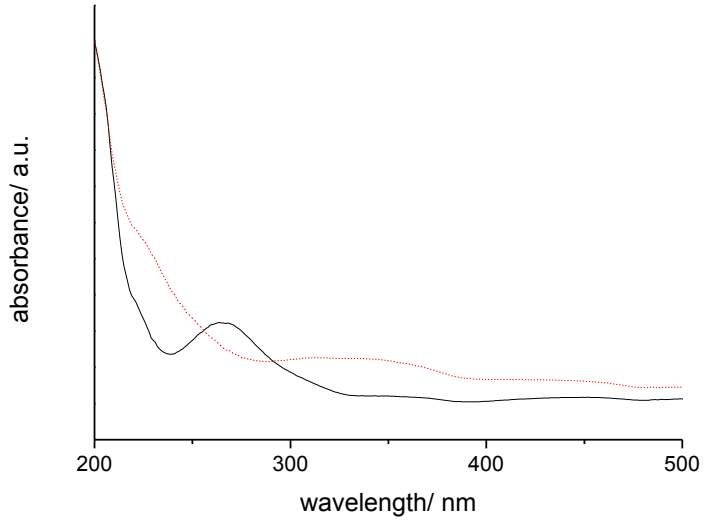

Figure 3.15: UV-Vis spectra of a film of poly(1-co-3) on CaF_2. Solid black line: prior to irradiation. Dotted red line: after UV-irradiation (E= 19.8 J cm^{-2}, λ> 300 nm)

The UV-Vis measurements performed prior to and after flood UV-illumination (E= 19.8 J cm^{-2}, λ> 300 nm) under nitrogen atmosphere revealed that poly(1-co-3) absorbs UV-light up to a wavelength λ~ 320 nm (peak maximum at λ~ 270 nm). The absorption peak in this range of the spectrum (s. Figure 3.15) is attributed to aryl chromophores with its π- π* transitions and the (n- π*) transitions caused by the C=O of the ester group. Strong absorbance was assigned to the C=O ester transition at 200 nm (π- π*). After flood UV-illumination performed under nitrogen atmosphere with an energy density E= 27 J cm^{-2} again a bathochromic shift of absorption (>300 nm) based on one hand on the UV induced generation of nitroso moieties as well as on the subsequent formation of azobenzenes was detected. These absorptions are assigned to π- π* and n- π* orbital transitions.

3.1.3.2.2 Investigation of the photoreaction by means of FTIR Spectroscopy

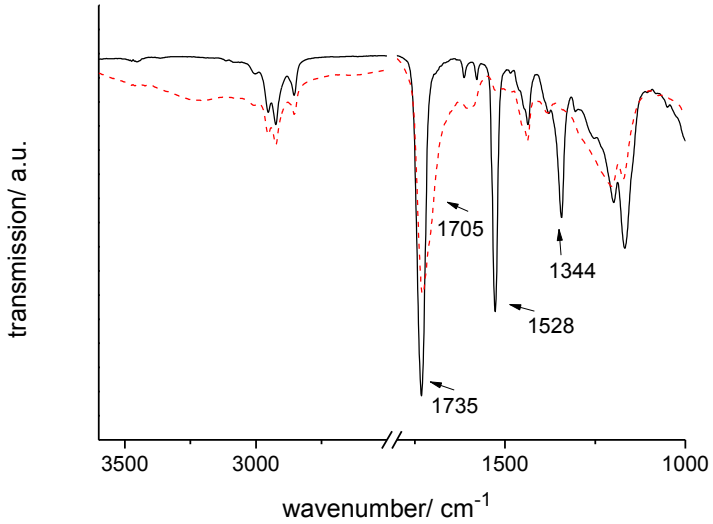

Figure 3.16: FTIR spectra a film of poly(1-co-3): prior to irradiation (solid black line); Dotted red line: after UV-irradiation (E= 19.8 J cm^{-2}, λ> 300 nm)

The FTIR spectra of a transparent film of poly(1-co-3) showed significant differences prior to and after polychromatic irradiation (s. Figure 3.16). The spectrum of the non-irradiated film revealed strong signals at 1735 cm^{-1} (C=O stretch) and at 1170 cm^{-1} (asym. C-O-C stretch) that are representative for the ester units. The strong signals at 1528 cm^{-1} and 1344 cm^{-1} are typical of the nitro group.

UV-irradiation induced significant changes observable in the FTIR spectrum of poly(1-co-3). The broad band emerging at 3400 cm^{-1} stems from the OH stretching vibration of hydroxyl groups. The signals of the ester group and the nitro group almost disappeared. New signal emerged at 1704 cm^{-1} and 1239 cm^{-1} representative for the formed carboxylic acid group. Furthermore, low absorption peaks at >1740 cm^{-1} and 1502 cm^{-1} indicated the minor formation of nitrosobenzaldehyde as side product.

3.1.3.3 POLY(ENDO,EXO-DI(2-NITROBENZYL) BICYCLO[2.2.1] HEPT-5-ENE-2,3-DICARBOXYLATE-CO- ENDO,EXO-DIPHENYL BICYCLO[2.2.1]HEPT-5-ENE-2,3-DICARBOXYLATE) (POLY(1-CO-2))

O-nitrobenzyl ester as well as phenyl ester chromophores are photoreactive moieties that undergo defined reactions upon exposure to UV-light. Both photoreactions are capable to form functional groups as photoproduct and to tune both surface and material properties by means of UV-irradiation. By combination of the o-nitrobenzyl ester and the phenyl ester moieties as realized in the statistical copolymer poly(1-co-2) the generation of two different functional groups can be accomplished by the choice of the UV-wavelength. The crucial parameter is the difference in absorption. As depicted in Figure 3.17 the UV-Vis spectrum of homopolymer poly-1 reveals a distinctive absorption well into the wavelength range of 300 and more nanometers. In contrast the homopolymer equipped with phenyl ester (p-1, poly(endo,exo-diphenyl bicyclo[2.2.1]hept-5-ene-2,3-dicarboxylate), s. chapter 2.2.2) moieties solely shows absorption up to 280 nm.

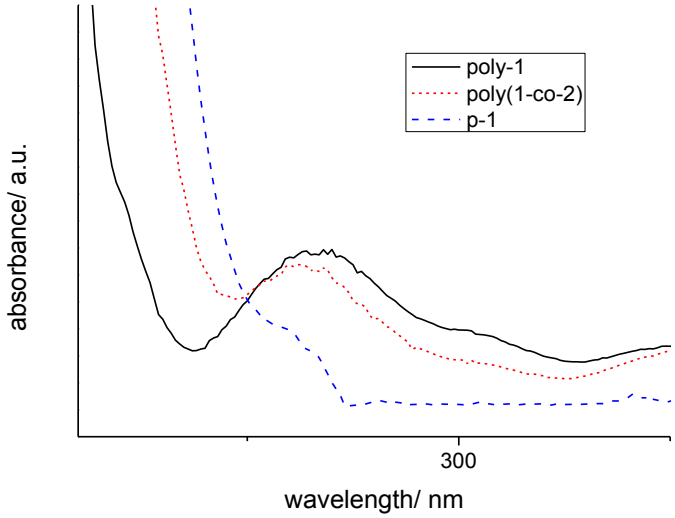

Figure 3.17: UV-Vis absorbance of poly-1, poly(1-co-2) and the photo-Fries polymer poly(endo,exo-diphenyl bicyclo[2.2.1]hept-5-ene-2,3-dicarboxylate) (p-1)

Thus, using UV-light of 300 nm and higher wavelength, only the o-nitrobenzyl ester units are expected to react selectively while in a second illumination step with monochromatic UV-light (254 nm) the formation of hydroxyketones can be induced. In the reaction scheme (s.

Figure 3.18) the two step illumination is displayed. The first step involves the photoinduced formation of the carboxylic acid units via selective illumination (>300 nm). A second irradiation (254 nm) step then generates ortho-hydroxyketones (photo-Fries rearrangement). Hence, two functional groups are formed and the versatility with respect to the tuning of both surface and material properties by means of UV-irradiation is significantly enhanced.

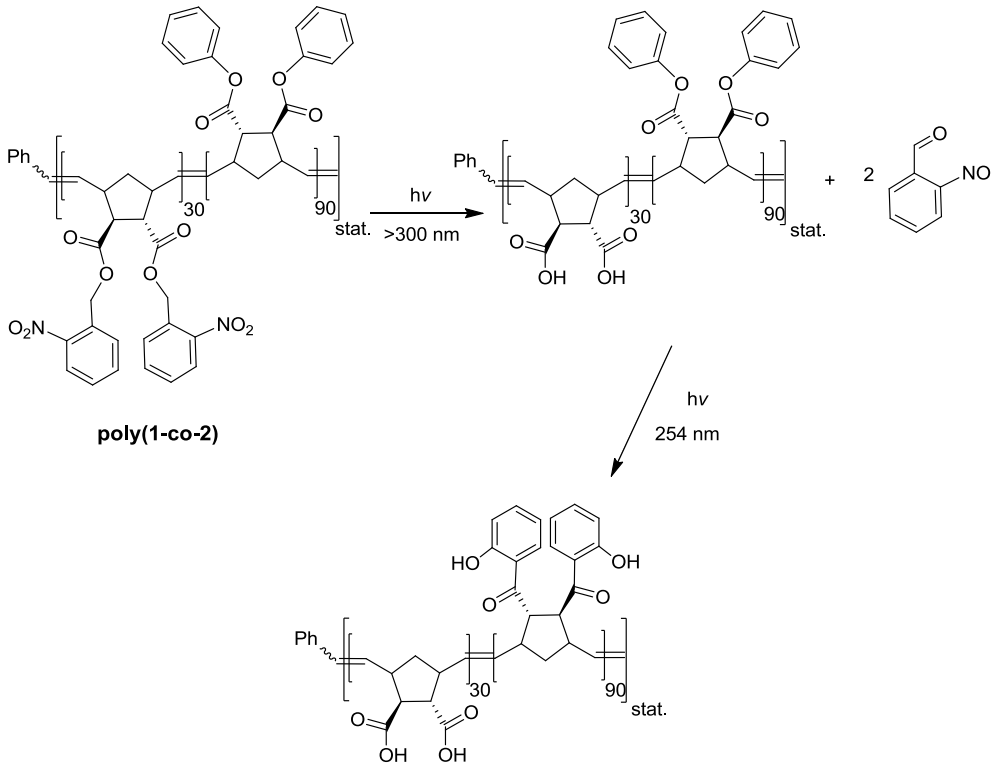

Figure 3.18: O-nitrobenzyl ester cleavage and photo-Fries rearrangement induced by wavelength-selective exposure to UV-light in poly(1-co-2)

3.1.3.3.1 Investigation of the photoreaction by means of UV-Vis spectroscopy

In Figure 3.19 the changes in absorption induced by exposure to UV-light are presented. The ester C=O group of the non-illuminated polymer (poly(1-co-2) absorbed at around 190 nm (π-π*) and with a peak maximum near 270 nm (n-π*). Polychromatic irradiation (>300 nm, J cm^{-2}) led to the UV-induced cleavage of the carboxylic acid groups and the subsequent generation of nitroso moieties accompanied by the formation of azobenzenes. Again a shift to higher wavelengths was observed. A further illumination with monochromatic light (254 nm, energy density E= 0.85 J cm^{-2}) caused the formation of two new absorbance maxima at

λ~ 260 nm and λ~ 330 nm, which revealed the generation of aromatic hydroxyketone units.[33,34]

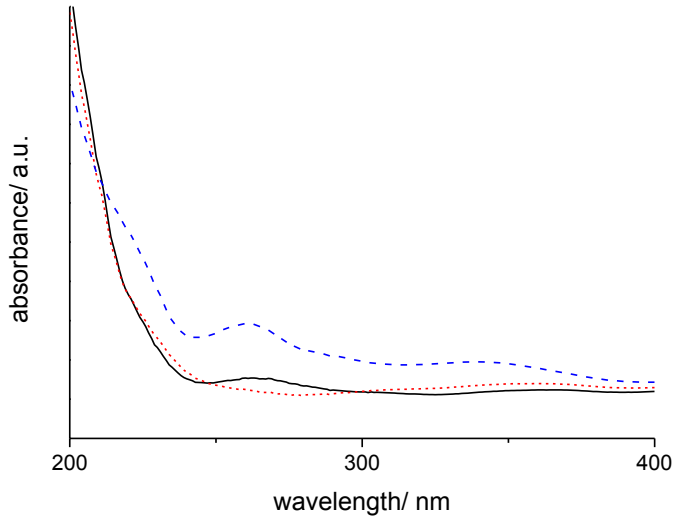

Figure 3.19: UV-Vis spectra of a film of poly(1-co-2) on CaF_2. Solid black line: prior to irradiation; Dotted red line: after UV-irradiation (E= 23.2 J cm^{-2}, λ> 300 nm); Dashed blue line: after second irradiation step (E= 0.854 J cm^{-2}, λ= 254 nm)

3.1.3.3.2 Investigation of the photoreaction by means of FTIR spectroscopy

The FTIR spectra (s. Figure 3.20) displays the depletion of the ester peaks at 1750 cm^{-1} (C=O stretch), respectively the loss of the nitro signals at 1528 cm^{-1} and 1343 cm^{-1} as a consequence of the first polychromatic illumination step performed. New signals emerged at 1705 cm^{-1} characterizing the formed carboxylic acid groups. The second illumination step (254 nm) was accompanied by the formation of bands at 3400 cm^{-1} for the O-H stretching of the hydroxyl group and 1631 cm^{-1}, which could be attributed to the formation of an ortho-hydroxyketone. Furthermore, a weak signal emerged at 1670 cm^{-1}. This signal described the formation of para-hydroxyketone groups. The spectrum of the signals at 1750 cm^{-1} (C=O stretch) and at 1164 cm^{-1} (asym. C-O-C stretch) were typical of the ester R_1-(C=O)-O-R_2 units with R_1 being an aliphatic moiety and R_2 being a phenyl ring.[106] Another band in this FTIR spectrum at 1509 cm^{-1} is related to the aromatic ring vibration.

The significant decrease of the ester peak (1750 cm^{-1}) observed is attributed to the conversion of the remaining phenyl ester moieties. These results are in good accordance with data obtained by literature.[107,108]

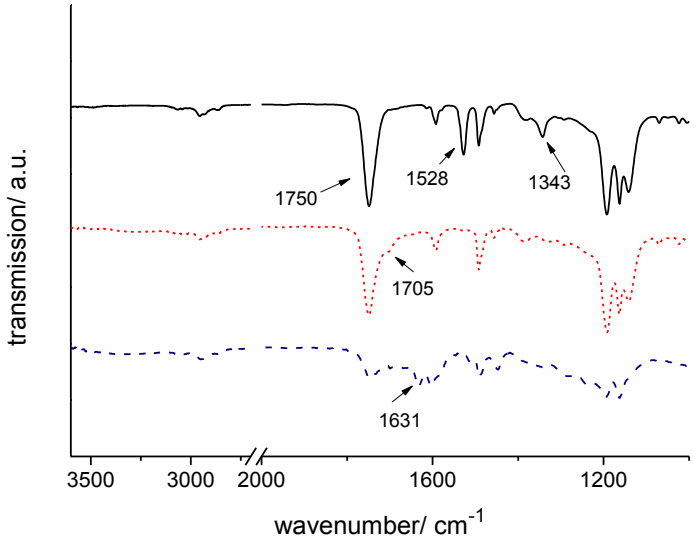

Figure 3.20: Comparison of FTIR spectra of poly(1-co-2) obtained by different illumination steps: Solid black line: prior to irradiation; Dotted red line: after UV-irradiation (E= 19.8 J cm^{-2}, λ> 300 nm); Dashed blue line: after 2nd illumination step (E= 0.85 J cm^{-2}, λ= 254 nm)

Furthermore, the yield of hydroxyketone was determined using the intensity of the ketone carbonyl signal in the range of 1631 cm^{-1}. Therefore, the infrared absorbance coefficients of hydroxy acetophenone and phenyl acetate were applied. The ketone unit in 2-hydroxy acetophenone (1631 cm^{-1}) absorbs with A_{1631}= 345 L mol^{-1} cm^{-1} and the absorption coefficient of phenyl acetate amounts to be A_{1750}= 420 L mol^{-1} cm^{-1} at 1750 cm^{-1}.[90] The ratio of the absorbance coefficients (ester:ketone) was figured out to be 1.2:1.0. This fact was considered to be sufficient for a rough comparison of the photoproducts and for the determination of the yield of o-hydroxyketones formed. Thus, as depicted in Figure 3.21 the amount of o-hydroxyketones formed was estimated to 30 %.

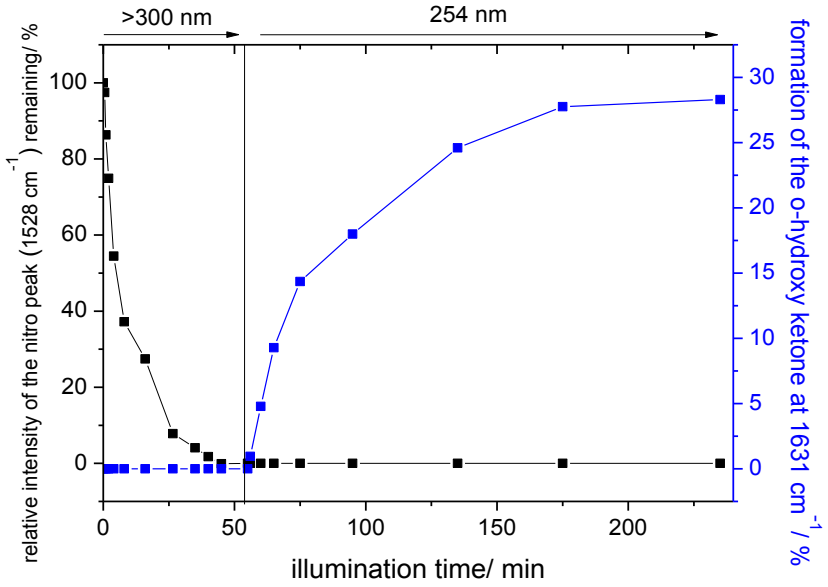

Figure 3.21: Decrease of the nitro peak and formation of the o-hydroxyketone signal dependent on the two step irradiation (1st step λ> 300 nm and 2nd step λ= 254 nm)

3.1.4 REFRACTIVE INDEX MODULATION IN POLY-1 AND POLY(1-CO-2)

The modulation of the refractive index via photo-Fries rearrangement going along with the possibility of adjusting the refractive index depending on the rate of photoconversion has been reported in literature.[35] Furthermore, Griesser et al.[3] have shown that the photoinduced formation of carboxylic acid groups in photo-Fries polymers results in a large decrease of the refractive index by approximately Δn_{589}= -0.043. Therefore, the functional o-nitrobenzyl ester moieties seem to be a promising candidate for obtaining a significant change in the refractive index.

The photoreactions, as well as the changes in refractive index upon irradiation, were investigated for thin films of both polymers (poly-1, poly(1-co-2)). The difference in light absorption of the o-nitrobenzyl ester group and the phenyl ester allows the selective excitation and the formation of the carboxylic acid using UV-light >300 nm whilst both reactions undergo changes via illumination with 254 nm. In Figure 3.22 the patterning of the refractive index in the polymeric film of poly-1 is illustrated.

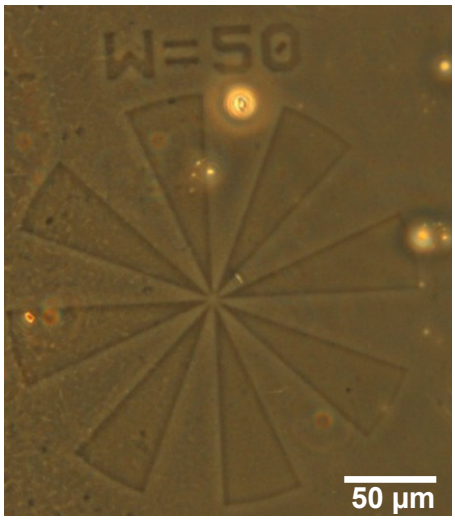

Figure 3.22: Phase contrast image of a film of poly-1 after UV-patterning with a mask aligner, (MJB4 from SUSS) using a 500 W HgXe lamp equipped with a filter for the range 270–353 nm

In Figure 3.23 the Cauchy fits of the dispersion of the refractive index of poly-1 before and after illumination with UV-light of >300 nm are depicted. After the irradiation process the refractive index at 589 nm changed from n_{589}= 1.570 to n_{589}= 1.523 (Δn_{589}= -0.047) at an energy dose of (E= 15.8 J cm^{-2}).

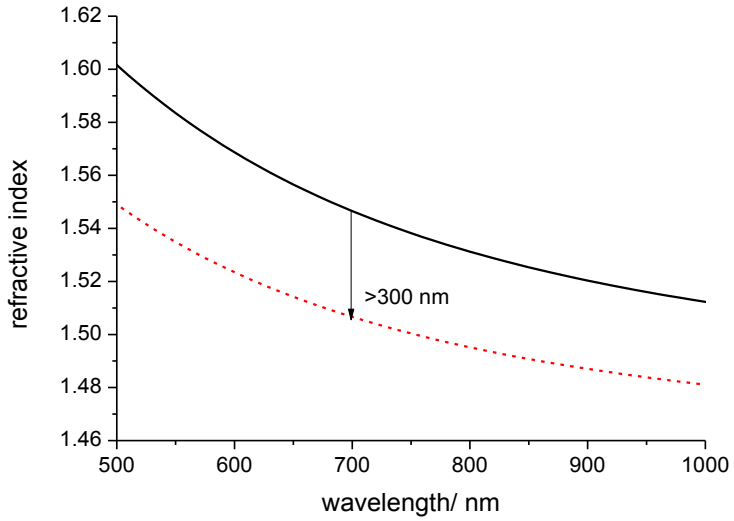

Figure 3.23: Cauchy fit of the dispersion of the refractive index of poly-1 before (black solid line) and after (red dotted line) illumination with UV-light of >300 nm (E= 18.2 J cm^{-2})

When poly(1-co-2) was irradiated in a first illumination step with wavelengths >300 nm (E= 15.8 J cm^{-2}), again a decrease of the refractive index was observable (Δn_{589}= 0.017). The second illumination step (>254 nm) achieved a change of Δn_{589}= +0.031.

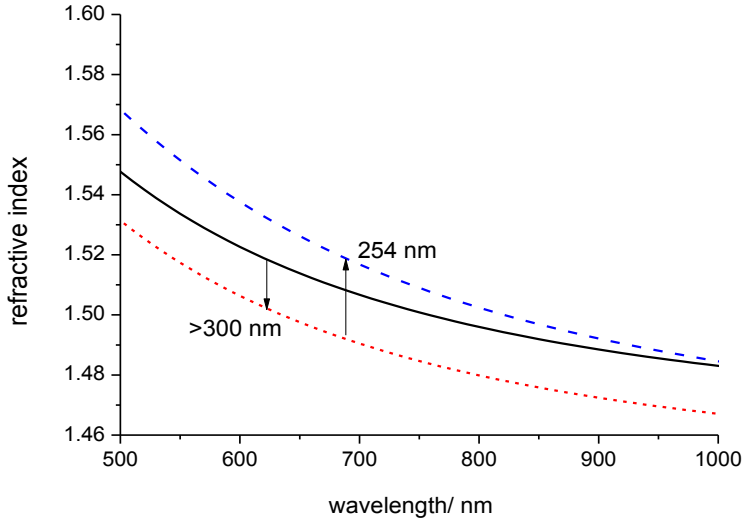

Figure 3.24: Cauchy fit of the dispersion of the refractive index of poly(1-co-2) before (black solid line); after the 1st illumination step (red dotted line) with UV-light of >300 nm (E= 18.2 J cm^{-2}); after 2nd illumination step (blue dashed line) using UV-light of 254 nm (E= 4.1 J cm^{-2})

Both polymers were illuminated to the maximum of photoconversion. Shorter irradiation times may result in lower index changes. Generally, the type and the amount of photoproducts determine the refractive index change in the illuminated polymer. Thus, the differences in the refractive index changes after illumination with different wavelengths could be explained by the cleavage of the o-nitrobenzyl ester group upon irradiation with UV-light of >300 nm as discussed above. Furthermore, the pronounced degradation of the ester groups using UV-light of 254 nm indicated that decarboxylation may be an important reaction that can be attributed to the change in the refractive index. As a consequence, the formation of the hydroxyketone accompanied by the photoinduced decarboxylation is responsible for the significant increase in the refractive index during the second illumination step.

Also photo-crosslinking, a generally observed side reaction or byproducts of the photo reactions have to be considered when evaluating the refractive index changes under UV-irradiation.

3.1.4.1 CONCLUSION

The o-nitrobenzyl ester groups in the new polymer poly-1 as well as o-nitrobenzyl ester and photo-Fries chromophores in poly(1-co-2) can both be excited by UV-light leading to a significant change in the refractive index of thin polymeric layers. While the selective excitation of the o-nitrobenzyl ester groups using wavelengths of >300 nm led to a decrease in the refractive index the irradiation of the copolymer poly(1-co-2) using a second illumination wavelength of 254 nm enabled an increase of the refractive index. In this case, the rise of the refractive index of Δn_{589}= 0.031 in copolymer poly(1-co-2) was based on the formation of the photo-Fries photoproduct. Thus, the choice of the irradiation wavelength and sequence allowed the modulation of the refractive index of the homopolymer and the copolymer in a wide range. This makes the UV-reactive material an interesting candidate for applications in optics. Moreover, the two step illumination procedure provides the possibility of erasing and even inverting the index contrast generated during the first illumination step.

3.1.5 APPLICATIONS OF PHOTOREACTIVE POLYMER LAYERS IN ORGANIC ELECTRONICS

3.1.5.1 TUNING THE CHARACTERISTICS OF ORGANIC THIN FILM TRANSISTORS (OTFTS)

Since the first publication of organic field effect transistors (OFETs) in 1986[109] the research area of organic field effect transistors has grown steadily. The advantages of low cost fabrication and large area coverage represent an interesting alternative to conventional inorganic semiconductors based on silicon technology. The field of potential application is manifold and OFETs are used as electrical switches, low cost sensors[110] and memory cards including radio frequency identification cards (RFIDs).[111,112] Organic thin film transistors (OTFTs), a special kind of OFETs, are three terminal devices. In Figure 3.25 the schematic view of a top contact OTFT is presented. The three electrodes are referred to as gate, source and drain electrode. Additionally, as gate dielectric (insulator) thermally grown SiOx on a highly doped silicon wafer (gate electrode) is applied. The organic semiconductor layer normally consists of highly conjugated small molecules or polymers such as pentacene[113], rubrene, poly(9,9-dioctylfluorene-co-bithiophene)[114], and poly(3-hexylthiophene) (P3HT).[115]

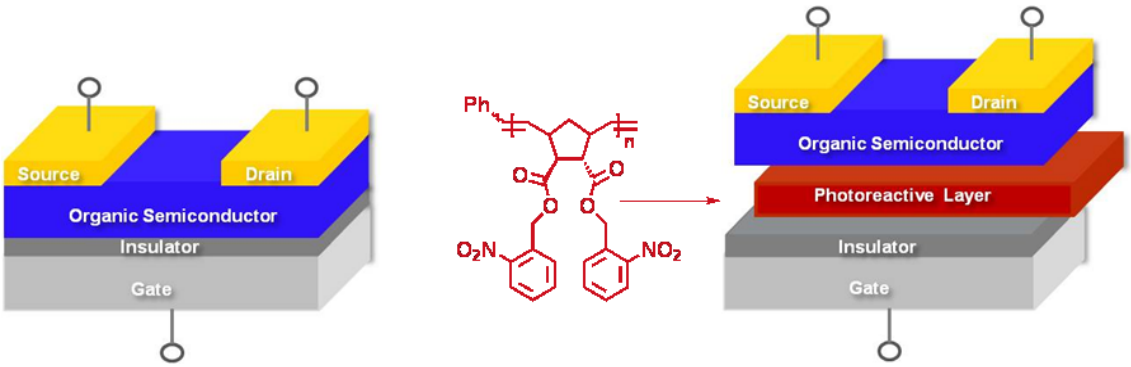

Figure 3.25: Set up of a standard OTFT and set up of an OTFT with additional photoreactive layer

Recent studies have shown that the performance of organic thin film transistors (OTFTs) is to a large extent governed by the properties of the interface between the organic semiconductor and the gate dielectric.[116] One commonly applied scheme for tuning those interface characteristics is the use of organo-silane based thin layers and self-assembled monolayers (SAMs)[5,6], covalently linked to the gate dielectric. A photoreactive interfacial layer is inserted between the gate dielectric and the organic semiconductor in the OTFT set up. In the following two approaches are shown how to control two of the most crucial device parameters- the charge carrier mobility (μ) and the threshold voltage (V_{Th}). The main goal for

most applications is the maximization of mobility[117], whereas the reproducible tuning of the threshold voltage (V_{Th}) over a broad range is desired, e.g. for inverter applications in integrated circuits.

3.1.5.2 PHOTOCHEMICAL CONTROL OF THE CARRIER MOBILITY IN PENTACENE-BASED ORGANIC THIN-FILM TRANSISTORS

In this study a thin layer of the photoreactive polymer poly(endo,exo-di(2-nitrobenzyl) bicyclo[2.2.1] hept-5-ene-2,3-dicarboxylate) (poly-1) was applied.[118] Due to the polar and protic acid groups the surface polarity increases dependent on the illumination time. To influence the growth of pentacene, a thin layer of poly-1 is spin cast on top of the SiO_2 gate dielectric. The chemical composition of the poly-1 surface can be tuned upon irradiation with UV-light. The photoreaction was investigated by FTIR spectroscopy. The signal of the ester group at 1744 cm^{-1} and the nitro peaks at 1526 cm^{-1} and 1343 cm^{-1} decreased significantly after 1200 s of illumination, whereas a new signal at 1706 cm^{-1} - attributed to the photogenerated carboxylic acid group - emerges. The photoconversion of the photoreactive layer leads to a change of surface energy from 47.4 mJ/m^2 to 42.0 mJ/m^2.

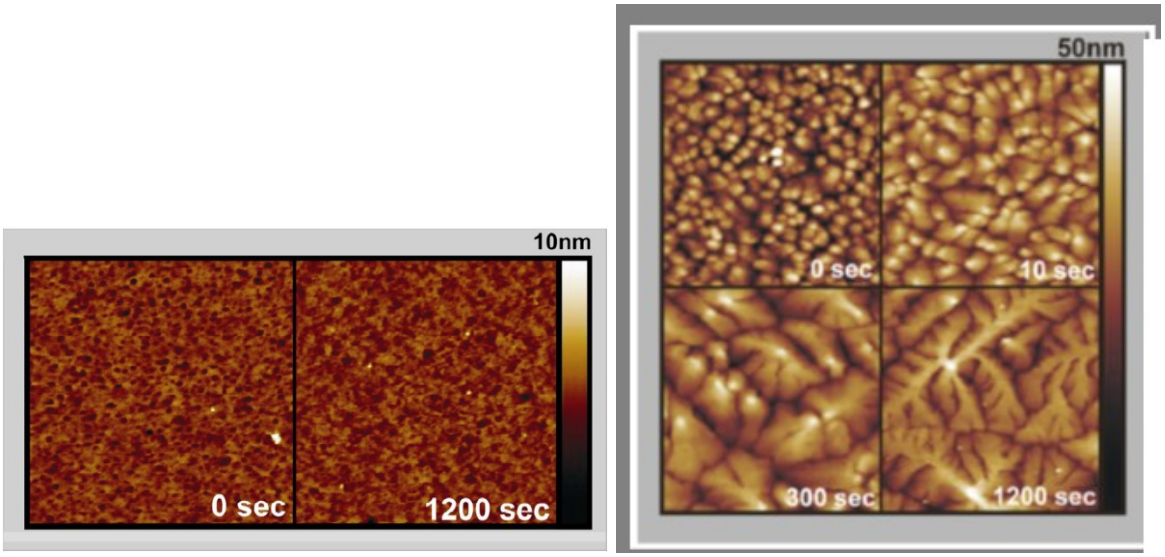

Figure 3.26 AFM image of the poly-1 layer prior to and after illumination (left); growth of the pentacene surface on poly-1 after different illumination times (right)[118]

In literature, the effect of the grain size in polycrystalline layers tuning the charge carrier mobility in OTFTs is still a controversial topic. The common definition in use complies that an

increase of charge carrier mobility scales with the grain size.[119,120] However, a few reports refer to the state that smaller grains result in higher mobilities.[121] A possible way to influence the morphology of pentacene is the application of a photoreactive substrate. The period the thin layer of poly-1 is exposed to UV-light is found to directly influence the morphology of the pentacene film grown on top of that layer.

In Figure 3.26 the AFM images of the grown pentacence crystals depending on the illumination time of the substrate (0 s, 10 s, 300 s, 1200 s) are presented. Pentacene growth on unexposed poly-1 caused high nucleation density with average grain sizes of 0.2 µm while after 1200 s of illumination dendritic growth occured. In addition, the morphology of the poly-1 layer was investigated. Therefore, AFM pictures of the poly-1 surface before and after illumination had been recorded. In Figure 3.26 the surface comparison of the non-illuminated, respectively of the irradiated layer (illumination time 1200 s) is depicted. No differences in morphology have been observed.

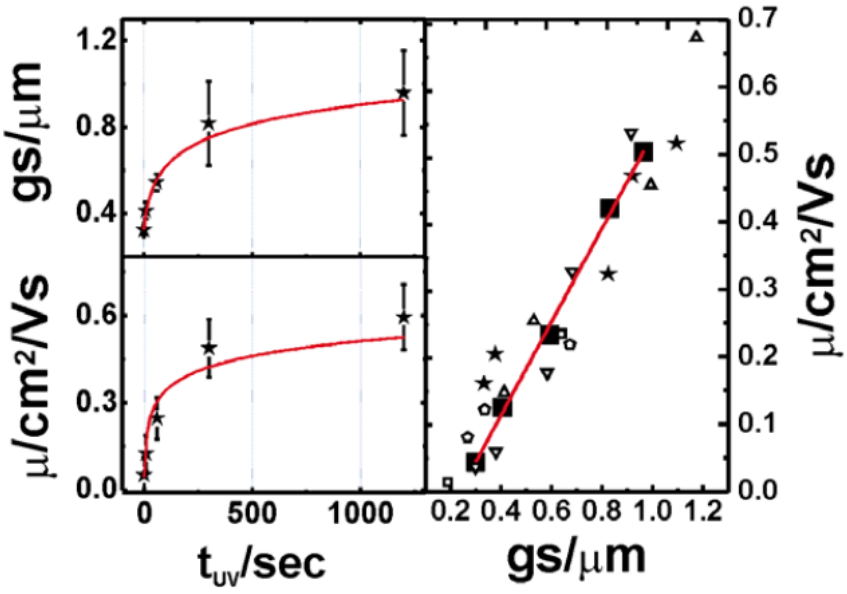

Figure 3.27: Top left: Average grain size as a function of illumination time. Bottom left: OTFT mobility as a function of illumination time. Right: OTFT mobility as a function of grain size. The large squares denote the average values for 0, 10, 60, 300, and 1200 s[118]

A linear relationship between the mobility and the grain size is observed, see Figure 3.27. The increase in the charge carrier mobility obtained in the OTFT by approximately one order of magnitude (from 0.06 to 0.7 cm^2 /Vs) is in accordance with literature reports on the linear relationship of the carrier mobility with grain size.[119] Therefore, influencing the morphology and the grain size, allows the control of the effective field effect mobility in OTFTs.

3.1.5.3 TUNING THE THRESHOLD VOLTAGE IN ORGANIC THIN-FILM TRANSISTORS BY LOCAL CHANNEL DOPING USING PHOTOREACTIVE INTERFACIAL LAYERS

Over the past years, a wide range of methods has been applied to tune threshold voltages, including the application of oxygen plasma[122] and UV-ozone treatments[123] to generate charged surface states at the dielectric semiconductor interface of an organic gate dielectric (parylene). V_{Th} is also shifted to more positive values by inserting a polarizable layer into the dielectric.[124] However, drawbacks including mechanisms and the operation with high "programming" voltages to tune V_{Th} are poorly understood. By insertion of self-assembled monolayers[113] or chemically reactive thin layers[22] local channel doping and dedoping processes using acid groups and bases are realized. A local patterning, important for the realization of integrated electronic circuits, is however, not obtainable. With the insertion of a thin poly-1 layer, acid groups are generated upon UV-irradiation and photochemical patterning is easily accomplished. In addition, the threshold voltage can be exactly controlled. The subsequent deprotonation of the acidic groups in the device due to the reaction with the organic semiconductor results in the formation of a space-charge region at the interface. A shift of V_{Th} is explained by the compensation of the formed conjugated bases by mobile holes. This has been shown by drift diffusion based modelling.[22]

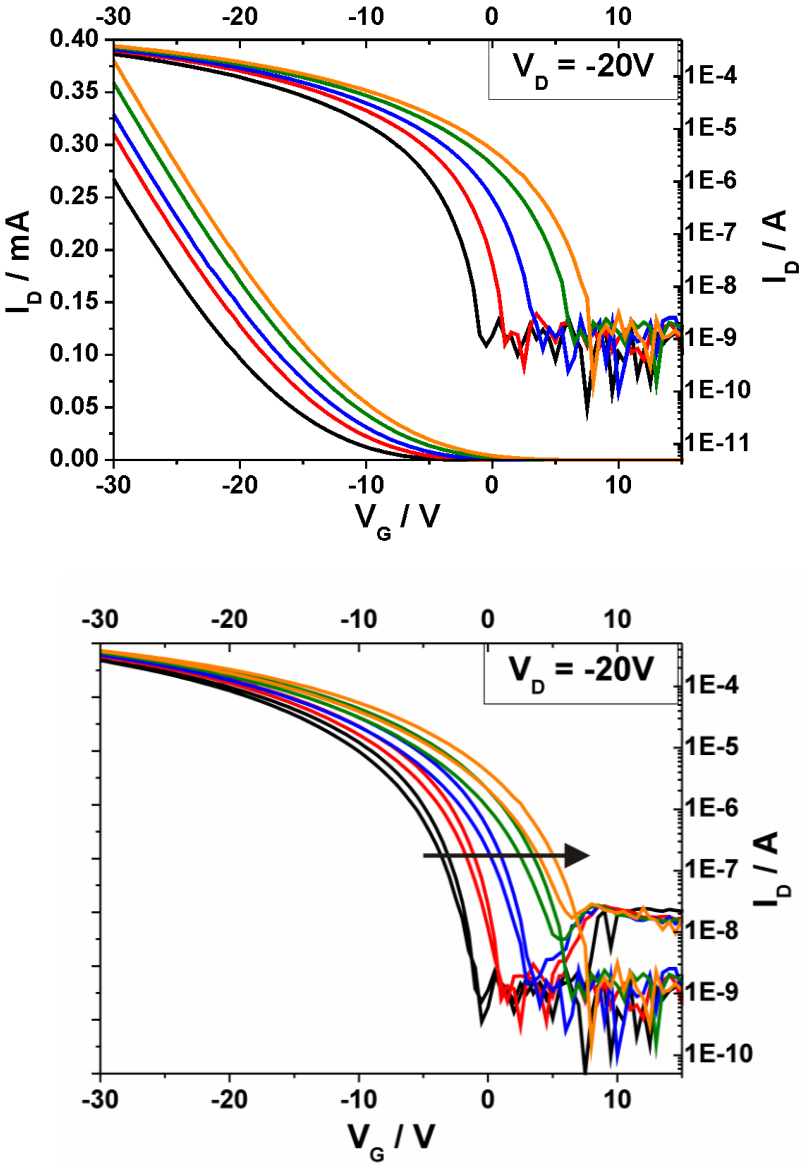

Figure 3.28: Transfer characteristics at V_D= -20 V of one series of pentacene/poly-1 OTFTs and output characteristics for a representative series of poly-1 OTFTs varying the illumination times. The arrow indicates an increase of illumination time.[125] Top: linear und logarithmic transfer characteristics without hysteresis; Bottom: logarithmic transfer characteristic with hysteresis

Figure 3.28 shows that the threshold voltage could be tuned by short time illumination. The shape of the curves is similar and during this short illumination the slopes and furthermore the mobility remains constant. Simultaneously, with an increased channel doping the drain current in the output characteristics rises and the hysteresis remains small (ΔV_G= 2 V at I_D= 0.10 mA).

Photolithographic patterns and interfacial doping processes enabled the local control of V_{Th} and thus, the possibility to define if a transistor works in depletion or enhancement mode.

Due to the application of photoreactive layers in a setup, integrated circuits such as depletion load inverters are easily fabricated. The setup of a depletion load inverter consists of an enhancement mode driven transistor and a depletion mode load transistor using only p-type OTFTs. The load transistor works in depletion mode and has a positive threshold voltage. The transistor is turned “on” due to the fact that it is already switched on at zero gate base bias. The switch TFT working in enhancement mode is normally an off transistor with a negative V_{Th}.

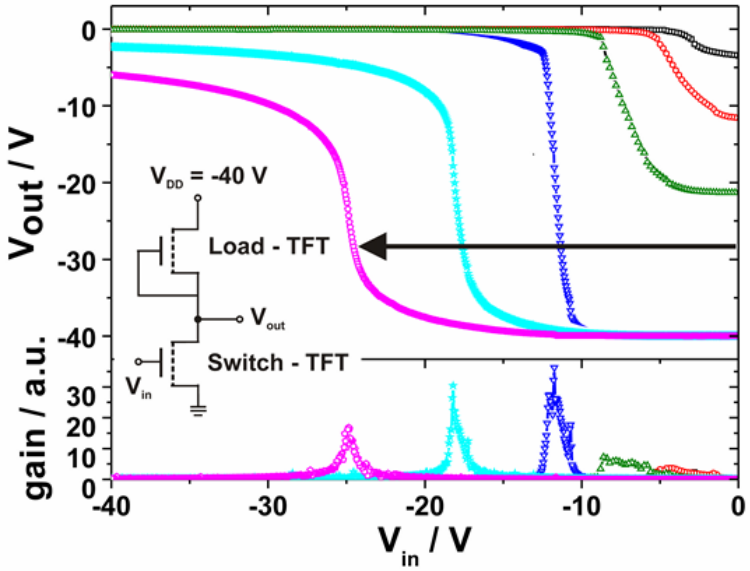

Figure 3.29: Inverter characteristics with short time illuminated load-TFTs (for 0,1,2,3,4 and 5 seconds); the trend for increasing illumination times is shown by the arrow; bottom: the corresponding gains of the inverters; inset: wiring diagram of a depletion-load inverter[125]

Both the switch and the load transistor in the inverter were equipped with a photoreactive layer. While the switch transistor remained non-illuminated, the load transistor was illuminated in 1 s steps. By increasing illumination time the load transistor shifted and the inverter characteristic improves significantly. After a 3 s illumination time a maximum gain of 40, based on the optimum value of V_{Th} with respect to the threshold voltage of the switch-transistor was reached. Further, exposure to UV-light, however, resulted in a deterioration of the inverter performance. In addition, it should be mentioned that any attempts for optimizing the inverter characteristics other than tuning V_{Th} had not been performed. Thus, a significant optimization can be realized by adapting the W/L ratio between load and switch respectively, optimizing the performance of individual transistors with respect to mobility, gate leakage etc.

3.1.5.4 CONCLUSION

With the application of photoreactive layers in OTFTs it was demonstrated that device characteristics such as mobility and threshold voltage can be easily tuned and adjusted. Thus, an easy and reproducible way to switch OTFTs from enhancement to depletion mode by a photochemical reaction using photoacid generators as interfacial layers is presented. Moreover, the fabrication of good quality depletion-load inverters with tuneable characteristics can be made feasible. Thus, the fabrication method presented offers the possibility for the fabrication of monolithical circuits by UV-lithography.

3.2 UV-PATTERNING AND DERIVATIZATION OF ORGANIC MOLECULAR LAYERS CONTAINING O-NITROBENZYL ESTER GROUPS

The functionalization of various inorganic substrates by thin organic layers is a widely applied and important technique for the fabrication of patterned plane materials with defined surface properties. In this context ultra-thin layers consisting of silane coupling agents with chloro- or alkoxysilyl groups reactive to various oxidic surfaces have attracted a lot of attention.[67,126] Favoured surface properties are easily achieved using bifunctional molecules with defined terminal groups. Thus, the extremely thin films are able to completely modify the surface properties such as wetting, adhesion, conductivity and friction. In general, the fabrication of micro- and nanostructured arrays based on organic thin films[127] provide an attractive method because of its broad practical utility in a large area ranging from nanotechnology, biotechnology to molecular electronics. Potential applications are the selective immobilization of several functional molecules, such as catalysts, nano particles, biomolecules[19,54,128] and the area of operation in organic electronic devices.[113,129,130]

Therefore, several microlithographic techniques such as photolithography[131], microcontact printing[132] and microwriting[133] have been applied to obtain micron-scale patterns. The generation of nanoscale patterns of self-assembled monolayers (SAMs) is even more challenging. Suitable utilities are scanning probe lithography (SPL)-based methodologies, such as nano grafting[134–136]/nano shaving[137,138] and dip-pen nanolithography.[137,139] Thereby, molecules suspended in droplets at the end of atomic force microscopy (AFM) tips are traced across a defined substrate and as consequence molecules acting as molecular ink are exactly deposited. Another convenient and versatile approach is photolithography. UV-photolithography of organic thin films has been explored as highly selective technique to obtain defined patterns with clean edges. However, the limit of resolution due to diffraction is restricted in the micron scale. A nanometer scale patterning can be performed by scanning near-field optical microscopy (SNOM).[18] Here, the exposure in the optical near-field is achieved by coupling an argon ion laser to a scanning near-field optical microscope. This lithographic technique yields high resolution in monolayer patterning. Thus, resolutions down to 9 nm have been obtained.[140]

Photopatterning processes, such as the photoinduced cleavage of organosilanes result in the removal of the organic alkyl chains by photocleavage of the Si-C or C-C bonds[141] and the formation of Si-OH groups. Furthermore, photooxidation reactions of terminal alkyl chains yield in the generation of aldehyde or carboxylic acid groups. For both approaches highly energetic irradiation is required. However, the attachment of UV-sensitive groups to the

silane based agents represents an alternative yielding in well-defined patterns without high energy input. These applications of reactions in 2D layers have demonstrated that thin layers possessing reactive sites can be further functionalized.

In this study the applicability of these bifunctional molecules for the preparation of thin photoreactive silane layers and patterned functionalized surfaces in the nano and micron regime is discussed. Therefore, two photoreactive bifunctional molecules, similarly set up, are presented.

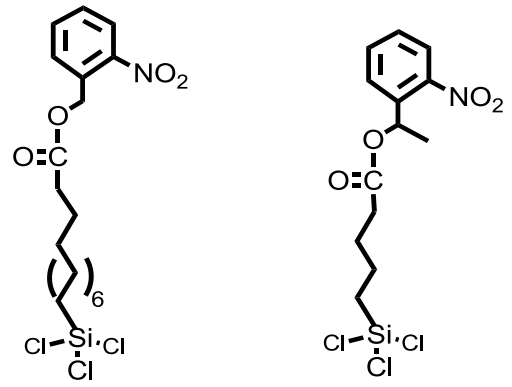

Figure 3.30: Structure of the molecules synthesized (SAM-1, SAM-2)

The bifunctional molecules depicted in Figure 3.30 are based on a trichlorosilane head group and a photoreactive o-nitrobenzyl ester tail group. The o-nitrobenzyl derivatives are well known as photocleavable protection groups for hydroxyl compounds, such as alcohols and carboxylic acids[11,28] or generating amine group.[142,143]

Using o-nitrobenzyl ester groups the occurring deprotection upon irradiation to UV-light leads to the associated formation of the carboxylic acid groups and is considered to be a photoacid generating (PAG) process. Therefore, nitrobenzyl ester groups are understood as photocleavable PAG groups. For further information on the mechanism see chapter 2.2.1.2.

The photoinduced formation of the carboxylic acid groups and the subsequent derivatization with fluorinated trifluoroethylamine were investigated for both molecules in thin layers. In addition to the photocleavage reaction, a photoreduction of the nitro group resulting in the generation of amines is mentioned in literature.[144] A consequence of the reduction is the associated loss of the ability for photodeprotection, which yields in lower carboxylic acid conversion. Beyond that the photoreaction and the subsequent post-exposure derivatization were measured in detail by X-ray photoelectron spectroscopy (XPS), contact angle

measurement, SIMS (secondary ion mass spectroscopy) and friction force microscopy (FFM). Furthermore, an exact adjustment of the layer thickness performed with the defined addition of water saturated toluene was investigated via XRR measurements.

3.2.1 2-NITROBENZYL 11-(TRICHLOROSILYL)UNDECANOATE (SAM-1)

3.2.1.1 SYNTHESIS

The photoreactive 2-nitrobenzyl 11-(trichlorosilyl)decanoate was synthesized in a two-step reaction. In the first step the photoreactive 2-nitrobenzyl undec-10-enoate was obtained via esterification reaction of undec-10-enoyl chloride added to a solution of 1.68 g (10.9 mmol) of (2-nitrophenyl)methanol and pyridine (0.88 ml, 10.9 mmol) in dichloromethane. A second step involved the hydrosilylation of 2-nitrobenzyl undec-10-enoate in the presence of a catalytical amount of H_2PtCl_6 using trichlorosilane. As solvent anhydrous dichloromethane was used. Due to the photoreactivity and the hydrolytic sensitivity of the silane group the reaction was performed under dry conditions and under exclusion of light.

3.2.1.2 ADJUSTMENT OF THE LAYER THICKNESS

According to the literature an increased thickness results from the presence of water, which results in partial crosslinking of the trichlorosilane groups and consequently in multilayer growth.[75] Therefore, an adjustment of the layer thickness was performed.

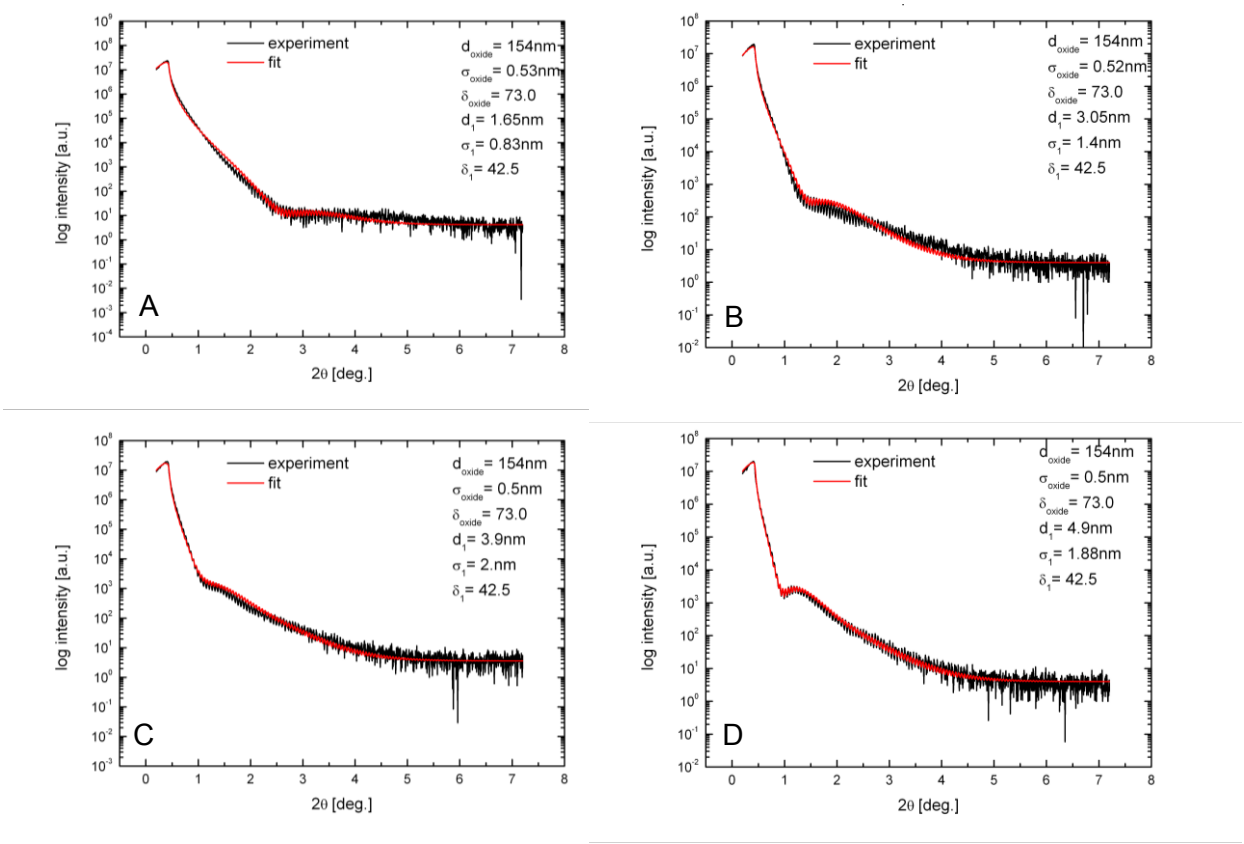

Figure 3.31: Influence of water on layer formation (A=0.5 ppm of water in toluene, B= 1.0 ppm of water in toluene, C=1.5 ppm of water in toluene, D=2.0 ppm of water in toluene)

A significant linear dependency between the layer thickness and the amount of water saturated toluene can be derived by Figure 3.31. Starting with 0.5 ppm of water in toluene a layer thickness of 1.65 nm was achieved. However, high values of surface roughness were obtained due to to polymerization of the trichlorosilane in the bulk solution.[70]

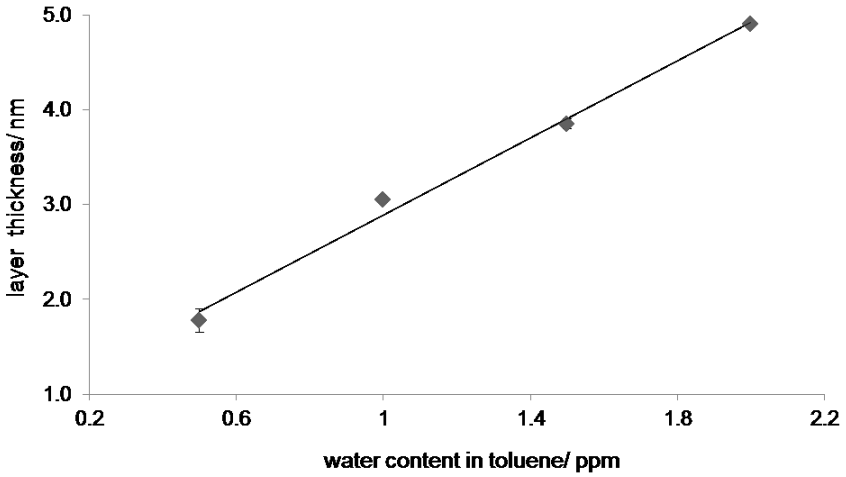

Figure 3.32: Adjustment of the layer thickness by the water content

Consequently, the development of the layer in the presence of water favors multilayer growth. Film thicknesses from 1.65 up to 5 nm were measured. For further experiments the initial layer thickness was measured to be approximately 1.5 nm (without water addition), which nearly corresponds to one layer of upright standing molecules (see also chapter 3.2.1.4.3).

3.2.1.3 Investigation of the photoreaction

The photoreaction as well as the absorption behavior of the photoreactive bifunctional units were investigated in the liquid phase by means of FTIR spectroscopy and UV-Vis measurements. In Figure 3.33 the photoreaction is depicted.

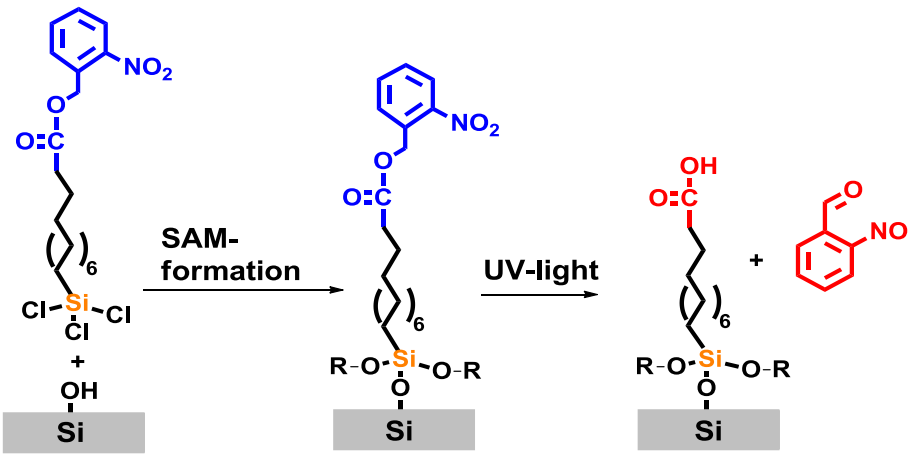

Figure 3.33: Illustration of the thin organic layer formation and the photoreaction induced upon irradiation with UV-light

3.2.1.3.1 FTIR SPECTROSCOPY

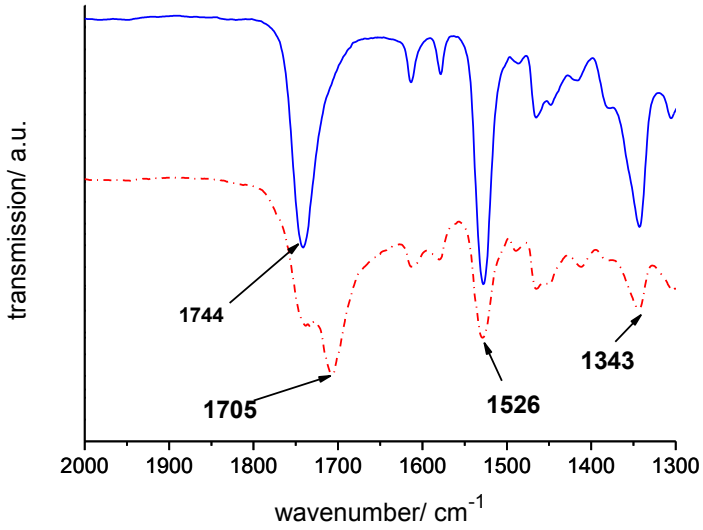

Figure 3.34: FTIR Spectra of SAM-1 in the bulk before (solid line, blue) and after (dotted line, red) illumination with UV-light of >300 nm (energy density E= 19.8 J cm^{-2})

Comparing the FTIR spectra prior to and after illumination (s. Figure 3.34) it can be seen that the signal of the ester group at 1744 cm^{-1} decreased significantly. Furthermore, the two peaks assigned to the nitro group at 1526 cm^{-1} and 1343 cm^{-1} nearly disappeared after 30 min of illumination. The new signal that emerged at 1706 cm^{-1} is representative for the formation of the carboxylic acid group.

3.2.1.3.2 UV-Vis Spectroscopy

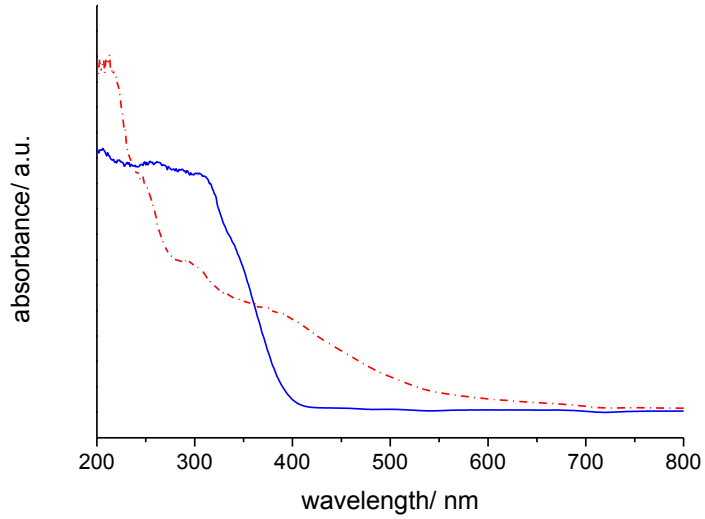

Figure 3.35: UV-Vis spectra of SAM-1 in the bulk before (solid line, blue) and after (dotted line, red) illumination with UV-light of >300 nm (energy density E= 19.8 J cm^{-2})

In accordance with the UV-Vis spectrum obtained it was decided to use an illumination source with a wavelength of >300 nm. Applying short-wavelength (deep UV, 254 nm) the generation of undesired products such as alcohols or aldehydes can emerge.[145] Selective modification of SAMs using soft UV (>300 nm) results in high-resolution patterned organic thin films. However, a crucial drawback of the ortho-nitrobenzyl-based processes is the fact that in solution the yield of this reaction is high, while in the range of thin films to molecular layer environment the yield is only moderate. The origin of these results is a competing photoreaction that reduces nitro groups to amines.[131,143,146,147]

3.2.1.3.3 Investigation of the photoreaction by means of TOF SIMS

For further investigation of the photocleavage reaction of o-nitrobenzyl ester groups, negative ion static SIMS spectra of the silane layers were recorded prior to and after exposure to UV-light.

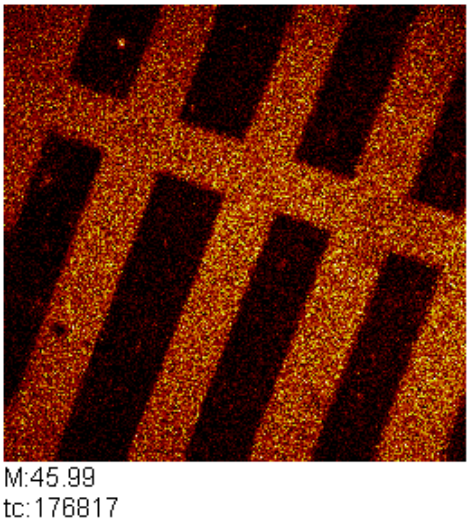

Figure 3.36: SIMS spectrum obtained by a photopatterned sample

As depicted in Figure 3.37, a distinct decrease of the nitro group before and after irradiation (at m/z 46) is presented. Furthermore, the negative ion spectra revealed a change in the low mass region. That region (m/z < 100) can be mainly attributed to hydrocarbons fragments, which were produced by the fragmentation of the alkyl spacer. The formation of the carboxylic acid was hardly detected by negative ion static SIMS measurements.

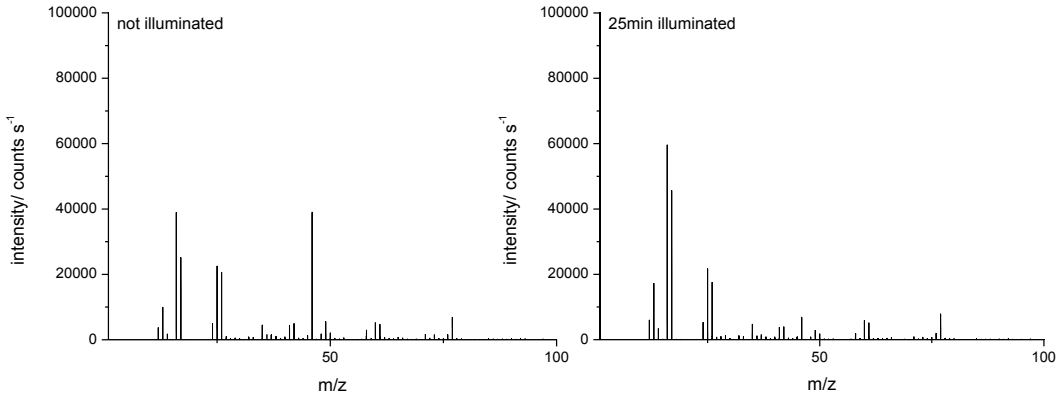

Figure 3.37: Comparison of the SIMS spectra of the illuminated (right) and non-illuminated part (left).

3.2.1.3.4 PHOTO INDUCED CHANGES OF SURFACE TRIBOLOGY BY MEANS OF FRICTION FORCE MICROSCOPY (FFM)

For the preparation of patterned functionalized surfaces with micron-scale resolution a contact mask and as UV-light source a laser with a wavelength of 325 nm were applied. The generation of nano structures was performed with a near-field scanning optical microscope coupled with the same UV-laser (325 nm).

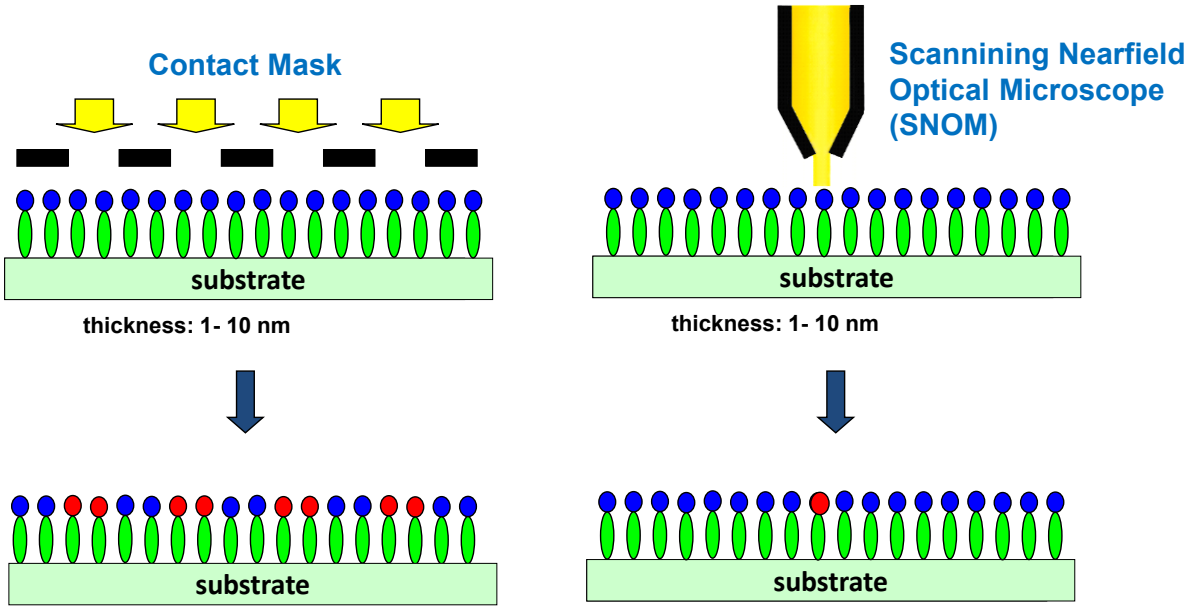

Figure 3.38: Depiction of photolithographical processes using a contact mask or SNOM

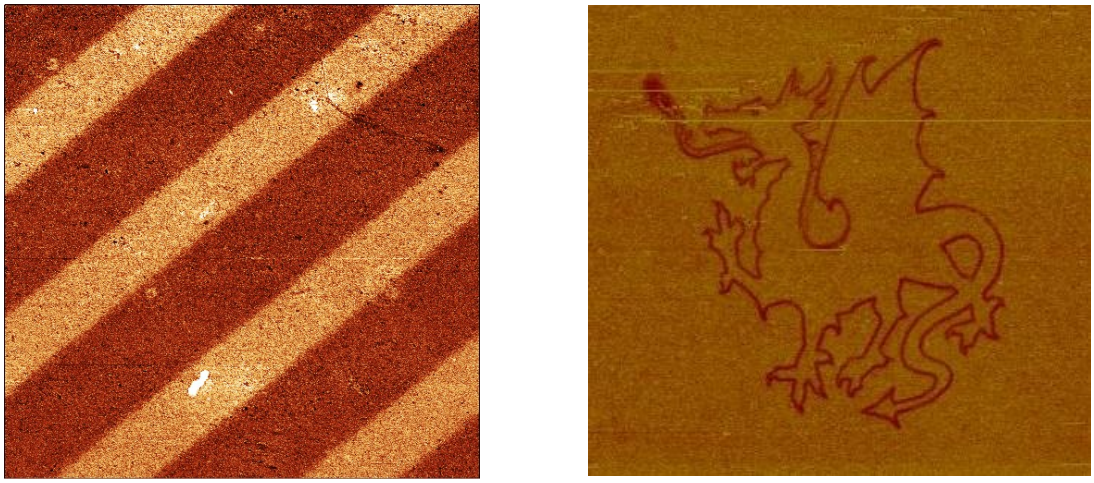

Figure 3.39: Friction force images after patterning using SNP under ambient atmosphere.

For the visualization of the structures the formed contrast between non-illuminated and illuminated or modified areas was measured under ambient conditions with friction force microscopy (FFM).[148] By using this special scanning technique a soft cantilever is scanned perpendicular to its long axis. Thus, lateral forces between tip and sample dependent on tip velocity and the different chemical end groups can be detected. The formation of the photoproduct leads to a different twist of the cantilever, which results in a significant contrast of friction in the AFM images (shown in Figure 3.39). The generation of nanometer-scale structures was realized using scanning near-field photolithography (SNP). The formed structures were also visualized with friction force microscopy (FFM). The illustrated high difference between the o-nitrobenzyl ester moieties and the photogenerated carboxylic acid units is achieved by the high contrast obtained in friction imaging. The exposed regions, in which the adsorbates have undergone the photocleavage reaction, give dark contrast (high friction), whereas the masked areas exhibit bright contrast. As the tip slides across the sample surface the contrast results from adhesive sample-to-tip interactions. In this specific case, the tip applied consists of a layer of polar silicon oxide predominantly showing strong interactions with polar regions of the sample. Compared to the photogenerated carboxylic acid group the nitrobenzyl ester interacts less strongly, which results in a reduced energy dissipation rate and consequently lower friction.

In addition to the formation of the organic thin film and the photoinduced deprotection of the carboxylic acid in the two dimensional layer a selective post-illumination modification reaction was investigated by contact angle measurements and XPS analysis. Furthermore, X-ray reflectivity measurements (XRR) characterizing the layer thickness were performed.

3.2.1.4 INVESTIGATION OF THE POST-MODIFICATION REACTION

Upon irradiation with UV-light, the bifunctional molecules undergo the o-nitrobenzyl ester cleavage and thus, the chemical reactivity of the illuminated areas is enhanced because of the formation of the carboxylic acid group. This carboxylic acid group can react with amine compounds to form amides. Using 2,2,2-trifluoroethylamine the post-modification step can be easily verified by various analysis techniques. Furthermore, surface properties such as surface energy can be tuned over a wide range. As coupling reagent 4-(4,6-dimethoxy-1,3,5-triazin-2-yl)-4-methyl-morpholinium chloride (DMT-MM) was used (s. Figure 3.40).

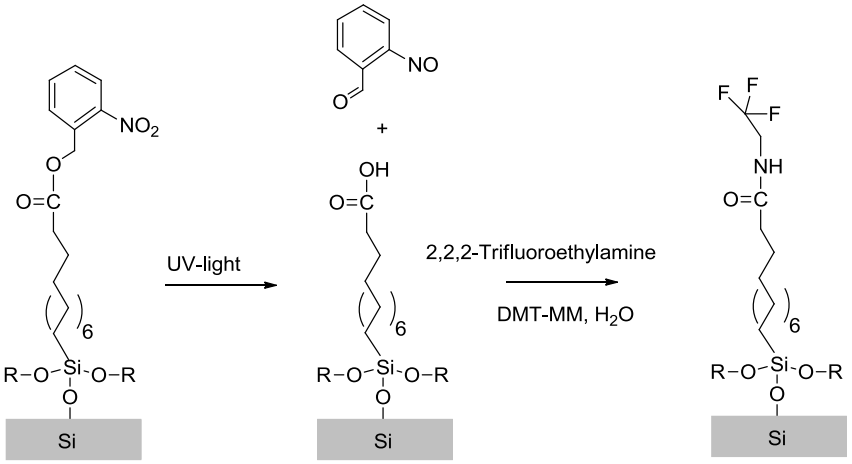

Figure 3.40 Photoreaction and post-illumination modification of SAM-1

3.2.1.4.1 CHANGE IN WETTABILITY AFTER IRRADIATION AND POST-MODIFICATION

Following the overall reaction scheme, shown in Figure 3.40, the advancing water contact angle of the monolayer SAM-1 prior to illumination was 71° (s. Table 2).

Table 2: Contact angle of water (sessile drop) on the investigated surfaces

	SAM-1		
	pristine	illuminated	fluorinated
Contact angle/ °	71.0 ±1.07	67.2 ±0.67	73.4 ±1.18

After illumination a slight decrease of the contact angle of water to 67° was observed.[149] This slight decrease of the photoreactive o-nitrobenzyl ester group can be referred to the incomplete formation of a highly ordered monolayer based on trichlorosilane. According to literature the partial crosslinking of the trichlorosilane moieties in the presence of water results in lying and not upright standing molecules. Furthermore, multilayer growth is favoured.[75] The subsequent derivatization using 2,2,2-trifluoroethylamine again showed an increase of contact angle to 73.4°.

3.2.1.4.2 Investigation of the post-modification reaction using X-ray photoelectron spectroscopy (XPS)

Besides contact angle measurements the photoreaction as well as the post-modification reaction were investigated by spatially resolved XPS. Therefore, XPS investigations prior to and after the illumination experiment were performed. XPS spectra are suitable to monitor the changes in the surface chemistry during the several reaction steps.

The XPS spectra were rapidly acquired to minimize the damage effects of the X-ray radiation observed at longer sample exposure. In addition, a selective post-modification with a fluorinated amine was performed. The use of fluorinated derivatization agents is advantageous, because they can be easily identified by XPS. Therefore, one half of the substrate was illuminated (energy density E= 19.8 J cm^{-2}) using a contact mask as shown in Figure 3.41. Subsequently, the whole sample was transferred into a solution of 2,2,2-trifluoroethylamine, 4-(4,6-Dimethoxy-1,3,5-triazin-2-yl)-4-methylmorpholinium chloride (DMT-MM) and milli-Q water (ultrapure). The illuminated side led to the reaction with the fluorinated amine while the non-illuminated side stayed unaffected. The selectivity of the derivatization reaction was evidenced by means of XPS. Thus, a comparison of pristine and modified area (2,2,2-trifluoroethylamine) was performed. For the visualization a line scan detecting the fluorine 1s signal, including 10 analysis spots (the distance is adjusted to be 1.5 mm), is depicted in Figure 3.41. The illuminated side of the sample showed a significant F1s signal, while only a weak fluorine signal could be detected in the non-illuminated area.

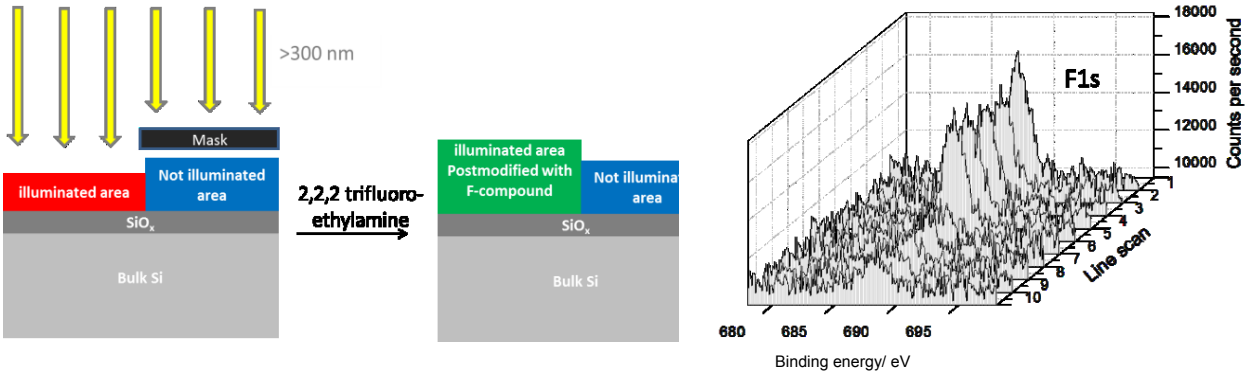

Figure 3.41: Comparison of the difference in the XPS-signal of fluorine between non-illuminated and illuminated area postmodified with fluorine compound using XPS

This minor fluorine contamination in the non-illuminated area is attributed to the fact that contaminants are physically adsorbed, or single carboxylic acid groups are already formed on the silane layers and thus can also react with the fluorinated compound.

However, the comparison of the fluorine signal integrals in Figure 3.42 indicates the high selectivity of the post-modification reaction in the illuminated area of the sample (ratio UV irradiated side to the non-illuminated side both exposed to the fluorine compound = 1:0.18).

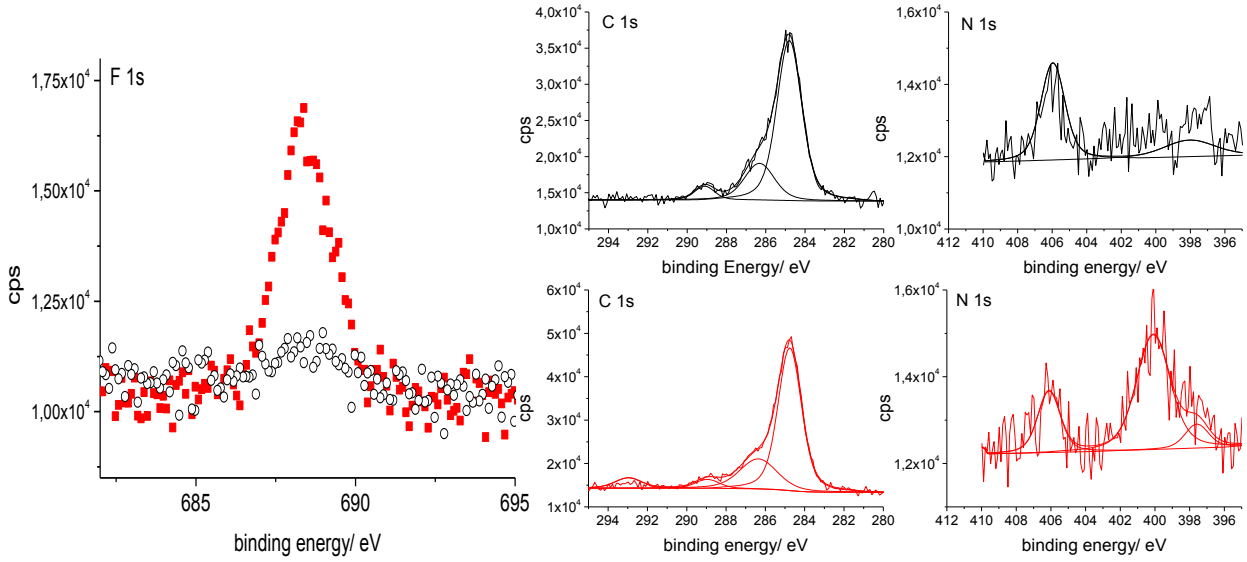

Figure 3.42: Comparison of F1s, C1s and N1s region of the XPS spectra of the SAM-1 layer prior to illumination (black) and of the irradiated and modified layer (red)

In addition, also changes in the signals of carbon and nitrogen were observed. After exposure to UV-light the conversion of the nitro moieties (reduction of the peak signal at 406 eV) was observed and the post-modification reaction led to the formation of an amide signal (400 eV) using trifluoroethylamine. Besides that a new carbon peak in the range of 293 eV (CF_3-) confirmed the attachment of the fluorinated amine compound (s. Figure 3.42).

3.2.1.4.3 CHANGES IN LAYER THICKNESS DURING IRRADIATION AND POST-MODIFICATION (MEASURED BY X-RAY REFLECTIVITY)

In addition, the quality of the layer and the change in layer thickness as a consequence of UV-irradiation and post-exposure reaction was investigated. For detailed information of the organic layer X-ray reflectivity measurements were performed. Therefore, the experimental and simulated data of the XRR-measurements are depicted in Figure 3.43. Besides the silicon oxide layer thickness the silane layer thickness was simultaneously determined. Based on the theoretical value of the molecular size (~1.6 nm) assuming upright standing molecules the height of the immobilized organic layer is supposed to be approximately 1.46 nm- a good accordance between theoretical and experimentally determined value.

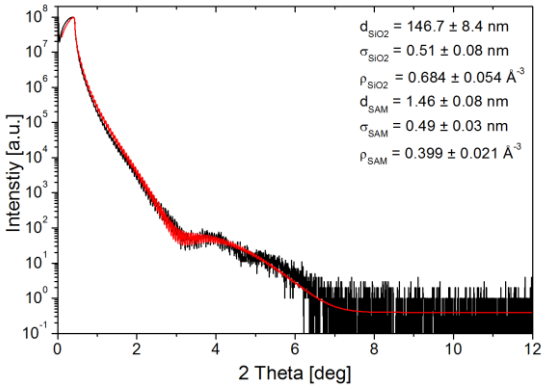

Figure 3.43: X-ray reflectivity measurement of a layer of SAM-1

After illumination (energy density E= 19.8 J cm^{-2}) a decrease in layer thickness to 1.09 nm was observed. The subsequent derivatization using trifluoroethylamine shows an increase again up to 1.5 nm. The data obtained are summarized in Table 3.

Table 3: Change of layer thickness prior to and after illumination and subsequent modification reaction

	SAM-1		
	pristine	illuminated	fluorinated
Layer thickness/ nm	1.46 ±0.08	1.08 ±0.08	1.51 ±0.1

3.2.2 1-(2-NITROPHENYL)ETHYL 5-(TRICHLOROSILYL) PENTANOATE (SAM-2)

3.2.2.1 INVESTIGATION OF THE PHOTOREACTION AND POST-MODIFICATION REACTION

A second photoreactive bifunctional molecule equipped with a trichlorosilane anchor group and the photoreactive o-nitrobenzyl ester unit was synthesized and characterized. By comparison of molecule SAM-1 and molecule SAM-2 the difference is based on a shorter spacer and an additional methyl group. It is known from literature that substitution of the parent o-nitrobenzyl group either on ring or α-position shall enable a significant improvement in the yield of photoreaction. Based on the methyl substitution[102], an increased abstraction of the benzylic hydrogen atom occurs due to the stabilization of the intermediate benzyl radical. Alternatively, the α-methyl group may alter the steric configuration of the molecule such that the reaction proceeds more readily.

3.2.2.1.1 INVESTIGATION OF THE PHOTOREACTION BY FTIR AND UV-VIS SPECTROSCOPY

The photoreaction as well as the absorbance behavior of the photoreactive bifunctional units was investigated in the liquid bulk by means of FTIR spectroscopy and UV-Vis spectroscopy. In Figure 3.44 the photoreaction is presented.

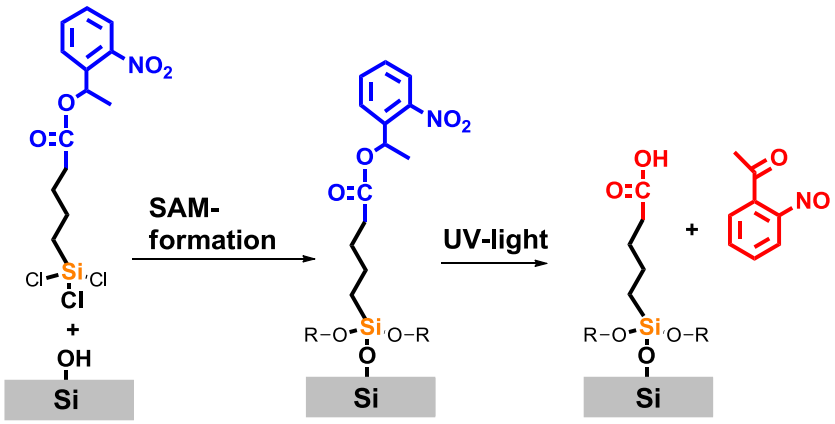

Figure 3.44: Depiction of the thin organic layer formation and the photoreaction induced upon irradiation with UV-light

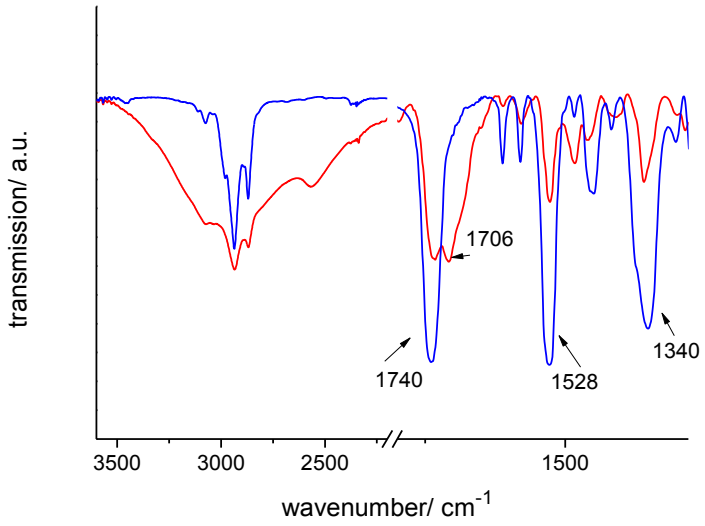

Figure 3.45: FTIR spectra of SAM-2 in the bulk before (solid line, blue) and after (dotted line, red) illumination with UV-light of >300 nm (energy density E= 19.8 J cm^{-2})

Comparing the FTIR spectra prior to and after illumination again the formation of a new peak typical of the formation of the carboxylic acid group (1706 cm^{-1}) could be observed. The peaks assigned to the carbonyl ester (1740 cm^{-1}) and the nitro group (1528 cm^{-1} and 1340 cm^{-1}) decreased significantly.

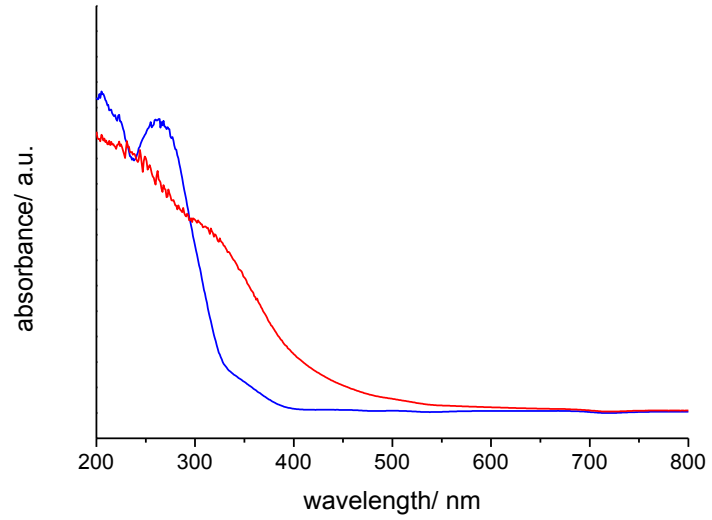

Figure 3.46: UV-Vis spectra of SAM-2 in the bulk before (solid line, blue) and after (dotted line, red) illumination with UV-light of >300 nm (energy density E= 19.8 J cm^{-2})

In accordance with the UV-Vis spectrum obtained it was decided to apply the same light source as used for SAM-1 (>300 nm). The same selective post-illumination modification reaction was investigated by contact angle measurements and XPS analysis. The overall reaction scheme is shown in Figure 3.47.

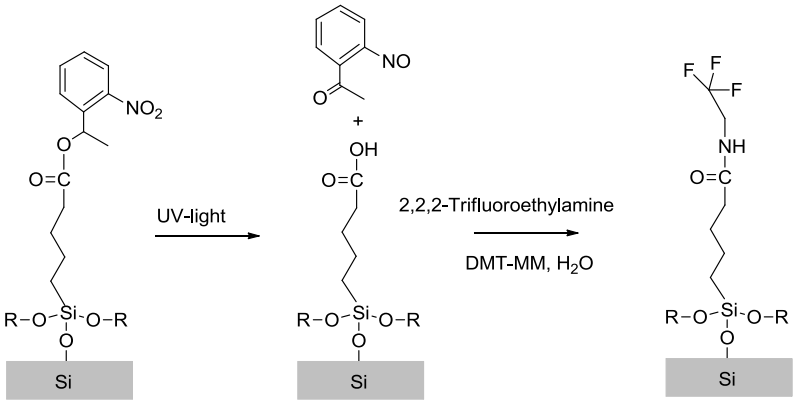

Figure 3.47: Photoreaction and post-illumination modification of the SAM-2 molecule

3.2.2.1.2 WETTABILITY OF THE MOLECULAR LAYERS

The formation of the organic thin film, the photoinduced deprotection of the carboxylic acid in the two dimensional layer and the selective post-illumination modification reaction were investigated by contact angle measurements and XPS analysis. The overall reaction scheme is shown in Figure 3.47.

Prior to and after illumination a higher difference in the contact angle of water was observed. Irradiation resulted in a significant decrease of the contact angle of water from 76° to 57°. The subsequent derivatization using 2,2,2-trifluoroethylamine again showed an increase of contact angle to 68.4°. Similar to SAM-1 multilayer growth is expected.

Table 4: Contact angle of water (sessile drop) on the investigated surfaces of SAM-2

	SAM-2		
	pristine	illuminated	fluorinated
Contact angle/ °	76.8 ±1.56	56.5 ±1.25	68.3 ±0.35

In comparison with SAM-1, the layer of SAM-2 showed a significant decrease in the contact angle of water after illumination. This result is consistent with previous literature which had reported about an increased yield of photogenerated carboxylic acid based on the α-substitution using a methyl group. In this case the α-methyl group influences the steric configuration of the molecule and as consequence the photoreaction in SAM-2 proceeds more readily. Thus, upon irradiation with UV-light the yield of carboxylic acid as photoproduct in SAM-2 is enhanced.

3.2.2.1.3 Investigation of the post-modification reaction using X-ray photoelectron spectroscopy (XPS)

XPS investigations prior to and after the illumination experiment were performed as shown by the following results. XPS spectra of the sample, again one half of the substrate was illuminated (energy density E= 1700 mJ cm^{-2}) by using a contact mask were performed (s. Figure 3.48). Subsequently, the whole sample was transferred into a solution of 2,2,2-trifluoroethylamine, 4-(4,6-Dimethoxy-1,3,5-triazin-2-yl)-4-methylmorpholinium chloride (DMT-MM) and water. A line scan measuring the F1s signal, depicted in Figure 3.48 revealed a significant difference in the intensity of F1s signal, while only a poor fluorine signal could be detected in the non-illuminated area.

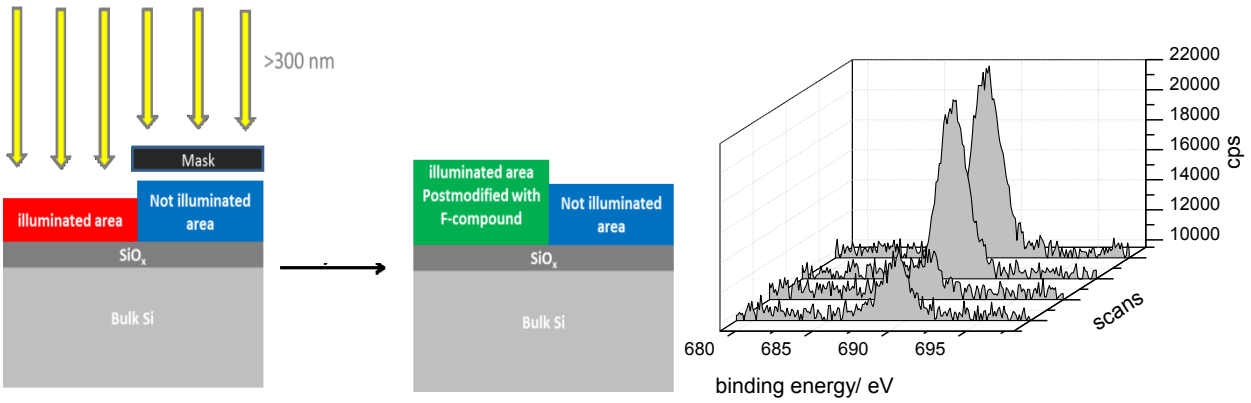

Figure 3.48: Comparison of the fluorine signal difference between non-illuminated and illuminated area post-modified with fluorine compound using XPS

Again a slight fluorine contamination in the non-illuminated area could be observed. However, in Figure 3.49 again a significant difference between the two areas is presented (ratio UV irradiated side to the non-illuminated side both exposed to the fluorine compound = 1.0:0.14).

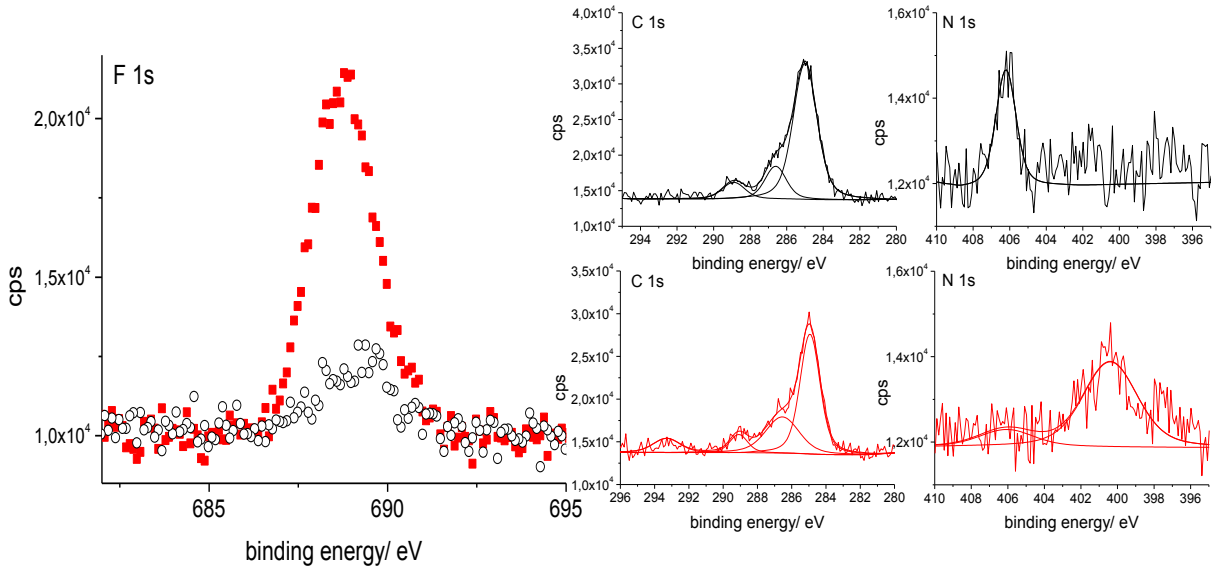

Figure 3.49: Comparison of F1s, C1s and N1s region of the XPS spectra of the pristine silane layer (black) and of the illuminated and modified layer (red)

The binding energies of the F1s peak at 689.3 eV is close to the literature values for organic fluorine compounds.[150] Furthermore, the reduction of the NO_2 signal (406 eV) after illumination and the formation of the amides at 399.9 eV were observed. The carbon peak in the range of 293 eV (CF_3-) measured after the derivatization confirmed the attachment of the fluorinated amine compound.

3.2.2.1.4 Investigation of the photoreaction by means of TOF SIMS

Direct comparison of the spectra showed in Figure 3.50 revealed a significant decrease of the peak at (m/z 47) related to the nitro group. Furthermore, the negative ion spectra indicated a change in the low mass region. The region m/z <100 are understood as fragments of hydrocarbons based on the fragmentation of the alkyl spacer. The formation of the carboxylic acid was hardly detected by negative ion static SIMS measurements.

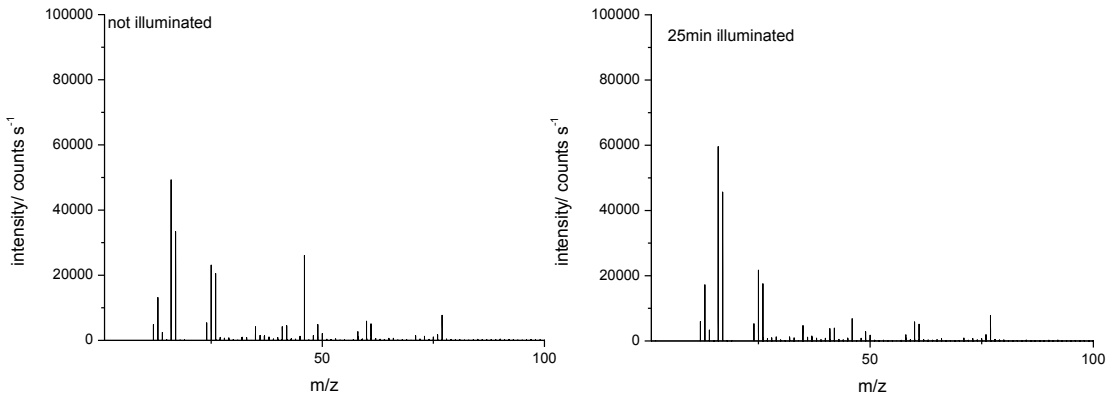

Figure 3.50: Comparison of the SIMS spectra of the illuminated and non- illuminated part of SAM-2

3.2.2.1.5 Investigation of the post-modification reaction by means of atomic force microscopy (AFM)

Micropatterning with a subsequent modification reaction of SAM-2 was performed. After 25 min of exposure to UV-light through a grid the sample was deposited in a solution of latex beads equipped with amine cappers. Here the latex beads should react with the illuminated areas, while an attachment of the beads shall not take place in the non-illuminated areas. As coupling reagent again DMT-MM was used.

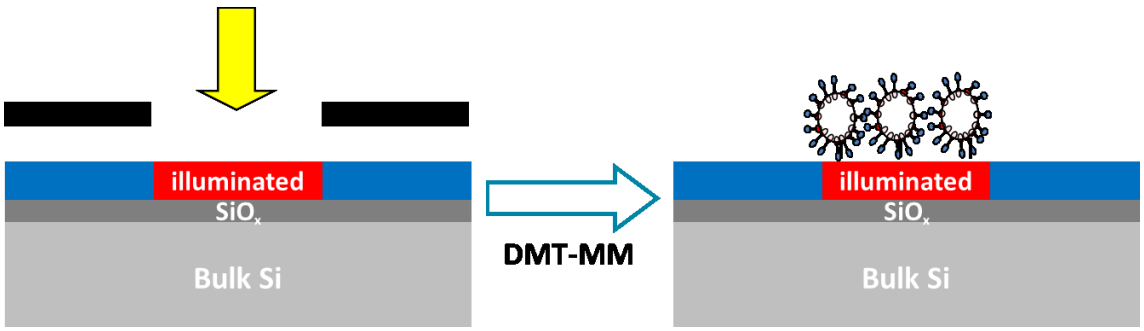

Figure 3.51: Depiction of the selective immobilization of latex beads

For visualization atomic force microscopy (tapping mode) was chosen. In Figure 3.52 the pattern obtained is displayed. Bright areas indicate the attached latex beads (high height areas), while the low height areas are representative for the non-irradiated regions.

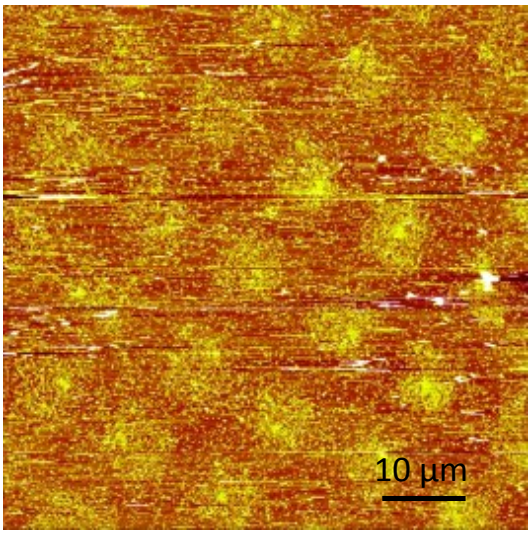

Figure 3.52: Atomic force microscopy (AFM) image of a thin photoreactive layer patterned with a TEM grid and reacted with amino functionalized latex particles

3.2.3 CONCLUSION

In this section the synthesis of two photoreactive trichlorosilane based bifunctional molecules has been presented. These molecules, equipped with a photosensitive o-nitrobenzyl ester group were applied for the formation of thin organic layers on oxidized silicon wafers. Upon irradiation with UV-light the induced formation of the carboxylic acid group, which is chemically more reactive than the ester units, enables the selective attachment of a variety of amino functionalized molecules. Thus, the selective immobilization, performed with a post-modification reaction using a fluorinated amine, was proven in evidence with XPS for both molecules. Besides the change in contact angle the high friction contrast determined by FFM measurements indicates a significant modification of the surface properties. Negative ion static SIMS spectra confirmed the progress of the photocleavage reaction. For SAM-1 patterned surfaces with micro scale arrays and even nano scale resolution were achieved by two different photolithographic techniques, either the application of illumination through a contact mask or SNOM. The resolution gained with the contact mask is approximately down to 1 µm, while scanning near-field photolithography (SNP) resolution was in the region of 250 nm. Moreover, the change in layer thickness during the individual reaction steps was observed by XRR measurements. Besides that, the adjustment of the organic layer thickness was found to be simply defined by the amount of water added. An increase in the yield of photoreaction is obtained by the introduction of an α-methyl compound. For SAM-2 a further post-modification was proved using latex beads equipped with amine cappers. The known simplicity of the photoreaction, the possibility to introduce a variety of functionalities by post-modification reactions tuning the surface properties as well as the application of photoreactive thin organic films with a defined layer thickness guarantee a broad field of application.

The results presented in this part of the thesis were achieved to a certain extent in cooperation with DI Simone Radl and are additionally published in the master thesis "Patterned Modulation of the Conductivity of Polyaniline Derivatives by Means of Photolithography" (Simone Radl, University of Leoben 2010)

3.3 PHOTOLITHOGRAPHIC PATTERNING OF UV-REACTIVE PRECURSORS OF POLYANILINE

The photolithographic adjustment of conductivity is based on a selective decarbonylation reaction proceeding in the polymer film when exposed to UV light. Next to the synthesis the exact characterization of the photoreaction was investigated by FTIR and UV-Vis spectroscopy, while the change in conductivity was measured using conductive atomic force microscopy (CAFM).

3.3.1 PHOTOREACTION OF POLY-N-FORMYLANILINE (EMERALDINE BASE)

The preparation of poly-N-formyl-aniline (FPANI) was performed using a mixture of acetic anhydride and formic acid as formylation agent and the emeralidine base of polyaniline (PANI) as starting material. FPANI was obtained in an appropriate yield of 60 % after precipitation in diluted ammonia solution (s Figure 3.53). By comparison of the FTIR-spectra in Figure 3.53 an almost quantitative conversion of a film of FPANI before (b) and after illumination (c) with UV-light (270-353 nm, mask aligner, 122.1 J/cm^2) is shown.

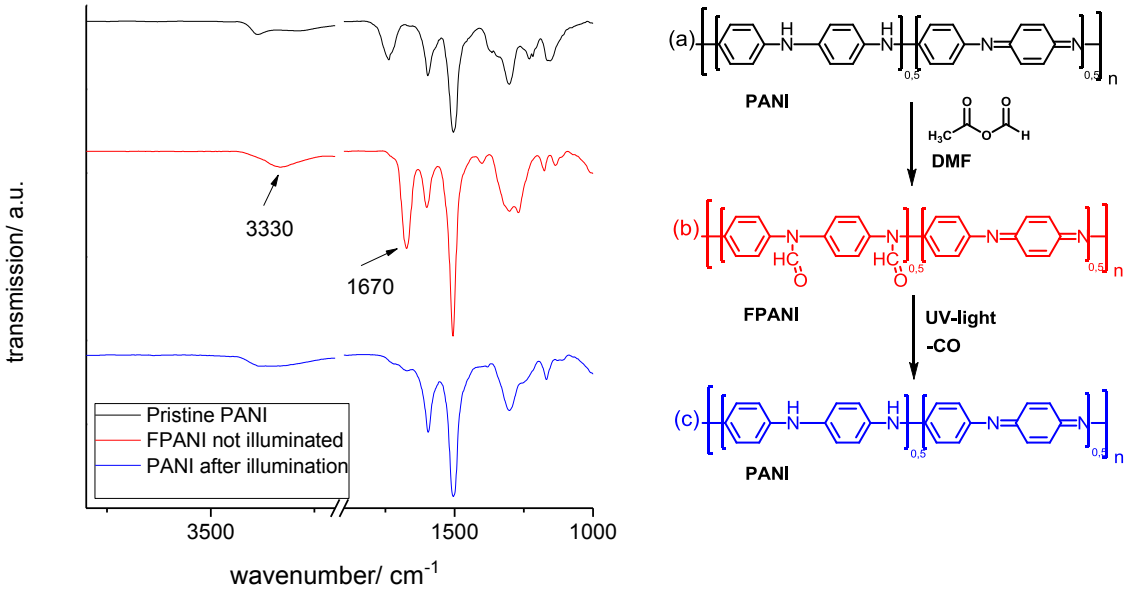

Figure 3.53: FTIR spectra of a film of starting material PANI (a), the synthesized FPANI before illumination with UV-light (mask aligner, 270-353 nm, 122.1 J/cm^2) (b) and after illumination (c)

In the spectrum of the non-irradiated film the signals at 1670 cm^{-1} (C=O stretch) and 3330 cm^{-1} (C-H stretch) are typical for N-formamides. After exposure to UV-light, the vibration band at 1670 cm^{-1} almost disappeared. Instead, a new broad peak at 3380 cm^{-1} has been arisen, which was attributed to N-H stretching vibrations of the formed secondary amino groups. The comparison of the FTIR spectrum of FPANI after irradiation (c) and the FTIR spectrum of the pristine polyaniline (a) resulted in the nearly identical spectra. Only, the N-H stretching vibration at 3380 cm^{-1} in the illuminated spectrum of FPANI is not that pronounced as in the spectrum of pristine PANI. As consequence polyaniline is recovered by the photodecarbonylation of the formamide groups. Moreover, side products are formed in minor degree and thus, the photoproduct corresponds with polyaniline formed in high yield. Similiar behaviour is evidenced by UV-measurements. Here, the UV-absorbance spectra of the polymer, depicted in Figure 3.54, changes upon illumination. The formylated PANI was characterized by a strong maximum at 310 nm. That absorption band at around 310 nm is referred to the π-π* transition, due to UV-irradiation and can be ascribed to the tertiary N-formamide moieties. The illumination (270-353 nm, mask aligner, 122.1 J/cm^2) resulted in a significant decrease (see Figure 3.54, red line). Furthermore, upon irradiation a new absorption maximum at 630 nm emerged, which is based on an intermolecular and/or intramolecular charge-transfer process from the benzenoid to the quinoid ring. This peak is

representative for the reformation of PANI. The UV-spectrum of the polyaniline obtained after irradiation is comparable to that found for pristine polyaniline emeraldine base as shown.

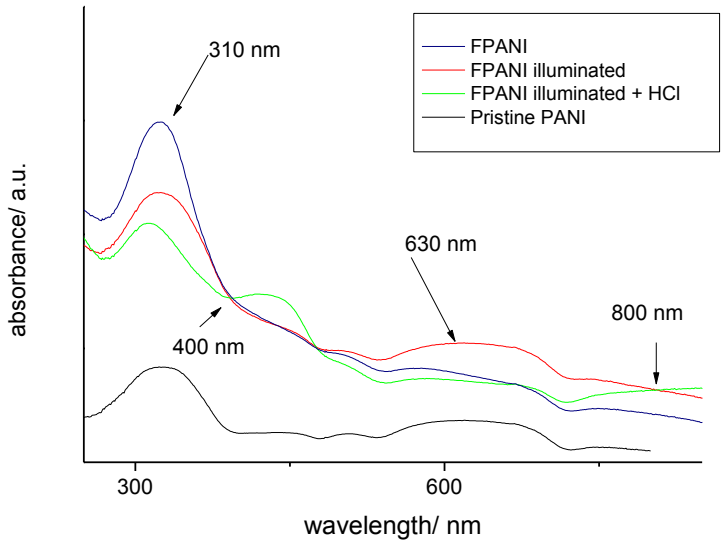

Figure 3.54: UV-Vis spectra of a thin film of FPANI before (blue line) and after irradiation (red line, mask aligner, 122.1 J/cm^2) and after treatment to gaseous hydrochloric acid (green line). For comparison the spectrum of Pristine PANI (black) is added

An exposure of the UV-illuminated FPANI to gaseous hydrochloric acid causes significant changes in the UV-absorbance spectrum (see Figure 3.54, green line). The obtained spectrum is comparable with the spectrum of pristine, doped PANI.[151] After the treatment with HCl the band at 630 nm disappeared and the band at 310 nm exhibited a significant reduction in intensity. While the disappearance of the peak at 630 nm is caused by the absence of excitons in the polar lattice, a process that takes place upon doping, the decrease in the absorption of the second peak can be related to the decreased number of species undergoing the π-π* transition. Simultaneously, two new bands around 800 nm and at 400 nm can be observed. These peaks are attributed to the transition from the highest and the second highest valence bands to the polaron band positioned in the middle of the band gap.

3.3.2 CHANGES IN THE CONDUCTIVITY OF THIN TILMS OF POLY-N-FORMYLANILINE (FPANI)

With the application of photosensitive FPANI, patterned polyaniline films could be achieved by lithographic methods. Thin films of FPANI were spincast on an ITO substrate using a DMF solution. Subsequently, an illumination performed by a mask aligner system equipped with a suitable quartz-chromium mask (122.1 J/cm^2, λ= 270-353 nm, contact lithography) was accomplished.

As mentioned before, the conductivity of doped PANI is dependent on its various oxidation state. While the acid doped emeralidine form shows the highest conductivity the formed N-acyl polyanillines exhibit a less conductive behaviour than the pristine PANI. This fact can be explained by the electron withdrawing effect of the acyl groups inducing a reduction of electrons on the polymeric backbone.[86] Moreover, a doping by protonation is inhibited by the N-acyl moieties, because the N-formamide groups are less basic compared to the secondary amino groups in PANI.

By exposure to UV-light, the N-formamide groups in the polymer chain cleavage and subsequent protonation of the photoinduced secondary amino groups ensure a significant increase of conductivity. A crucial parameter tuning the generation of secondary amines is the illumination time. This approach represents a convenient method for the modulation of the relative sheet conductivity of thin FPANI films (s. Figure 3.55).

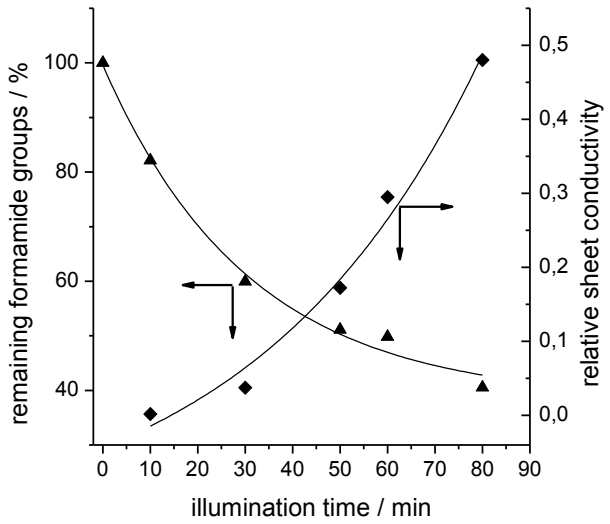

Figure 3.55: Modulation of conductivity via illumination time[90]

Thin films of FPANI were exposed to UV-light using various irradiation times. Subsequently, a treatment of all films with gaseous HCl was performed. The occurring difference in sheet conductivity of these films was measured with a two point measurement setup. In addition, the sheet conductivity of thin layer of acid doped, pristine PANI was investigated. Due to the fact that several parameters (e.g. the dopant and the molecular weight) influence the conductivity, doped pristine PANI has been applied as reference. The amount of formamide units converted (medium pressure mercury lamp, λ= 260-320 nm, P= 13.2 mW cm^{-2}) was determined from the decrease of the carbonyl vibration signal at 1670 cm^{-1}. The maximum sheet conductivity reached is amounted to be approximately 50 % of pristine PANI. Therefore, 60 % of all N-formyl units have been cleavaged during 80 min illumination time. Further conversion of formamide groups does not result in increased sheet conductivity. Presumably, prolonged illumination will reduce the conductivity due to degradation reactions of the polymer. However, the sheet conductivity obtained by this approach is in positive contrast to the data reported for PANI/PAG blends where conductivities of about 10 % of pristine doped PANI have been reported.[89]

Furthermore, conductive atomic force microscopy (CAFM) images of photopatterned and protonated polyaniline are recorded. CAFM is a special atomic force microscopy mode, which is able to map the local film conductivity by conductive cantilevers. Thus, a significant contrast of conductivity between photopatterned and respectively doped regions of the samples was visualized. The CAFM images yield in bright contrast indicating high conductivity in the areas exposed to UV-light. The non-irradiated regions with (low conductivity) resulted in darker contrast. In addition, a slight increase in conductivity was observed in the illuminated region after UV-irradiation. This effect can be attributed to the photoinduced elimination of the formamide group, causing a depletion of the electron withdrawing effect, which is conveyed in higher conductivity. A subsequent treatment with HCl shows a significant increase of conductivity, fitting well with our expectations. A current, even above the amplifier's saturation limit of 100 pA could be measured in the illuminated areas.

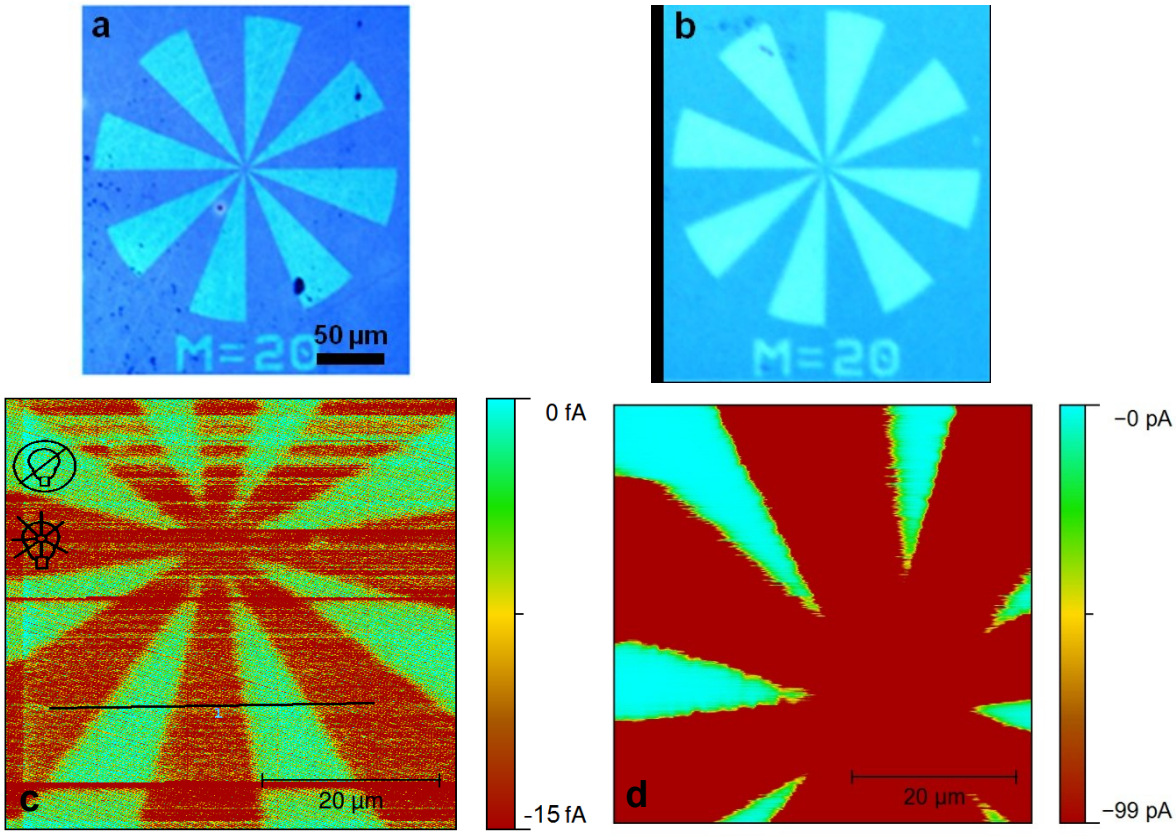

Figure 3.56: Thin film of FPANI on an ITO substrate after patterned illumination (mask aligner, λ= 270-353 nm, 122 J cm^{-2}) (a) respectively, after patterned illumination and exposure to gaseous hydrochloric acid (b). Conductive atomic force microscopy (CAFM) image of sample **a** after patterned illumination (c) respectively CAFM image of **b** after patterned illumination and subsequent protonation using gaseous hydrochloric acid (d) recorded at +10 V

In addition to the change of conductivity a difference of work function between non-illuminated and illuminated/protonated FPANI layers is in the focus of interest. Therefore, KPFM has been performed using a TiN coated tip. The work function of the TiN coated tip is supposed to be 5 eV. The measured KPFM signals were –0.100 V ±0.005 V for the illuminated/protonated areas and –0.160 V ±0.005 V for the non-illuminated areas. The negative signals obtained, imply that the work functions are higher than work functions of the tip. Thus, a work function of 5.1 eV for the illuminated/protonated and 5.16 eV for the non-illuminated areas are found. By this way a reduction of the work function in the illuminated areas was observed. An absolute work function, however, was not determined as a consequence of several parameters, e.g. ambient conditions and a water film, significantly influencing the results.

3.3.3 APPLICATION OF PHOTOREACTIVE POLYMERIC LAYERS IN OLEDS

Organic light-emitting diodes (OLEDs) represent a widely used application method in today's display technology. In general, the basic OLED set up consists of a film of fluorescent organic material, embedded between two electrodes: a transparent conducting anode and a metallic cathode.[152]

As soon as an appropriate bias is applied to the device, holes are injected from the anode and electrons from the cathode. The occurring recombination between holes and electrons results in electroluminescence. With the application of a photoreactive organic layer, patterned OLEDs with structured fluorescent surfaces can be obtained. Next to photostructuring, FPANI was further tested in the field of organic light emitting diodes acting as photopatternable charge injection layer. Literature already mentions the successful application of thin films of PANI as hole injection layer in OLEDS and organic photovoltaic cells.[153] Properties, such as transparency, chemical stability and the high conductivity makes PANI a suitable candidate as alternative choice to well-established PEDOT/PSS charge injection layers.

As a consequence of UV-irradiation the photoinduced conversion of FPANI yields in the nearly entire formation of PANI - with similar conductivity (in the protonated state) and similar UV-Vis transmittance. That is why especially this photoreactive polymeric material is suited for the application as photopatternable charge injection layers in optoelectronic devices.

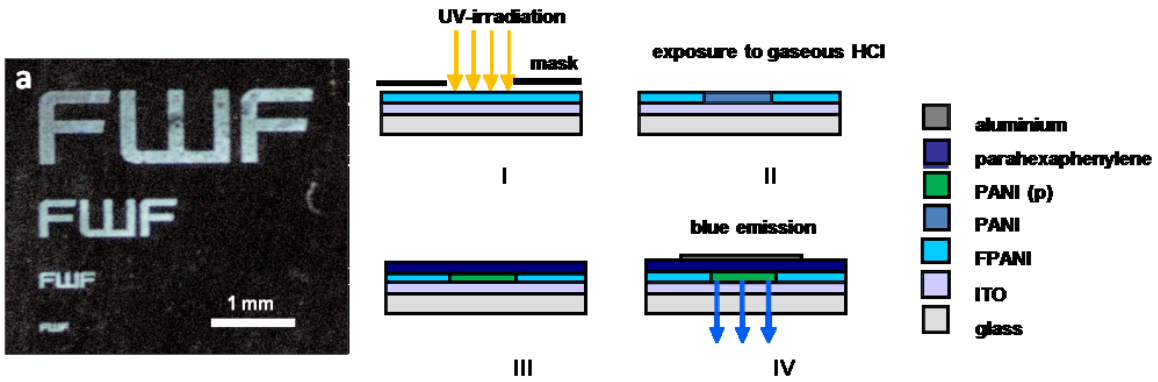

Figure 3.57: Photograph of a structured OLED when operated at 9 V (left) and scheme of the preparation of a structured OLED

The setup of a photopatterned OLED device (s. Figure 3.57) was accomplished on an indium-tin oxide (ITO) coated glass substrate. The transparent ITO electrode then was

covered with a spin cast film of FPANI. Photo structuring using a mask aligner (λ = 270-353 nm, 122 J cm^{-2}) was performed and afterwards the photogenerated PANI was exposed to gaseous HCl. Subsequently, a thin layer (20 nm) of para-hexaphenylene as emissive component was deposited by hot wall epitaxy. Finally, on top of this device a layer of aluminium (100 nm) was attached (contact electrode). Furthermore, a photograph of the structured OLED when operated at 9 V is presented (s. Figure 3.57 a).

In addition, the electrical properties of the OLED have been investigated. A current/voltage characteristic has been acquired and is plotted in Figure 3.58.

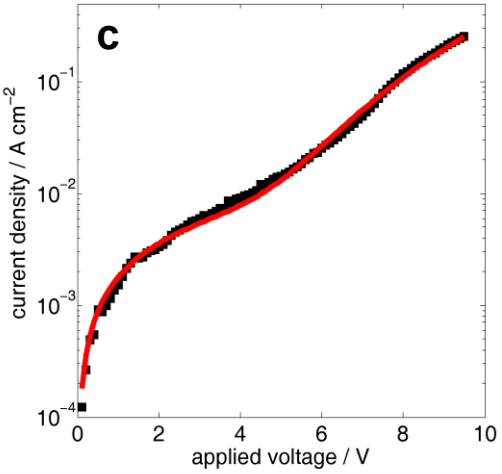

Figure 3.58: Logarithmic representation of the J-V characteristics. Black squares are the measured values and the red line shows a fit representing a tunneling process for carrier injection at the electrodes and a parallel resistance accounting for leakage in the diode[90]

The data are achieved using the formula of Fowler-Nordheim tunnelling[154] as given in equation 3. The description of the current by a tunnelling model was chosen due to the high applied electric field of more than 10^8 V/m.[155]

$$J = \frac{V}{R \cdot A} + V^2 \cdot C \cdot \exp\left(-\frac{8\pi\sqrt{2m}\varphi^{3/2}}{3qh} \cdot \frac{d}{V} \right) \tag{3}$$

J is the current density, V is the voltage applied, R stands for parallel resistance, while A and d are the area and the thickness of the active layer. Furthermore, C is a constant of proportionality, m is the mass of the charge carriers which is assumed to equal the free

electron mass, q represents the elementary charge and *h* is Planck's constant. For the barrier height is φ introduced. Based on this equation a value of 7.5 kΩ for the parallel resistance and an estimate of 0.35 eV for the hole injection barrier was determined.

3.3.4 CONCLUSION

A patterned modification of the conductivity in photoreactive polyformylaniline films can be accomplished by means of UV-light. UV-irradiation leads to a decarbonylation reaction of the pendant N-formamide groups and polyaniline as well as carbon monoxide are formed. Further treatment with gaseous HCl acid results in the insoluble and conductive emeraldine salt. Photoinduced changes in conductivity were corroborated by conductive AFM measurements. A direct dependency of conductivity in FPANI based on the conversion of the N-formamide groups enables selective adjustment of the conductivity controlled by exposure to UV-light. In addition, the application as photopatternable charge injection layer for structured OLEDs is demonstrated. The fabrication of planar conductive pattern embedded in a non-conductive matrix represents a field of application as electrodes and interconnects in various organic electronic devices.

4 EXPERIMENTAL SECTION

4.1 SYNTHESIS OF THE BIFUNCTIONAL MOLECULES

4.1.1 SYNTHESIS OF 2-NITROBENZYL 11-(TRICHLOROSILYL)UNDECANOATE (SAM-1)

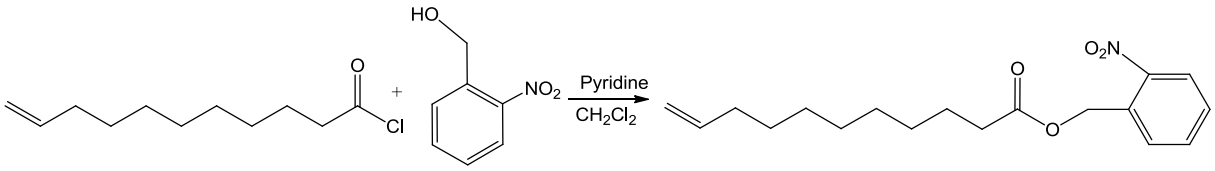

The photosensitive bifunctional molecule was synthesized in a two step reaction.

Step 1:

2.0 g (9.9 mmol) of undec-10-enoyl chloride were added to a solution of 1.68 g (10.9 mmol) of (2-nitrophenyl)methanol, dissolved in a mixture of 0.88 ml (10.9 mmol) of pyridine and 40 ml of dichloromethane. To exclude light from the reaction aluminium foil was used. The reaction was stirred for 48 h at ambient temperature until a complete conversion was observed. The organic phase was extracted with diluted hydrochloric acid (1.5 %) then with saturated $NaHCO_3$ and finally with deionized water and dried over anhydrous sodium sulfate. The solvent was removed in vacuum and subsequently a column separation cyclohexane/ethyl acetate (8:1) for product purification was performed.

Yield: 2.63 g of a white solid (83 % of theoretical yield).

^{1}H-NMR: (δ, 400 MHz, 20°C, $CDCl_3$): 8.05 (dd, 1H, ph^3); 7.62 (t, 1H, ph^4); 7.57 (d, 1H, ph^6); 7.46 (t, 1H, ph^5); 5.76 (m, 1H, =CH-); 5.48 (s, 2H, O-CH_2-ph); 4.91 (dd, 2H, CH_2=); 2.38 (t, 2H,-C2-(COO)); 2,00 (q, 2H,C9); 1.63 (quint, 2H,C3); 1.27 (m, 10H,C4-C8) ppm.

^{13}C-NMR: (δ, 125 MHz, 20°C, $CDCl_3$): 172.30 (1C, COO); 147.56 (1C, ph^2-NO_2); 137.13 (1C, C10(C=C)); 135.20 (1C, ph^1); 134.24 (1C, ph^5); 128.36 (2C, $ph^{4,6}$); 125.67(1C, ph^3);

115.15 (1C, C11(C=C)); 63.76 (1C,(COO)-CH_2-ph); 34.05 (1C,C9); 34.00 (1C,C2); 29.27 (1C,C8);29.18 (1C,C7); 29.07 (1C,C6); 29.04 (1C,C5); 28.87 (1C,C4); 24.93 (1C,C3) ppm.

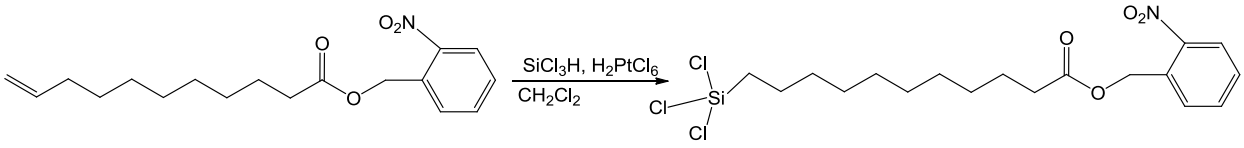

SAM-1

Step 2:

1.0 g (7.4 mmol) of trichlorosilane was added to a solution of 1.0 g (3.1 mmol) of (2-nitrobenzylundec-10-enoate, dissolved in 5 ml of dichloromethane. As catalyst hexachloroplatinic acid was used. To exclude light from the reaction aluminium foil was used. The reaction was stirred for 24 h at ambient temperature until a complete conversion was observed.

Yield: 1.38 g of a white, yellowish liquid (97.3% of theoretical yield).

^{1}H-NMR: (δ, 400 MHz, 20°C, $CDCl_3$): 8.05 (dd, 1H, ph^3); 7.59 (t, 1H, ph^4); 7.53 (d, 1H, ph^6); 7.43 (t, 1H, ph^5); 5.48 (s, 2H, (O-CH_2-ph)); 2.35 (t, 2H,-C2-(COO)); 1.61 (m, 2H,C3); 1.51 (m, 2H,C10); 1.35 (quint, 2H,C11); 1.28 (m, 12H,C4-C9) ppm.

^{13}C-NMR: (δ, 125 MHz, 20°C, $CDCl_3$): 173.12 (1C, COO); 147,64 (1C, ph^2-NO_2); 133.61 (1C, ph^6); 132.23 (1C, ph^1); 129.1 (1C, ph^4); 128.73 (1C, ph^5); 125.01 (1C, ph^3); 62.76 (1C,(COO)-CH_2-ph); 34.13 (1C,C2); 31.75 (1C,C9); 29.32 (1C,C8); 29.23 (1C,C7); 29.15 (1C,C6); 29.07 (1C,C5); 28.94 (1C,4); 24.84 (1C,C3); 24.27 (1C,C11); 22.23 (1C,C10) ppm.

IR-Data (CaF_2, cm^{-1}): 2925; 2853; 1742; 1613; 1578; 1528; 1447; 1343.

4.1.2 SYNTHESIS OF 1-(2-NITROPHENYL)ETHYL 5-(TRICHLOROSILYL) PENTANOATE (SAM-2)

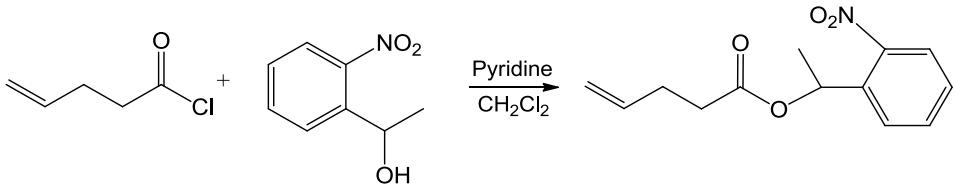

The photosensitive bifunctional molecule was synthesized in a two step reaction.

Step 1:

0.75 g (6.3 mmol) of pent-4-enoyl chloride were added to a solution of 1.17 g (7.0 mmol) of 1-(2-nitrophenyl) ethanol, dissolved in a mixture of 0.55 ml (7.0 mmol) of pyridine and 30 ml of dichloromethane. To exclude light from the reaction aluminium foil was used. The reaction stirred for 48 h at ambient temperature until a complete conversion was observed. The organic phase was extracted with diluted hydrochloric acid (1.5 %) then with saturated $NaHCO_3$ and finally with deionized water. The solvent was removed in vacuum and subsequently a column separation cyclohexane/ethyl acetate (8:1) for product purification was performed.

Yield: 1.51 g of a white solid (78.6 % of theoretical yield).

^{1}H-NMR: (δ, 400 MHz, 20°C, $CDCl_3$): 7.95 (dd, 1H, ph^3); 7.63 (m, 2H, ph^4, ph^6); 7.43 (m, 1H, ph^5); 6.34 (m, 1H, =CH-); 5.79 (s, 1H, O-(CH_3)CH-ph); 5.00 (m, 2H, CH_2=); 2.41 (m, 2H,-C3-); 2.36 (m, 2H,-C2-(COO); 1.65 (d, 3H, -CH_3) ppm.

^{13}C-NMR: (δ, 125 MHz, 20°C, $CDCl_3$): 171.81 (1C, COO); 137.96 (1C, ph^6); 136.41 (1C, C4(C=C); 133.43 (1C, ph^5); 128.31 (1C, ph^2-NO_2); 127.18 (2C, $ph^{1,3}$); 125.40 (1C, ph^4); 115.61 (1C, C5(C=C)); 68.06 (1C,(COO)-CH_2(-CH_3)-ph); 33.51 (1C,C2); 28.67 (1C,C3); 21.99 (1C,-CH_3) ppm.

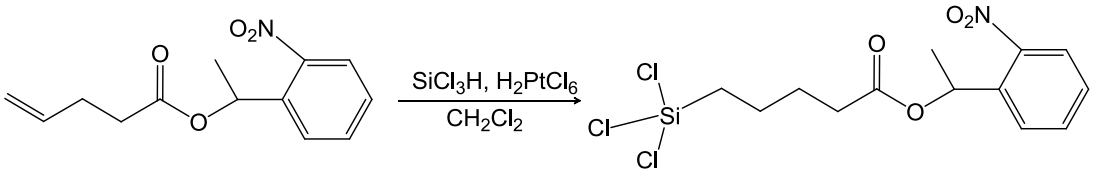

SAM-2

Step 2:

1.0 g (7.4 mmol) of trichlorosilane was added to a solution of 1.0 g (4.0 mmol) of 2-nitrobenzylpent-4-enoate, dissolved in 5 ml of dichloromethane. As catalyst hexachloroplatinic acid was used. To exclude light from the reaction aluminium foil was used. The reaction stirred for 24 h at ambient temperature until a complete conversion was observed.

Yield: 1.38 g of a white, yellowish liquid (97.3 % of theoretical yield).

^{1}H-NMR: (δ, 400 MHz, 20°C, $CDCl_3$): 7.92 (dd, 1H, ph^3,); 7.59 (m, 2H, ph^4, ph^6); 7.43 (m, 1H, ph^5); 6.23 (m, 1H, (O-CH_2-ph)); 2.35 (m, 2H,-C2-(COO)); 1.73 (m, 2H,C3); 1.65 (d, 3H,-CH_3); 1.63 (m, 2H,C4); 1.41 (quint, 2H,C5) ppm.

^{13}C-NMR: (δ, 125 MHz, 20°C, $CDCl_3$): 172.9 (1C, COO); 137.61 (1C, (1C, ph^6); 135.1 (1C, (1C, ph^5); 130.0 (1C, ph^2-NO_2); 129,8 (1C, ph^3); 128.9 (1C, ph^4); 128.7 (2C, ph^1); 67.76 (1C,(COO)-CH_2(-CH_3)-ph); 33.7 (1C,C2); 31.75 (1C,C3); 27.1 (1C,C5); 29.23 (1C,C4); 18,9 (1C,-CH_3) ppm.

IR-Data (CaF_2, cm^{-1}): 2933; 2868; 1740; 1613; 1581; 1528; 1448; 1353; 1192.

4.2 SYNTHESIS OF THE MONOMERS

4.2.1 SYNTHESIS OF ENDO,EXO-DI(2-NITROBENZYL) BICYCLO[2.2.1]HEPT-5-ENE-2,3-DICARBOXYLATE (M-1)

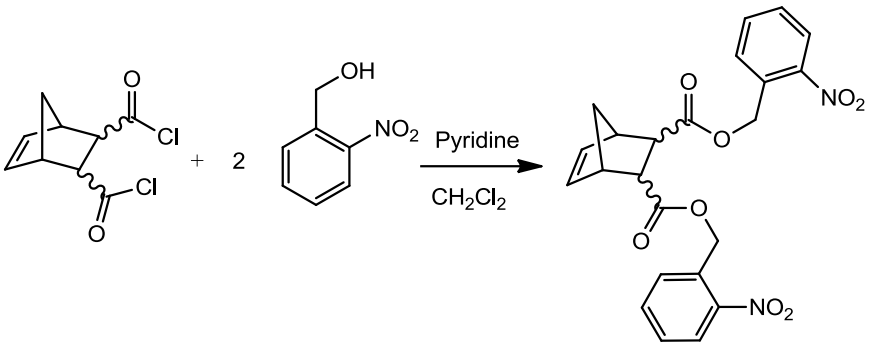

M-1

The photosensitive monomer was synthesized in an one-step reaction. 2.42 g (15.8 mmol) of (2-nitrophenyl)methanol were added to a stirred solution of 1.56 g (7.18 mmol) of bicyclo[2.2.1]hept-5-ene-2,3-dicarbonyl dichloride and 1.24 ml (15.8 mmol) of pyridine in dichloromethane. To exclude light from the reaction aluminium foil was used. The reaction stirred for 48 h at ambient temperature until a complete conversion was observed. The organic phase was extracted with diluted hydrochloric acid (1.5 %) then with saturated $NaHCO_3$ and finally with deionized water. The solvent was removed in vacuum and subsequently a column separation cyclohexane/ethyl acetate (10:1) for product purification was performed.

Yield: 2.69 g of a white solid (83 % of theoretical yield).

^{1}H-NMR: (δ, 400 MHz, 20°C, $CDCl_3$): 8.09 (m, 2H, ph^3); 7.63 (m, 2H, ph^4); 7.58 (m, 2H, ph^5); 7.49 (d, 2H, ph^6); 6.30, 6.11 (m, 2H, $nb^{5,6}$); 5.55, 5.47 (m, 4H, O-CH_2-ph); 3.51 (m, 1H, nb^3); 3.36 (s, 1H, nb^4); 3.21 (s, 1H, nb^1); 2.83 (m,1H, nb^2); 1.67, 1.54 (d, 2H, nb^7) ppm.

^{13}C-NMR: (δ, 125 MHz, 20°C, $CDCl_3$): 173.6, 172.4 (2C, COO); 137.71 (2C, ph^2-NO_2); 137.62, 135.16 (2C, $nb^{5,6}$);133.74, 133.63 (2C, ph^5); 131.98, 131.67 (2C, ph^1); 129.26, 129.15 (2C, ph^4); 128.87 (2C, ph^6); 125.87, 125.02 (2C, ph^3); 63.31, 63.54 (2C, O-CH_2-ph); 48.67 (1C, nb^1); 47.60 (1C, nb^4); 47.57 (1C, nb^2); 47.20 (1C, nb^3); 45.78 (1C, nb^7) ppm.

IR-Data (CaF_2, cm^{-1}): 1733; 1613; 1578; 1525; 1447; 1342; 1306; 1163.

4.2.2 SYNTHESIS OF ENDO,EXO-DIPHENYL BICYCLO[2.2.1]HEPT-5-ENE-2,3- DICARBOXYLATE (M-2)

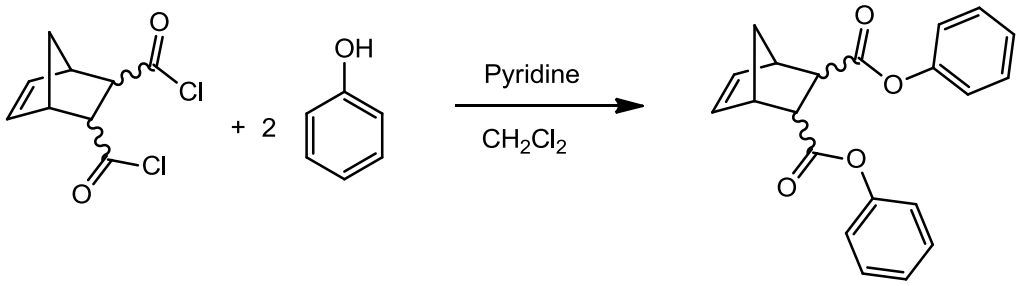

M-2

The photosensitive monomer was synthesized by an one-step reaction. 2.42 g (15.8 mmol) of bicyclo[2.2.1]hept-5-ene-2,3-dicarbonyl dichloride were added to a stirred solution of 4.0 g (42.5 mmol) of phenole and 10.0 g (126.5 mmol) of pyridine in dichloromethane. For cooling an icebath was used. To exclude light from the reaction aluminium foil was used. The reaction stirred until a complete conversion was observed. The formed pyridinium salt was removed by filtration and then the organic phase was extracted with diluted hydrochloric acid (1.5 %), with saturated $NaHCO_3$ and finally with deionized water. The solvent was removed in vacuum and subsequently a column separation cyclohexane/ethyl acetate (10:1) for product purification was performed.

Yield: 4.98 g (76 %) of a white solid.

^{1}H-NMR: (δ, 400 MHz, 20°C, $CDCl_3$): 7.41, 7.39 (m, 4H, $ph^{3,5}$); 7.26 (m, 2H, ph^4); 7.13, 7.07 (d, 4H, $ph^{2,6}$); 6.45, 6.30 (m, 2H, $nb^{5,6}$); 3.79 (m, 1H, nb^3); 3.54 (s, 1H, nb^4); 3.42 (s, 1H, nb^1); 3.10 (m,1H, nb^2); 1.80,1.64 (d, 2H, nb^7) ppm.

^{13}C-NMR: (δ, 125 MHz, 20°C, $CDCl_3$): 173.1, 171.8 (2C, COO-ph); 150.9 (2C, ph^1); 138.1, 135.3 (2C, $nb^{5,6}$); 129.6 (4C, $ph^{3,5}$); 126.1 (2C, ph^4); 121.6 (4C, $ph^{2,6}$); 48.3 (2C, $nb^{1,4}$); 47.6 (2C, $nb^{2,3}$); 46.2 (1C, nb^7) ppm.

IR-Data (CaF_2, cm^{-1}): 3098-2875; 1750; 1592; 1492; 1456; 1305; 1263; 1242; 1192; 1163; 1150; 1107.

4.3 SYNTHESIS OF THE POLYMERS

4.3.1 SYNTHESIS OF POLY(ENDO,EXO-DI(2-NITROBENZYL) BICYCLO[2.2.1] HEPT-5-ENE-2,3-DICARBOXYLATE) (POLY-1)

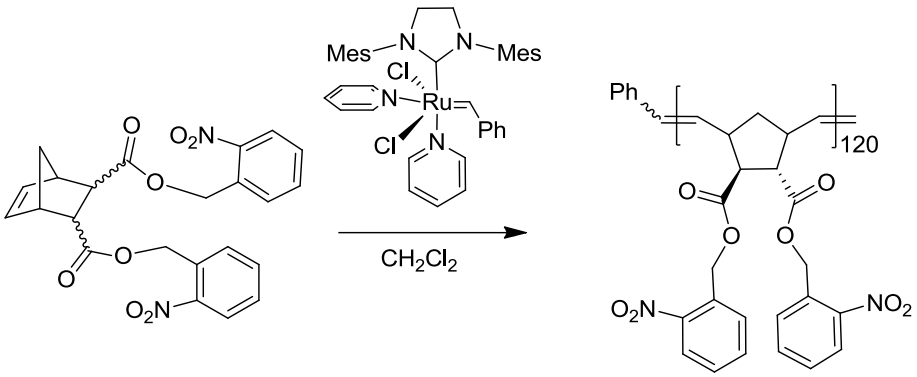

M-1 **poly-1**

500 mg of monomer (M-1) dissolved in 3 ml of dichloromethane were added to a solution of 6.7 mg of G-3 dissolved in 2 ml of CH_2Cl_2 and was stirred at RT for 3 h. After complete conversion (TLC), the reaction was stopped by adding of 0.15 ml ethylvinylether. Then the polymer was recrystallized two times in cold methanol and dried under vacuum.

Yield: 420.2 mg of a white solid (84 %).

^{1}H-NMR: (δ, 400 MHz, 20°C, $CDCl_3$): 8.01 -7.23 (8H, ph); 5.6-5.1 (2H, (CH=CH) + 4H, (O-CH_2-ph)); 3.74-3.03 (4H, nb^{1,2,3,5}); 1.91-1.55 (2H, nb^4) ppm.

IR-Data (CaF_2, cm^{-1}): 2963-2850; 1736; 1611; 1576; 1518; 1448; 1336; 1164; 1002.

SEC: (THF): M_W= 47900 g/mol; M_N=45600 g/mol; PDI=1.05.

T_g: 57.9 °C

4.3.2 SYNTHESIS OF POLY(ENDO,EXO-DI(2-NITROBENZYL) BICYCLO[2.2.1] HEPT-5-ENE-2,3-DICARBOXYLATE-CO- ENDO,EXO-DIMETHYL BICYCLO[2.2.1]HEPT-5-ENE-2,3-DICARBOXYLATE) (POLY(1-CO-3))

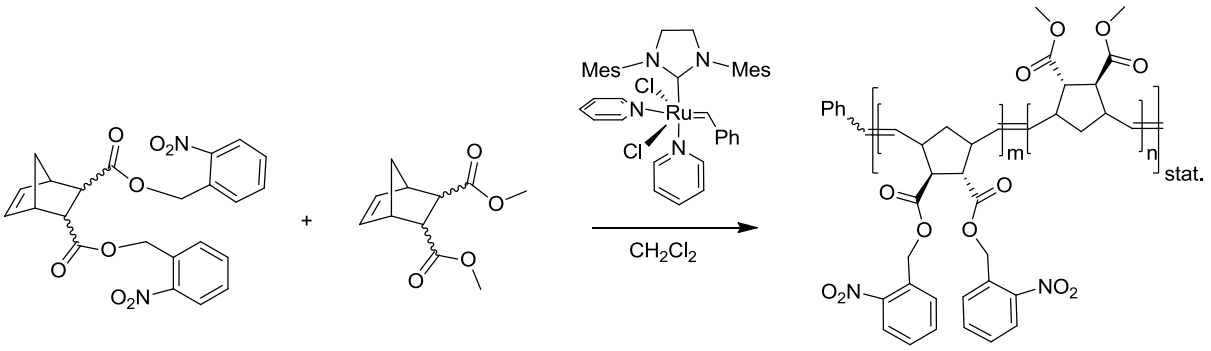

M-1 **M-3** **poly(1-co-3)**

A solution of 10.7 mg of Grubbs 3rd generation catalyst (G-3) dissolved in 1 ml of CH_2Cl_2 was added to 831 mg of monomer M-1 and 1.158 g of M-3 dissolved in 5 ml of dichloromethane and stirred at RT for 3 h. After complete conversion (TLC), the reaction was stopped by adding of 0.15 ml ethylvinylether. Then the polymer was recrystallized two times in cold methanol and dried under vacuum.

Yield: 1.625 g (81.7 %)

^{1}H-NMR: (δ, 400 MHz, 20°C, $CDCl_3$): 8.01 -7.37 (8H, ph); 5.6-5.1 (4H, (CH=CH) + 4H, (O-CH_2-ph)); 3.74-3.03 (8H, $nb^{1,2,3,5}$), (6H,-CH_3); 1.91-1.55 (4H, nb^4) ppm.

IR-Data (CaF_2, cm^{-1}): 3037-2860; 1736; 1620; 1578; 1518; 1430; 1336; 1198; 1168

SEC (THF): M_W= 32080 g/mol; M_N=30850 g/mol; PDI=1.04.

T_g: 62 °C

4.3.3 SYNTHESIS OF POLY(ENDO,EXO-DI(2-NITROBENZYL) BICYCLO[2.2.1] HEPT-5-ENE-2,3-DICARBOXYLATE-CO- ENDO,EXO-DIPHENYL BICYCLO[2.2.1]HEPT-5-ENE-2,3-DICARBOXYLATE) (POLY(1-CO-2))

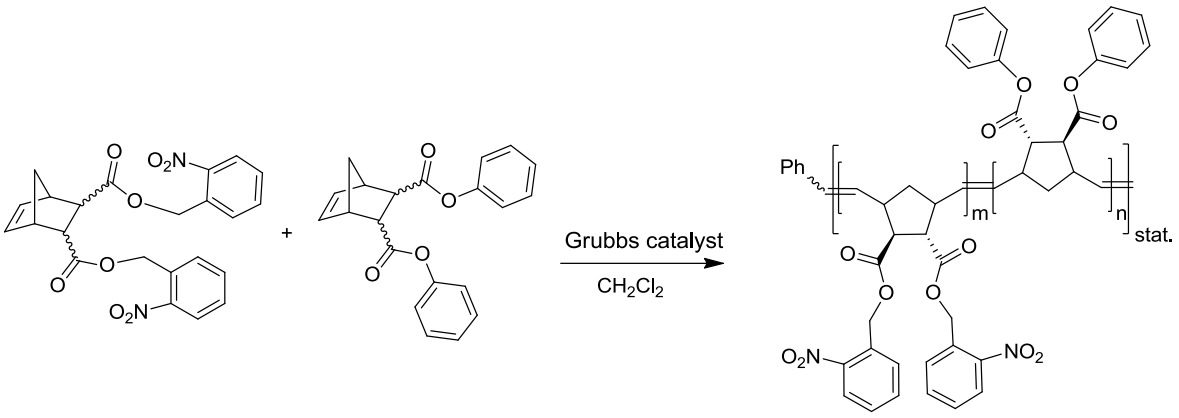

M-1 **M-2** **poly(1-co-2)**

A solution of Grubbs generation catalyst dissolved in 2 ml of CH_2Cl_2 was added to a mixture of monomer (M-1) and monomer (M-2) dissolved in 3 ml of dichloromethane and was stirred at RT. After complete conversion (TLC), the reaction was stopped by adding of 0.15 ml ethylvinylether. Then the polymer was recrystallized two times in cold methanol and dried under vacuum.

Table 5: Specific polymerization data using Grubbs 1st or 3rd generation catalyst

polymer	monomer	mmol	Ratio catalyst monomer	catalyst	µmol	Yield / %
poly(1-co-2)	M-1	0.11	1:120	G-1	2.21	86
	M-2	0.33				
poly(1-co-2)	M-1	0.11	1:120	G-3	2.21	89
	M-2	0.33				

^{1}H-NMR: (δ, 400 MHz, 20°C, $CDCl_3$): 8.01 -7.37 (18H, ph); 5.6-5.1 (4H, CH=CH) (4H, O-CH_2-ph); 3.74-3.03 (8H, $nb^{1,2,3,5}$); 1.91-1.55 (4H, nb^4) ppm.

IR-Data (CaF_2, cm^{-1}): 3125-2800; 1747; 1591; 1528; 1491; 1456; 1380; 1340; 1198; 1160; 1142.

SEC:

Grubbs 1st generation

(THF): M_n= 36700 g/mol; M_w=40.900 g/mol; PDI=1.11.

Grubbs 3rd generation-type

(THF): M_n= 37020 g/mol; M_w=39890 g/mol; PDI=1.08.

Elemental analysis:

70.23 % C, 5.32 % H, 2.17 % N; calculated: 71.2 % C, 5.30 % H, 1.9 % N.

T_g: 79.9 °C

4.3.4 SYNTHESIS OF POLY-N-FORMYLANILINE (EMERALDINE BASE)

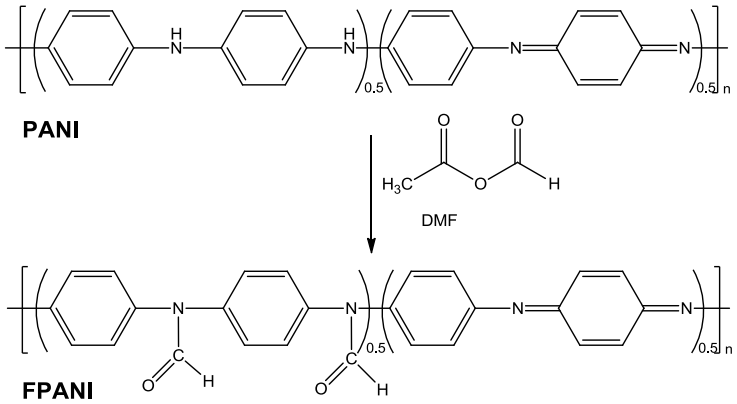

3 ml of a mixture of acetanhydride and formic acid (2:1 vol. ratio) was added under stirring to a solution of 100 mg of polyaniline in 50 mL dimethylformamide (anhydrous). To exclude light from the reaction aluminium foil was used. The reaction stirred at 50 °C for 48 h under exclusion of light. The colour of the mixture turned slowly from dark blue into dark brown. In a next step the product was precipitated by adding 20 ml ammonium hydroxide solution (10 %). After four hours of stirring the precipitate was filtered and rinsed with distilled water. The product was dried in the vacuum oven at 50 °C.

Yield: 69.6 mg of a dark brown solid.

^{1}H-NMR: (δ, 400 MHz, 20 °C, DMSO): 8.73-8.42 (m, 1H, H-C=O-N); 7.51-6.83 (m, 4H, CH) ppm.

IR-Data: (CaF_2, cm^{-1}): 3332; 1674; 1604; 1511; 1430; 1319; 1270; 1138.

T_g: 160 °C

4.4 SYNTHESIS OF GRUBBS-TYPE 3RD GENERATION (G-3) CATALYST

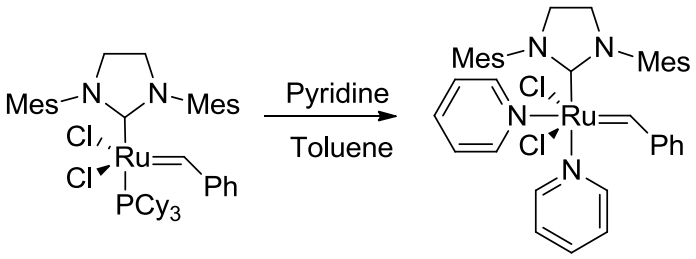

G-3

A solution of G-2 catalyst (H_2IMes)-(PCy_3)$(Cl)_2$Ru=CHPh (155.3 mg; 0.18 mmol) dissolved in 5 ml of toluene was added dropwise to pyridine under stirring (736 mg; 9.31 mmol). A discolouration from purple to green was observed. After 3 h a precipitation of the catalyst from solution using 40 ml of degassed n-heptane was performed under stirring. After filtration and cleaning with n –heptane the catalyst was dried under vacuum.

Yield: 126.5 mg (95 %) of a green solid.

4.5 CHEMICALS AND SUBSTRATES APPLIED

4.5.1 CHEMICALS

Solvents used for the synthesis, such as toluene have been distilled and dried under ambient conditions. All other chemicals were purchased from commercial sources and used without further purification. All experiments were carried out under inert atmosphere using Schlenk techniques or a glove box.

Table 6: List of chemicals used

Substances	Company	Purity
Acetic acid	Roth	Rotipuran 100 % p.a.
Acetic anhydride	Sigma-Aldrich	p.a.
Acetone	Roth	98 %
Acetonitrile	Riedel-de Haën	SPECTRANAL
Ammonium hydroxide	Sigma-Aldrich	28.0-30.0 % NH_3 basis
Aniline	Sigma-Aldrich	>99 %
Anisol	Sigma-Aldrich	purum, ≥99.0 % (GC) (Fluka)
Bicyclo[2.2.1]hept-5-ene-2,3-dicarbonyl dichloride	Sigma-Aldrich	98 %
Chloroform-d_1	Chemotrade	>99.8 % D
Cyclohexane	Roth	p.a.
Dichloromethane	Merck	p.a.
Diethylether	Merck	p.a.
4-(4,6-Dimethoxy-1,3,5-triazin-2-yl)-4-methylmorpholinium chloride	Sigma-Aldrich	>96 %
Dimethylformamide	Sigma-Aldrich	anhydrous, 99.8 % (Sigma-Aldrich)
DMSO- d_6	Eurisotop	H_2O < 0.02 %
Ethanol	Sigma-Aldrich	chromosolv
Ethyl acetate	Fluka	p.a.
Ethyl vinyl ether	Sigma-Aldrich	98 %
Formic acid	Fluka	puriss. p.a., ~98 % (T) (Fluka)
Grubbs catalyst 1st generation	Sigma-Aldrich	Not stated
Grubbs catalyst 2nd generation	Sigma-Aldrich	Not stated
n-Heptane	Sigma-Aldrich	99.00 %
Hexachloroplatinic acid	Sigma-Aldrich	99.90 %
Hydrochloric acid	Roth	Rotipuran 37 %
Hydrogen Peroxide	Sigma-Aldrich	ACS reagent, 30 wt. % in H_2O

Substances	Company	Purity
Methanol	Riedel-de Haën	purum, ≥99.5 %
1-(2-nitrophenyl)ethanol	Accela Bio Chem	97 %
(2-nitrophenyl)methanol	Sigma-Aldrich	97 %
PEDOT:PSS	Baytron	Not stated
Pent-4-enoyl chloride	Sigma-Aldrich	98 %
Phenol	Sigma-Aldrich	99 %
Phenyl acetate	Sigma-Aldrich	≥99 %
Polyaniline	Sigma-Aldrich	
Pyridine	Sigma-Aldrich	chromosolv
Sodium bicarbonate	Fluka	purum
Sodium sulfate	Fluka	purum, anhydrous, ≥99.0 %
Sulfuric acid	Roth	Rotipuran 98 %
Tetrahydrofurane	Merck	p.a.
Toluene	Roth	≥99.8 %
Trichlorosilane	Sigma-Aldrich	99 %
Trichloromethane	Sigma-Aldrich	NMR reference standard, 1% in acetone-d6 (99.9 atom % D) (Fluka)
Trichloromethane	Roth	≥99 %
2,2,2-Trifluoroethylamine	Sigma-Aldrich	99.5 %
Undec-10-enoyl chloride	Sigma-Aldrich	97 %

4.5.2 SUBSTRATES

Based on the application, various types of substrates have been used.

4.5.2.1 SILICON WAFER AS SUBSTRATE

Single side polished silicon wafers with a native silicon oxide layer from Taisil Electronic Materials Corp. (200mm/CZ/1-0-0/Boron/p-type/ Resis/9-8) have been used as substrates for silane based photoreactive bifunctional molecules as well as substrates for thin spin cast polymeric films.

4.5.2.2 GLASS SUBSTRATE WITH AN ITO (INDIUM TIN OXIDE) LAYER

ITO substrates (CG-61IN) from Delta Technologies were used as conductive substrates for the characterization of spin cast FPANI layers. ITO is well known as electrode material that is fixed on a fused silica substrate by sputtering technique. Features and benefits are high transparency, in the visible range of wavelength, high electrical conductivity (approximately 30 Ω) and excellent work function (4.7 eV).

4.5.2.3 CALCIUM FLUORIDE SUBSTRATE (CaF_2)

Optically polished CaF_2 disks from Korth Kristalle GmbH were applied as substrates for the characterization of the thin polymeric layers. (Ø 20 mm-0.1mm x 2 ±0.1 mm).

4.5.2.4 GOLD SUBSTRATE

Gold substrates from the Arrandee company were also applied as conductive substrates for the characterization of spin cast FPANI layers. The gold substrate consists of borosilicate an interfacial chromoxide layer (2.5 +/-1.5) and a goldlayer (thickness 250 nm) on top of the substrate.

4.6 ANALYTICAL EQUIPMENT AND METHODS

4.6.1 THIN-FILM-CHROMATOGRAPHY

The reactions were monitored by TLC (Silica gel 60 F_{254} on aluminium, Merck). Detection: UV-light (254 nm and 365 nm for fluorescent/phosphorescent compounds)and staining with molybdate/H_2SO_4 (dip: a solution of 10 g ammonium molybdate in 1000 mL 10 % H_2SO_4 and a solution of 8 g cerium sulphate tetrahydrate in 80 mL 10 % H_2SO_4 were mixed) or potassium permanganate (2 % dissolved in H_2O deionized). As mobile phase mixtures of ethyl acetate und cyclohexane were used.

4.6.2 FTIR SPECTROSCOPY

The FTIR spectroscopy was performed with a Fourier-Transformation-Infrared-spectrometer (Perkin Elmer Spectrum One instrument). The spectral range lies in between 4000 cm^{-1} and 800cm^{-1}. All IR spectra were recorded in transmission mode using a pyroelectrical DTGS-detector. (DTGS = DeuteratedTriglycineSulphate). The samples were investigated as thin films spin cast on CaF_2 discs.

4.6.3 UV-VIS SPECTROSCOPY

UV-Vis spectra were recorded with a Varian Cary 50 conc.-spectrophotometer. Therefore, all UV-Vis spectra were measured in absorbance mode, in a range of 200 nm - 800 nm. The samples were investigated as thin films spin cast on CaF_2 discs.

4.6.4 NUCLEAR MAGNETIC RESONANCE SPECTROSCOPY (NMR)

^{1}H-NMR and ^{13}C-NMR spectra were performed using a Varian 400- NMR spectrometer operating at 399.66 and 100.5 MHz, respectively, and were referenced to Tetramethylsilane $Si(CH_3)_4$. A relaxation delay of 10s and 45° pulses were used for acquisition of the ^{1}H-NMR spectra. Peak shapes are indicated as follows: s (singlet), d (doublet), dd (doublet of

doublet), t (triplet), m (multiplet). Solvent residual peaks were used for referencing the NMR spectra to the corresponding values given in literature.[156]

4.6.5 CONTACT-ANGLE MEASUREMENTS

The surface tension σ of the sample surfaces was determined by measuring the contact angle with a Drop Shape Analysis System DSA100 (Krüss GmbH, Hamburg, Germany) using water and diiodomethane as test liquids (drop volume ~ 15 μL). The contact angles were obtained by means of the sessile drop method and were measured within 2 s. Based on the Owens-Wendt method, the surface tension σ as well as the dispersive and polar components (σ^d and σ^p) were calculated.

4.6.6 ATOMIC FORCE MICROSCOPY (AFM)

Atomic force microscopy (AFM) in intermittant contact mode and lateral force mode (also termed friction-force microscopy; FFM) were employed to characterize the surface properties of the prepared films. Friction force microscopy measurements were carried out on an Asylum MFP-3D atomic force microscope (Asylum Research).The probes used were silicon nanoprobes. The nominal force constants of these probes were 0.06 or 0.12 N m^{-1}.

4.6.7 CONDUCTIVE ATOMIC FORCE MICROSCOPY (CAFM)

The conductivity of patterned films in the submicron-scale is studied with conductive atomic-force microscopy (CAFM) measurements, operating in contact mode, using a Asylum MFP-3D atomic force microscope (Asylum Research). A home-made CAFM amplifier allowed current detection with a peak to peak noise level below 30 fA. TiN coated single crystal n-doped Si cantilevers from NT-MDT with a force constant between 0.003 N m^{-1} and 0.13 N m^{-1} and a tip radius of about 35 nm were used. For these experiments, FPANI was coated on ITO/glass substrates in order to provide a conductive substrate.

4.6.8 KELVIN PROBE FORCE MICROSCOPY (KPFM)

The KPFM measurements on an illuminated and protonated sample were performed employing TiN coated cantilevers with a force constant from 0.35 to 6.1 N m^{-1} and a resonance frequency between 47 and 150 kHz.

4.6.9 ELLIPSOMETRY

For ellipsometric measurements and a 10 mg/mL solution of the corresponding polymer dissolved in anisole was spincast on silicon wafers. Ellipsometric measurements were carried out with a Woolam VASE spectroscopic ellipsometer (Xenon short arc lam, wavelength range 240-1100 nm, spectral bandwidth 4 nm). The implemented software uses the Levenberg-Marquardt fit algorithm.

4.6.10 SECONDARY ION MASS SPECTROMETRY (SIMS)

Samples for analysis were cut to 2 × 15 mm size to maximise the number of samples that can be analyzed. As there was contact between the metal surface and the sample holder, surface charging was therefore not a problem. Static SIMS experiments were carried out using a TOF-SIMS IV instrument (Ion-ToF GmbH, Münster, Germany) equipped with a Bismuth ion gun and a single-stage reflectron time-of-flight analyser. A minimum of 2 spectra per sample and multiple samples were analyzed. All spectra were plotted as intensity (counts per second) vs. m/Z.

4.6.11 X-RAY PHOTOELECTRON SPECTROSCOPY (XPS)

XPS spectra were performed with a monochromatic K-Alpha spectrometer equipped with an Al X-ray source (1486.6 eV) operating with a base pressure in the range of 10^{-8} to 10^{-10} mbar. Charge compensation for insulator samples were compensated with an Ar Flood gun. High resolution scans of the F1s region were acquired at pass energy of 20 eV and a step size (resolution) of 0.1 eV. Survey scans were acquired with pass energy of 100 eV and a step size of 1.0 eV. All spectra have been normalized to the Au 4f7/2 peak. To minimize

irradiation damage caused by X-rays, a low excitation power was used and only one scan at each point was performed. All samples had a size of 1x1 cm^2 and only one half was UV illuminated while the other half was covered. The spatial resolution of the analyzer (400 µm diameter) ensured that each half could be measured separately.

4.6.12 X-RAY REFLECTIVITY (XRR)

XRR measurements have been performed on the PANalytical Empyrean diffractometer with a multilayer mirror and a Pixcel detector using copper radiation (λ=1.54 nm). The measured XRR data has been simulated with the software package X´Pert Reflectivity 1.3 (PANalytical), which uses the Parratt[157] formalism and the Névot approach[158] to get the layer quantities. The software comprises a genetic fitting algorithm to simulate the measured data.

4.6.13 SIZE EXCLUSION CHROMATOGRAPHY (SEC)

Weight and number average molecular weights (M_w and M_n), as well as the polydispersity index PDI=M_w/M_n, were determined by size exclusion chromatography (SEC) using Polymer Laboratories chromatograph GPC-50 (Church Stretton, UK) equipped with a differential refractometer. Separation columns from Polymer Laboratories (7.5 mm*300 mm, PLgel Mixed-C, STV 5 µm grade size) were applied. Polystyrene standards from Polymer Standard Service were used for calibration. All SEC runs were performed with THF as eluent.

4.7 UV-IRRADIATION EXPERIMENTS

In these experiments different types of lamps have been applied. For the cleavage of the o-nitrobenzyl ester groups the illumination process was carried out with a medium pressure Hg lamp (100 W, from Newport, model 66990) equipped with a filter for the wavelength >300 nm (power density of 13.2 mW cm^{-2}).

Photolithographic patterning was performed using a mask aligner (model MJB4 from SUSS, Germany) with a 500 W HgXe lamp and equipped with a filter transmissive for the wavelength range 270–353 nm (P= 37 mW cm^{-2}).

For photo-Fries-rearrangement the light of a monochromatic medium pressure mercury lamp (Heraeus) with a power density of 178 µW cm^{-2} was used. In these irradiation experiments, the light intensity (power density) at the sample surface was measured with a spectroradiometer (Solatell, Sola Scope 2000TM, spectral range from 230 to 470 nm) and the intensity needed was analyzed separately.

Additionally, a laser system operating at a wavelength of 325 nm for scanning near field optical microscopy was used. Therefore, the laser was coupled to a Thermo Microscopes Aurora III near-field scanning optical microscope (Veeco UK, Cambridge, U.K.) fitted with a fused-silica fiber probe (Veeco, Cambridge, U.K.). The probe scan velocity was 0.1 µm s^{-1}.

5 ANALYTICAL METHODS FOR THIN FILM CHARACTERIZATION

5.1 CONTACT ANGLE MEASUREMENT

The Contact angle measurement (CA) represents a simple and extremely sensitive method for surface analysis. A conveniant approach is the sessile drop technique, where drops of liquid with a defined volume are deposited on smooth solid surfaces. Using this method the surface energy of solids, measured in units of Joules per area, is determined. Therefore, a droplet of liquid is directly placed on the solid. After reaching equilibrium at the three phase boundary (intersection of liquid, gas and solid) a tangent line drawn from the droplet to the touch of the solid surface forms an angle between the tangent line and the solid surface.[159] This angle is called the contact angle. Using liquids with well-known properties the resulting interfacial tension can be used to identify the nature of the solid.

In 1805 YOUNG had already formulated a relationship between the interfacial tensions at a point on a 3-phase contact line.

$$0 = \sigma_S - \sigma_{SL} - \sigma_L \cdot \cos\theta \tag{4}$$

Where the σ_S and σ_L represent the surface tension indices of the two phases and σ_{SL} is the interfacial tension between the two phases. θ represents the contact angle between the vectors σ_L and σ_{SL}.

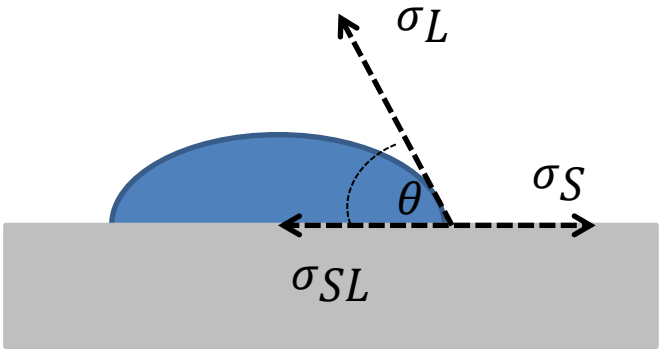

Figure 5.1: Contact angle formation on the three phase method according to YOUNG

Furthermore, OWENS, WENDT, RABEL and KAELBLE extended the calculation of surface tension by additionally splitting up each phase into a polar and a disperse fraction:

$$\sigma_L = \sigma_l^p + \sigma_l^d \quad (5)$$

$$\sigma_S = \sigma_s^p + \sigma_s^d \quad (6)$$

The drop applied on a defined sample surface is analyzed and interpreted by a DSA 100 (Krüss GmbH, Hamburg, Germany). This optical system includes a camera that records the drop shape and subsequently the drop shape is analyzed by a drop shape analysis software, using various models, e.g., the Owens Wendt method.[160]

Moreover, measuring the contact angle the sessile drop method can be performed using static or dynamic drops. While for static measurements the drop volumes remains constant, the drop shape is enlarged or reduced by the dynamic method.

5.2 X-RAY PHOTOELECTRON SPECTROSCOPY (XPS)

X-ray photoelectron spectroscopy, also known as Electron Spectroscopy for Chemical Analysis (ESCA) is a highly sensitive surface analysis technique. The basic idea behind this spectroscopic technique is the determination of the elemental composition as well as chemical and electronical states within the top atomic layers of the samples. Except hydrogen and helium nearly every element can be detected. The technique appears to have first been applied by Kai Siegbahn, who reported about this specific analysis method by investigating cleaved NaCl.

XPS spectra itself are gained by irradiation of materials with sufficiently high energy, i.e. X-rays. Consequently, a special form of photoemission is generated. In this process (depicted in Figure 5.2) an electron of the inner core shell (K shell) gets excited and leaves the sample. With the determination of the recorded kinetic energy, the binding energy (E_B) of the electrons ejected can be calculated and thus, the parent element and atomic energy level are determined. By recording the energies of the photoelectrons ejected a spectrum is obtained where peaks corresponding to the energy bands of core levels are displayed. For that quantitative XPS analysis is accomplished by correlation of the area under a certain peak with the relative concentration of a corresponding atomic species.[161]

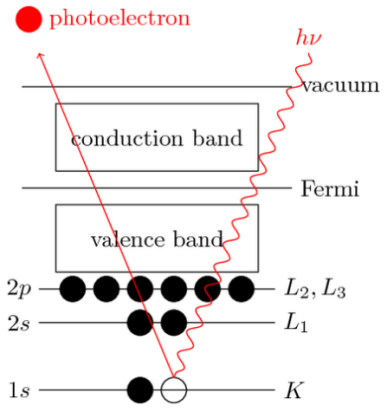

Figure 5.2: Depiction of the principles of X-ray photoelectron spectroscopy[162]

Using equation 7 the binding energy is calculated by the parameters listed below.[163,164]

$$E_B = h\nu - E_{kin} - \phi_W \quad (7)$$

The radiation is emitted from an X-ray source with an energy of 1486.6 eV (Al-Kα) and 1253.6 eV (Mg-Kα) respectively using an aluminum or magnesium anode. For the reduction of the X-ray line width and to avoid satellite peaks a monochromator, e.g., made of glass, is used. As a consequence of exposure to soft X-ray radiation photoelectrons are ejected from the core levels of the sample surface atoms. While the X-rays may penetrate deep into the sample, the escape depth of the ejected electrons is limited. That means, for energies around 1400 eV, ejected electrons from depths greater than 10 nm have a low probability of leaving the surface without undergoing an energy loss event.

The energy of the electrons emitted is subsequently analyzed by a spectrometer. Therefore, the emitted photoelectron has to pass a series of lenses and the hemispherical sector analyser. While the lenses retard the electrons with high kinetic energy and thus increase the resolution the photoelectrons have to pass a pair of concentric hemispherical electrodes. Thus, an electron energy analyser is able to disperse the emitted electrons according to their kinetic energy and to additionally separate the flux of emitted electrons of a particular energy. The electrons arrived are count by a detector. Therefore, electron multipliers are used (channeltrons and channelplates).[165]

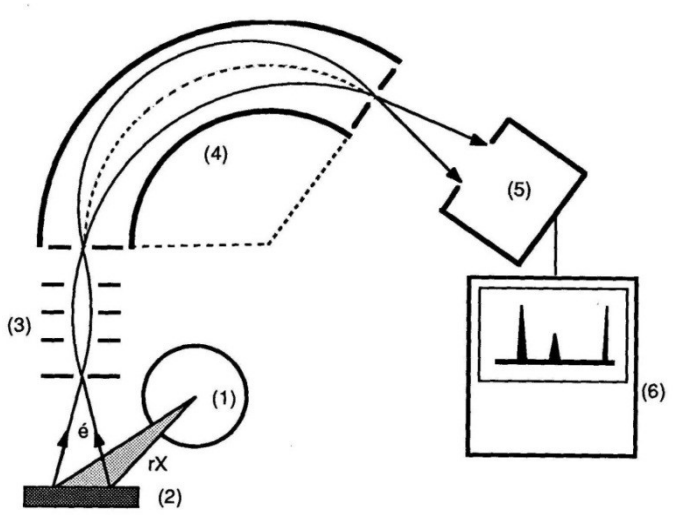

Figure 5.3: X-ray photoelectron spectrometry system. (1) X-rays tube; (2) Sample; (3) Electronic focusing system; (4) Spectrometer; (5) Electrons detector (channeltron); (6) Data acquisition[166]

Furthermore, ultra high vacuum (UHV) conditions are required to enable the emitted photoelectrons to be analyzed without interference from gas phase collisions. It is noteworthy that XPS only detects those electrons that have actually escaped into the vacuum of the instrument.

Special features, such as depth profiling or cleaning of the surfaces are made possible by an ion gun. An additional flood gun enables charge compensation and thus, correct energy peaks are obtained.

5.3 X-RAY REFLECTIVITY METHOD

X-ray scattering analysis are used in material research for investigations of surfaces and interfaces on length scales of several orders of magnitude. X-ray reflectivity (XRR) is a specular diffraction technique which capitalizes on the optical properties of X-rays. During the measurement the incidence angle of the beam is equal to the angle of the diffracted beam (Figure 5.4). The technique utilizes the fact that the refractive index n of any material is less than unity and the phenomena of external total reflection occurs if the incidence angle of the beam is smaller than the critical angle of the material. A further increase of the incident angle results in a deeper beam penetration into the material and constructive interference occurs at the interfaces at a certain angle, which will be measured. The XRR method yields important quantities of single thin films like layer thickness, surface roughness, interface roughness and electron density (scattering decrement) as well as at multilayer arrangements.[167]

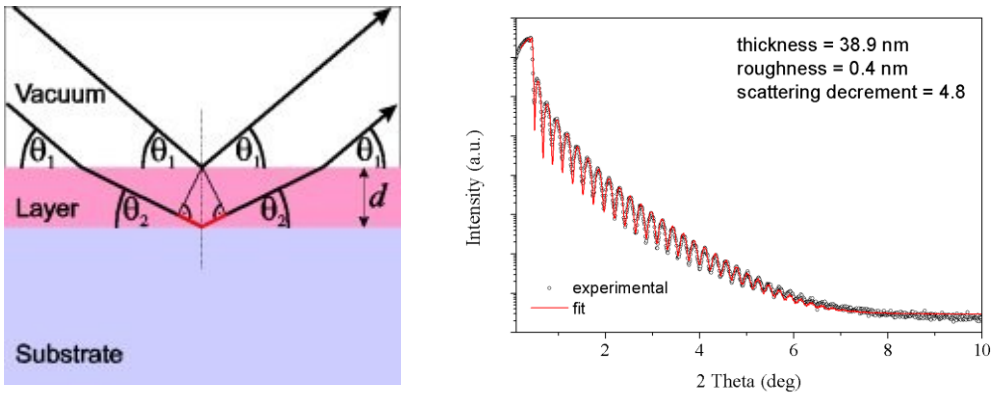

Figure 5.4: Scheme of the X-ray beam path in the sample during an X-ray reflectivity scan (left) and a typical XRR diagram with the layer properties (thickness, roughness and scattering decrement) extracted from simulation of the experimental data (right)[168]

5.4 SCANNING PROBE MICROSCOPY

SPM techniques are based on the interaction of a tip with the sample surface. Local physical quantities are recorded and the surface studied can be visualized by detailed images.

5.4.1 ATOMIC FORCE MICROSCOPY (AFM)

Atomic force microscopy, invented by Binning et al. in 1986, consists of a fine tip, usually made of silicon, that is fixed on the free end of a cantilever.[169] In proximity of the sample surface attractive or repulsive forces resulting from interactions between the tip and the surface cause a positive or negative deflection of the cantilever according to Hooke's law. The deflection is detected by means of a laser beam, which is reflected from the back side of the cantilever into an array of photo diodes. Using a suitable software, images of the sample surface are formed.

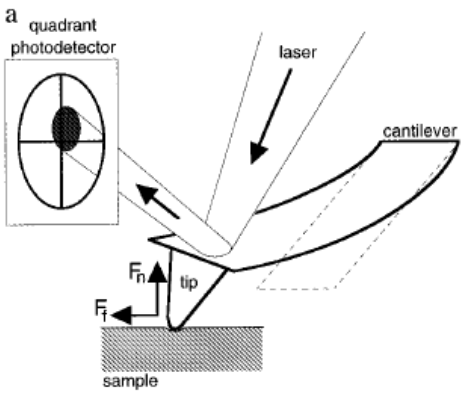

Figure 5.5: Set up the optical beam deflection used for AFM[170]

The application of AFM is widespread. Thus, several types of materials such as metal semiconductors, or biological samples as well as conductive and non-conductive materials can be investigated. Depending on the morphology of the surface resolutions up to fractions of nanometers are possible.

Several forces can be measured by the tip surface interactions, such as contact force, chemical bonding, Van der Waals forces, capillary forces, electrostatic forces, magnetic forces etc.[171]

If the cantilever is positioned less than a few angstroms from the sample surface (contact regime) the interatomic forces between the cantilever and the sample based on electrostatic

regimes are repulsive. In the non-contact regime (distance approximately hundreds of Angstroms) interactions between the cantilever and sample surface are attractive (based on long Van der Waals interactions).

For AFM three different modes of operation are applied:

Contact mode:

Using contact mode two measurement modes can be realized: constant height and constant force. For both modes a soft “physical contact” has to be accomplished. Either using constant height or constant mode the tip has to scan in small height above the sample keeping the condition constant according to the mode applied.

Non-contact mode:

The probe operates in the attractive force region and as a consequence the tip-sample interactions are minimized. The advantage results in a non-destructive measurement method. However, results of sample details do not show that high resolution.

Intermittent contact mode:

In intermittent contact mode (tapping mode) the cantilever is oscillating close to its resonance frequency. Thus, an electronic feedback loop applied has the task to remain the oscillation amplitude constant. The relative contrast in the cantilever oscillation amplitude while scanned over a surface reveals differences in the local sample elasticity. Furthermore, less damage of the sample surface is caused.

5.4.2 LATERAL FORCE MICROSCOPY

Lateral force microscopy, also known as friction force microscopy is a secondary contact AFM mode. Differences of frictional forces are investigated by sliding contacts. A tip is brought into contact with the sample surface and lateral forces that have an impact on the cantilever are collected by the twisting of the cantilever. While the sample surface and the tip slide relative to each other the cantilever is twisted along its axis and consequently leads to a deflection which is detected by a laser beam and the photodetector applied. Usually, to differentiate between changes in the friction of the sample’s surface and the influence of

topography a trace and retrace scan has to be performed. Thus, a decisive change in friction next to topography can be recorded simultaneously. Legett et al.[172] showed that friction force provides information with nm spatial resolution on the properties of molecular structures. Controlling the tip chemistry enables the determination of mixed monolayer systems or the investigation of the alkyl chain organization of these systems. In this thesis FFM measurements are performed to visualize the difference in friction obtained by illumination.

5.4.3 CONDUCTIVE ATOMIC FORCE MICROSCOPY (CAFM)

Conductive atomic force microscopy (CAFM) is a particular mode of AFM for the determination of variations in conductivity of resistive samples. In contrast to STM (Scanning tunnel microscopy), for both methods a voltage has to be applied between the sample and the tip, a conductive cantilever is applied that scans the sample surface in contact mode. This method provides the possibility of mapping the local film conductivity on the nanometre scale using conductive cantilevers. Thus, next to the measurement of localized conductivity, current flows in the range of micro to even femtoamps can be determined, at the same time topography can be captured. The convenient conditions of measurement using conductive AFM attract many applications, such as conductive polymers, ferro-electric films or nanotubes. Conductive atomic force microscopy turned out to be an appropriate method to visualize the obtained contrast of the conductivity between the non-illuminated and the illuminated/doped regions of the patterned FPANI samples.

5.4.4 KELVIN PROBE FORCE MICROSCOPY (KPFM)

KPFM a noncontact atomic force microscopy measurement determines the contact potential difference between tip and sample surface.[173] An electrostatic force between the tip and the sample is caused by different Fermi energies. This electrostatic force can be nullified by applying a bias voltage which ideally is the contact potential difference (difference in work function).Since KPFM is sensitive to electrostatic forces, any source of electrostatic potential influences the KPFM signal. The KPFM results obtained clearly demonstrate a reduction of the work function on the illuminated areas of FPANI.

5.5 SPECTROSCOPIC ELLIPSOMETRY

Spectroscopic ellipsometry is a common optical technique for characterizing thin films and bulk materials. Different samples are characterized by light reflection, respectively transmission of light. Ellipsometry measures a change in polarization as light reflects or transmits from a material structure.[174]

Ellipsometry measures the complex reflectance ratio, ρ

$$\rho = \tan(\Psi)\, e^{i\Delta} \tag{8}$$

The polarization change is represented as an amplitude ratio, Ψ, and the phase difference, Δ between light waves known as p- and s-polarized light waves. The s component oscillates perpendicular to the plane of incidence and parallel to the sample surface, while the p- component is oscillating parallel to the plane of incidence.

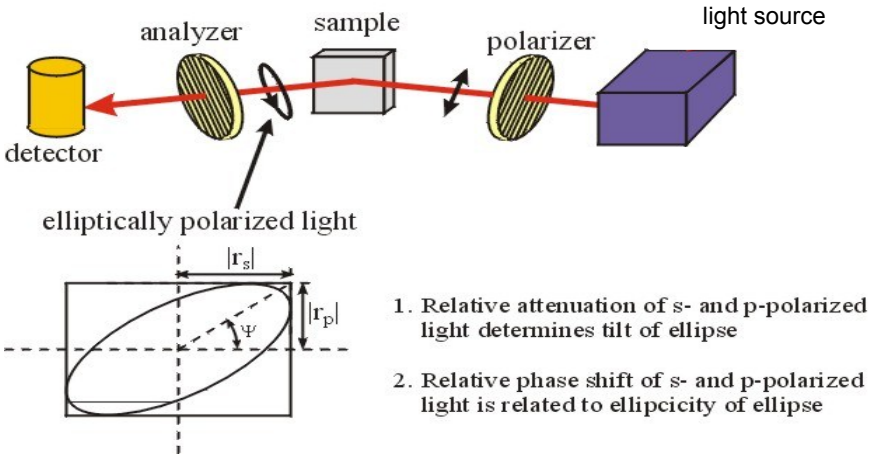

Figure 5.6: Schematic setup of an ellipsometric measurement[175]

Typical ellipsometry configuration, where linearly polarized light is reflected from the sample surface and the polarization change is measured to determine the sample response.

The name ellipsometry itself can be derived from the fact that polarized light, that is necessary for the measurements, becomes “elliptical” upon light reflection. Ellipsometry is a versatile tool for the investigation of optical constants and thin-film thicknesses of samples.[176]

Generally there exist two major restrictions on the ellipsometry measurement:

- A small surface roughness is required
- Oblique incidence has to be ensured

Since the interpretation of the measurement results via amplitude ratio, Ψ, and the phase difference, Δ is complicated an optical model is needed for data analysis. Using this form of data analysis the physical properties including the optical constants and film thicknesses of the sample can be determined. Unlike reflectance/transmittance measurement, ellipsometry allows the direct determination of the refractive index n and extinction coefficient k, which are also referred to as optical constants. These two values are used to determine how light interacts with a material.

5.6 SECONDARY ION MASS SPECTROMETRY (TIME OF FLIGHT)

Secondary ion mass spectrometry (SIMS) is a surface analysis technique that provides detailed information about the first 1 or 2 nm of the sample's surfaces. In SIMS an ion beam is rastered over the surface. The impact of the heavy ions leads to the emission (sputtering) of surface material. Characteristically, one to several atoms are ejected per incident ion. During the ejection process fragmentations of the surfaces become charged atoms or molecules. Positive as well as negative ions can be detected. Furthermore, Time-of-flight of any molecular ion reaching the detector is taken and converted into a molecular mass. By mapping all elements, including helium and hydrogen can be detected and furthermore, imaging of the chemical composition of the surface can be measured.[177] Besides that SIMS high mass resolution enables ions with very similar m/z to be exactely distinguished. The Imaging capability is excellent. Full SIMS spectra with a sub micron spatial resolution are obtained. Images demonstrating the spatial distribution of specific spectral features can be extracted.

5.7 PREPARATION OF THE PHOTOREACTIVE FILMS

5.7.1 PREPARATION OF THIN POLYMERIC FILMS

For photochemical characterizations, thin films of the various polymers (poly-1, poly(1-co-2), poly(1-co-3)) were dissolved in tetrahydrofurane or CH_2Cl_2 (10 mg/ml) and spin cast onto CaF_2-discs. For some distinctive measurements the polymer was spincast as a homogeneous film on silicon wafers. All films of the investigated polymers were coated using the Photo Resist Spinner (Model 4000, Electronic Micro Systems). Depending on the spin coater settings and the solvent the film thickness was determined to be in the range of 60-155 nm. For refractive index measurements film thicknesses of 23-25 nm using anisol were determined.

Due to the poor film forming properties of FPANI, CaF_2 discs, gold/glass substrates and the ITO/glass, were preheated to 100 °C for 30 minutes. The deposition of FPANI layer was performed by spin coating from dimethylformamide solutions (30 mg/ml). In addition the FPANI/DMF solution was heated to 50 °C before deposition.

Table 7: Schedule of the settings for spin casting

Polymer specific data			**Spin cast data**		
polymer	**solvent**	**substrate**	**speed / rpm**	**ramp / rpm s^{-1}**	**dwell / s**
Poly-1, poly(1-co-2), poly(1-co-3)	THF, Anisol, CH_2Cl_2	CaF_2 Ø 20 mm	2000	100	100
Poly-1, poly(1-co-2), poly(1-co-3)	THF, Anisol, CH_2Cl_2	Si Wafer 10x10mm	4000	100	100
FPANI (10-30 mg/mL)	DMF	CaF_2 Ø 20 mm	250	5	800
FPANI (10 mg/mL)	DMF	gold/glass	500	10	800
FPANI (10 mg/mL)	DMF	ITO/glass	500	10	800

5.7.2 PREPARATION OF THIN ORGANIC FILMS (SAMS)

The silicon wafers were first cleaned by piranha solution (70:30, v/v, H_2SO_4/H_2O_2) and subsequently heated to 70°C for 20 min in solution of $NH_4OH/H_2O_2/H_2O$ (1:1:5). The substrates were then rinsed with Milli-Q water and dried.

Immediately after the water dip step, the clean Si/SiO_2 substrates were placed in a 7 mmol solution of SAM-1 respectively SAM-2 in pure toluene (10 ml) for 1h. Adjusting the layer thickness, a defined amount of water saturated toluene was added. After removing the samples from the solution, the samples were rinsed with toluene and dried in a stream of CO_2.

5.8 IRRADIATION EXPERIMENTS

Illumination experiments were performed in a premium steel chamber equipped with a quartz glass, transparent for UV-radiation. Furthermore, the chamber was flushed by nitrogen before (5 min) and during the illumination process. The exposure length stated has to be understood as optimized illumination time, especially in terms of photolithographic structuring. Photo kinetic experiments required longer illumination times.

5.8.1 IRRADIATION OF PHOTOREACTIVE POLYMERS

The irradiation of the photosensitive polymers (poly-1, poly(1-co-2), poly(1-co-3)) was carried out by using a medium pressure Hg lamp (100 W, from Newport, model 66990) equipped with a filter for the wavelength >300 nm. Depending on the experiment performed illumination times were varied.

Furthermore, the second irradiation step for poly(1-co-2) initiating the photo-Fries rearrangement was performed by using a monochromatic (254 nm) low pressure Hg lamp. Depending on the experiment performed illumination times were varied.

Mask Aligner irradiations (MJB4, SUSS Microtec) for the photosensitive polymers (poly-1, poly(1-co-2), poly(1-co-3) were required to last for 3-5 min ($P = 37$ mW cm^{-2}).

UV-irradiation experiments of FPANI were carried out with a medium pressure Hg lamp (100 W, from Newport, model 66990) equipped with a filter for the range of 260 – 320 nm. Photolithographic patterning was carried out 45 min using a mask aligner (model MJB4, SUSS Microtec).

5.8.2 IRRADIATION AND POST-MODIFICATION REACTIONS OF THIN ORGANIC FILMS BASED ON BIFUNCTIONAL MOLECULES (SAMS)

The illumination steps were performed on two different instruments by using an ozone-free mercury medium-pressure UV lamp (100 W, from Newport, model 66990, >300 nm) with a power density of 13.2 mW/cm^2 (irradiation time typically 30 min) and a laser system operating at a wavelength of 325 nm for scanning near field optical microscopy. Flood UV-illumination was carried out in inert atmosphere (N_2).

After the illumination step, the substrates were immersed in a solution of 4-(4,6-Dimethoxy-1,3,5-triazin-2-yl)-4-methylmorpholinium chloride (DMT-MM)[178,179] in milli-Q water. 100 µL of 2,2,2-Trifluoroethylamine were added and reacted for 24 h. The samples then were then rinsed with milli-Q water and dried in a stream of nitrogen.

6 CHARACTERIZATION OF THE ORGANIC THIN FILM TRANSISTORS (OTFTS)

The organic thin film transistor characterized is a three terminal device consisting of a bottom-gate top-contact configuration with gate source and drain electrode.[180] The drain electrode has to be grounded. The device setup is depicted in Figure 6.1.

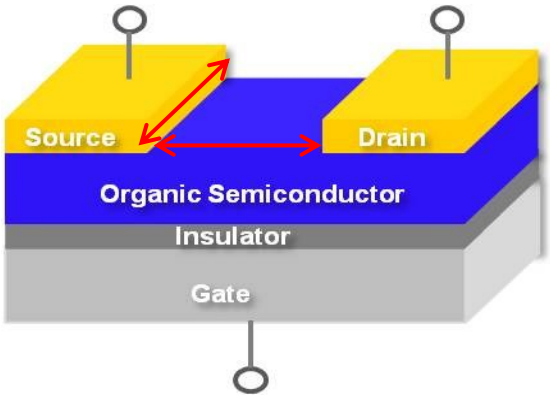

Figure 6.1: OTFT setup: bottom-gate top-contact

Once a voltage (V_G) is applied to the gate electrode charge carriers are accumulated at the semiconductor –insulator interface and a conductive channel is formed. With the increase of the drain voltage, V_D, the source-drain current, I_D, increases linearly. The current flow can be modulated by the gate voltage (V_G) applied. That kind of transistor is known to be turned off when the gate voltage is 0. Inversely the current flow increases as soon as a higher voltage is applied and more mobile charges are generated in the channel.

6.1 OUTPUT CHARACTERISTICS AND TRANSFER CHARACTERISTICS OF AN OTFT

The characterization of the transistor is based on two main parameters: The output characteristics and the transfer characteristics. One obtains the transfer characteristic by sweeping V_G while V_D is fixed. The output characteristic is obtained by a sweep of V_D while V_G is fixed. The typical output characteristics of an OTFT are presented in Figure 6.2.

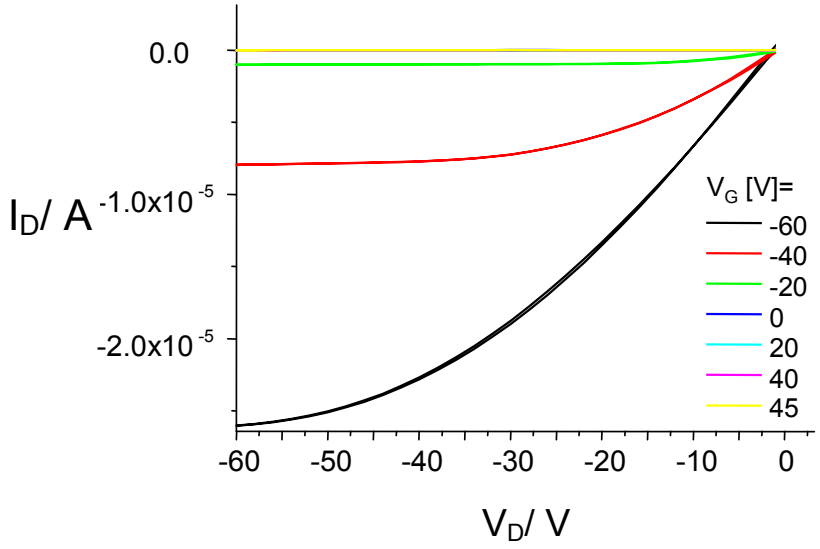

Figure 6.2: Classical OTFT output characteristics. The drain current (I_D) is plotted against the source-drain voltage V_D. V_G is fixed[66]

The application of different constant gate voltages (V_G) results in the linear up to the saturation regime. The linear region is marked by high gate voltages and smaller drain voltage and the drain current increases linear with regard to the drain voltage. As soon as the drain voltage reaches higher values the drain current decreases until the saturation regime is obtained and the so called pinch-off is observed. From the output characteristics the saturation behavior and possible problems with a too high contact resistance can be readily seen.

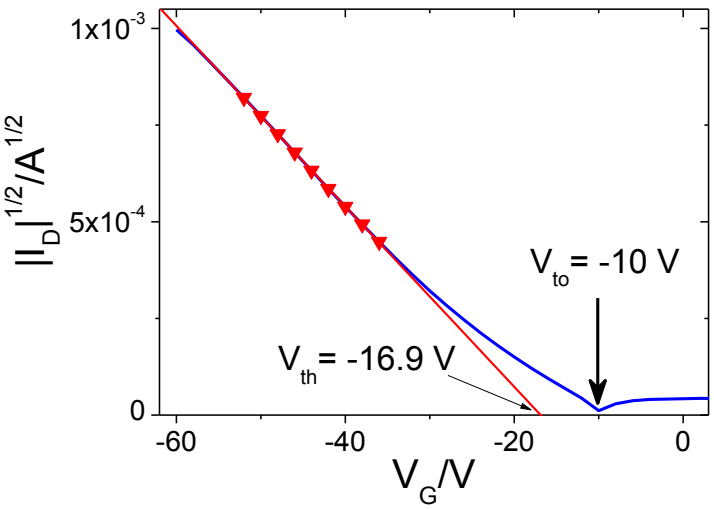

Figure 6.3: Classical transfer characteristics of an OTFT[66]

Important transistor facts can be extracted from the transfer characteristic: the threshold V_{TH} and turn-on V_{TO} voltages. The Turn-on voltage is understood as the gate voltage when the drain current starts to flow. For determination of the charge-carrier mobility and threshold voltage some approximations are essential.[117, 118]

6.2 PREPARATION OF AN ORGANIC FIELD EFFECT TRANSISTOR

Highly p-doped silicon wafers with a 155 nm thick layer of thermally grown SiO_2 purchased from Siegert Consulting e.K. (Aachen, Germany) were used as gate electrode and insulator layer. All wafers were O_2-plasma etched for 30 s and then rinsed in deionized H_2O in an ultrasonic bath for 120 s. Subsequently, the photoreactive polymer poly-1 was spin-cast from a solution in tetrahydrofuran (4 mg mL^{-1}) at 1000 rotations per minute (rpm) for the first 9 s and at 2000 rpm for the following 40 s. The films obtained showed a thickness of 35 nm, as determined by X-ray reflectivity measurements. Afterwards, pentacene layers with an average thickness of 35 nm (measured with a quartz-microbalance) were evaporated at a base pressure of 1×10^{-5} mbar, while the substrates were kept at room temperature. The first 5 nm were evaporated at a rate of 0.02 A s^{-1} and the subsequent 30 nm at a rate of 0.1 A s^{-1}. Then a 50-nm-thick Au source and drain electrodes were deposited through a shadow mask at a base pressure of 4×10^{-6} mbar. The resulting channel length and width were 50 µm and 7 mm, respectively.[118,125]

7 APPENDIX

7.1 ABBREVIATION LIST

AFM	Atomic force microscopy
CaF_2	Calcium fluoride
CAFM	Conductive atomic force microscopy
CD	Compact disc
CH_2Cl_2	Dichloromethane
CO_2	Carbon dioxide
DFB	Distributed feedback
DMF	*N,N*-Dimethylformamide
DMSO	Dimethyl sulfoxide
DMT-MM	4-(4,6-Dimethoxy-1,3,5-triazin-2-yl)-4-methylmorpholinium chloride
DVD	Digital versatile disc
E_B	Binding energy
EB	Emeraldine base
E_{kin}	Kinetic energy
ES	Emeraldine salt
ESCA	Electron spectroscopy for chemical analysis
FFM	Friction-force microscopy
FPANI	Formylated polyaniline
FTIR	Fourier transform infrared spectroscopy
h	Planck`s constant
HgXe-lamp	Mercury-xenon lamp
HCl	Hydrochloric acid
HNO_3	Nitric acid
I_D	Drain current
ITO	Indium tin oxide
J	Current density
KPFM	Kelvin probe force microscopy
LES, LEB	Leuco emeraldine base/salt
m	Mass
Milli-Q	Water, typically 18.2 MΩ·cm
M_W	Weight average molar mass

M_N	Number average molar mass
N_A	Number of molecules reacting
N_Q	Number of photons absorbed
N_2	Nitrogen
NaCl	Sodium chloride
$NaHCO_3$	Sodium bicarbonate
n	Refractive index
Δn	Change in refractive index
n-doped	Negative doped
$(NH_4)_2S_2O_8$	Ammonium persulfate
NCS	Isothiocyanate
NMP	*N*-methylpyrrolidone
NMR	Nuclear magnetic resonance
OTFT	Organic thin film transistor
OLED	Organic light emitting diode
P	Power density
PAG	Photo acid generator
PANI	Polyaniline
PB, PS	Pernigraniline base(salt)
PDI	Poly dispersity index
p-doped	Positive doped
PEDOT/PSS	Poly(3,4-ethylenedioxythiophene) poly(styrenesulfonate)
PMMA	Polymethylmethacrylate
q	Elementary charge
S_1	Excited singlet state
SAM	Self assembled monolayer
SCN	Thiocyanate
SEC	Size exclusion chromatography
Si	Silicon
SiO_2	Silicon oxide
SIMS	Secondary ion mass spectrometry
T_1	Excited triplet state
Tg	Glass transition temperature
THF	Tetrahydrofurane
TLC	Thin layer chromatography

TiN	Titanium nitride
UV	Ultraviolet
UV-Vis	Ultraviolet-visible
V_D	Drain voltage
V_G	Gate voltage
V_{TH}	Threshold voltage
V_{TO}	Turn on voltage
XPS	X-ray photoelectron spectroscopy
XRR	X-ray reflectivity

θ	Contact angle
λ	Wavelength
μ	Mobility
σ_L	Surface tension index of the liquid phase
σ_{SL}	Interfacional tension index (solid-liquid)
σ_S	Surface tension index of the solid phase
σ^d	Dispersive part of surface tension
σ^p	Polar part of surface tension
ϕ_W	Work function
ϕ	Overall quantum yield
φ	Barrier height
Ψ	Amplitude ratio

7.2 LIST OF FIGURES

7.3 LIST OF TABLES

7.4 LIST OF PUBLICATIONS

2012

Edler, M.; Mayrbrugger, S.; Fian, A.; Trimmel, G.; Radl, S.; Kern, W.; Griesser, T.
Wavelength selective refractive index modulation in a ROMP derived polymer bearing phenyl- and ortho-nitrobenzyl ester groups.
Submitted, October 2012

Moser, A.; Flesch, H.-G.; Marchl, M.; Edler, M.; Grießer, T.; Außerlechner, S. J.; Haase, A.; Smilgies, D.-M.; Jakabovic, J.; Resel, R.
Crystallization of pentacene thin films on polymeric dielectrics.
Synthetic Metals 161 (2012), 2598 – 2602

Grießer, T.; Radl, S.; Köpplmayr, T.; Wolfberger, A.; Edler, M.; Pavitschitz, A.; Kratzer, M.; Teichert, C.; Rath, T.; Trimmer, G.; Schwabegger, C.; Sitter, H.; Kern, W.
UV-induced modulation of the conductivity of polyaniline: towards a photo-patternable charge injection layer for structured organic light emitting diodes.
Journal of Materials Chemistry 22 (2012), 2922 – 2928

Schenk, V.; Ellmaier, L.; Rossegger, E.; Edler, M.; Grießer, T.; Weidinger, G.; Wiesbrock, F.
Water-developable poly(2-Oxazoline)-based negative photoresists.
Macromolecular Rapid Communications 33 (2012), Issue 5, 396 – 400

Edler, M.; Rath, T.; Schenk, A.; Fischereder, A.; Haas W.; Edler, M.; Chernev, B.; Kunert, B.; Hofer, F.; Resel, R.; Trimmel, G.
Copper zinc tin sulfide layers prepared from solution processable metal dithiocarbamate precursors.
Journal of Materials Chemistry and Physics 136, 2-3, (2012) 582-588

2011

Marchl, M.; Edler, M.; Haase, A.; Fian, A.; Trimmel, G.; Grießer, T.; Stadlober, B.; Zojer, E.
Tuning the threshold voltage in organic thin-film transistors by local channel doping using photoreactive interfacial layers.
Advanced Materials 22 (2011), 5361 - 5365

2010

Marchl, M.; Golubkov, A. W.; Edler, M.; Grießer, T.; Pacher, P.; Haase, A.; Stadlober, B.; Belegratis, M.; Trimmel, G.; Zojer, E.
Photochemical control of the carrier mobility in pentacene-based organic thin-film transistors.
Applied Physics Letters 96 (2010), 213303 – ff

26 contributions to conference presentations (talks and posters) at national and international conferences.

7.5 CURRICULUM VITAE

Personal data

Name	Matthias Edler, Dipl.-Ing. (M.Sc.)
Born	03.06.1982, Graz, Austria
Nationality:	Austria

Career history

06/2000	Matura at the BG, BRG Graz-Seebachergasse
10/2000 – 05/2001	Military service
10/2001 – 09/2008	Studies in Technical Chemistry at the TU Graz Diploma Thesis: „Optimization of a pharmaceutical tank, mass transfer and rheological behaviour”
06/2006 – 09/2006	Research Stay as Summer Student at Syracuse University (USA)
02/2007 – 06/2007	Erasmus student exchange at UTC Compiègne (FRANCE)
01/2009 – 2012	PhD work on tuning of surfaces by photoreactive thin films and monolayers, NFN- Project: “Interface controlled and functionalized organic films“ under supervision of Univ.-Prof. Mag.rer.nat. Dr.techn. Wolfgang Kern
01/2012 –	Research assistant at the CD-Laboratory for Polymer-Based Printer Ink, University of Leoben

8 LITERATURE

1 H. Klauk, *Organic electronics: Materials, manufacturing and applications*, Wiley-VCH, Weinheim **2006**.

2 T. Griesser, J.-C. Kuhlmann, M. Wieser, W. Kern, G. Trimmel, *Macromolecules* **2009**, *42*, 725–731.

3 T. Griesser, T. Höfler, G. Jakopic, M. Belzik, W. Kern, G. Trimmel, *J. Mater. Chem.* **2009**, *19*, 4557.

4 T. Griesser, A. Wolfberger, M. Edler, M. Belzik, G. Jakopic, G. Trimmel, W. Kern, *J. Polym. Sci. A Polym. Chem.* **2010**, *48*, 3507–3514.

5 H. Klauk, D. J. Gundlach, Jackson Thomas N., IEEE **1999**, *20*.

6 C. Huang, H. E. Katz, J. E. West, *Langmuir* **2007**, *23*, 13223–13231.

7 J.-P. Fouassier, *Fundamentals and methods*, Elsevier Applied Science, London **1993**.

8 J.-P. Fouassier, *Photoinitiation, photopolymerization, and photocuring: Fundamentals and applications*, Hanser; Hanser/Gardner, New York, Cincinnati **1995**.

9 S.-J. Sung, K.-Y. Cho, J.-H. Yoo, W. S. Kim, H.-S. Chang, I. Cho, J.-K. Park, *Chemical Physics Letters* **2004**, *394*, 238–243.

10 S. Lochbrunner, M. Zissler, J. Piel, E. Riedle, A. Spiegel, T. Bach, *J. Chem. Phys.* **2004**, *120*, 11634.

11 C. Bochet, *J. Chem. Soc., Perkin Trans. 1* **2002**.

12 L. Sharma, T. Kimura, *Polym. Adv. Technol.* **2003**, *14*, 392–399.

13 G. Berkovic, V. Krongauz, V. Weiss, *ChemInform* **2000**, *31*, no.

14 H. Kudo, M. Yamamoto, T. Nishikubo, O. Moriya, *Macromolecules* **2006**, *39*, 1759–1765.

15 S. C. Martin, N. Singh, S. C. Wallace, *J. Phys. Chem.* **1996**, *100*, 8066–8069.

16 M. Hoshino, F. Ebisawa, T. Yoshida, K. Sukegawa, *Journal of Photochemistry and Photobiology A: Chemistry* **1997**, *105*, 75–81.

17 J. Träger, J. Heinzer, H.-C. Kim, N. Hampp, *Macromol. Biosci.* **2008**, *8*, 177–183.

18 G. J. Leggett, *Chem. Soc. Rev.* **2006**, *35*, 1150.

19 S. Sun, D. Thompson, U. Schmidt, D. Graham, G. J. Leggett, *Chem. Commun* **2010**, *46*, 5292.

20 P. Ribič, V. Kalihari, C. Frisbie, G. Bratina, *Phys. Rev. B* **2009**, *80*.

21 G. Hernandez-Sosa, C. Simbrunner, T. Höfler, A. Moser, O. Werzer, B. Kunert, G. Trimmel, W. Kern, R. Resel, H. Sitter, *Organic Electronics* **2009**, *10*, 326–332.

22 P. Pacher, A. Lex, V. Proschek, H. Etschmaier, E. Tchernychova, M. Sezen, U. Scherf, W. Grogger, G. Trimmel, C. Slugovc, E. Zojer, *Adv. Mater.* **2008**, *20*, 3143–3148.

23 W. S. Klug, M. R. Cummings, *Concepts of genetics*, Prentice Hall, Upper Saddle River, N.J **op. 1997**.

24 B. Wardle, *Principles and applications of photochemistry*, Wiley; John Wiley distributor, Hoboken, N.J, Chichester **2008**.

25 K. Fries, G. Finck, *Ber. Dtsch. Chem. Ges.* **1908**, *41*, 4271–4284.

26 J. Anderson, Reese C.B., *Proc. Chem. Soc.* **1960**.

27 C. E. Kalmus, D. M. Hercules, *J. Am. Chem. Soc.* **1974**, *96*, 449–456.

28 H. Barzynski, D. Sänger, *Angew. Makromol. Chem.* **1981**, *93*, 131–141.

29 Giacomo Ciemioian und P. Silber **1901**.

30 J. A. Barltrop, P. J. Plant, P. Schofield, *Chem. Commun. (London)* **1966**.

31 C. H. Bamford, R. G. W. Norrish, *J. Chem. Soc.* **1935**.

32 T. Köpplmayr, M. Cardinale, G. Jakopic, G. Trimmel, W. Kern, T. Griesser, *J. Mater. Chem.* **2011**, *21*, 2965.

33 T. Höfler, T. Grießer, M. Gruber, G. Jakopic, G. Trimmel, W. Kern, *Macromol. Chem. Phys.* **2008**, *209*, 488–498.
34 T. Griesser, T. Höfler, S. Temmel, W. Kern, G. Trimmel, *Chem. Mater.* **2007**, *19*, 3011–3017.
35 T. Höfler, T. Grießer, X. Gstrein, G. Trimmel, G. Jakopic, W. Kern, *Polymer* **2007**, *48*, 1930–1939.
36 H.-G. Unger, *Planar optical waveguides and fibres*, Clarendon Press, Oxford;, New York **1977**.
37 R. A. Lessard, G. Manivannan, *Selected papers on photopolymers: Physics, chemistry, and applications*, SPIE Optical Engineering Press, Bellingham, Wash **1995**.
38 T. D. Milster, Y. Zhang, *MRS Bull.* **2006**, *31*, 318–323.
39 R. S. Moshrefzadeh, D. K. Misemer, M. D. Radcliffe, C. V. Francis, S. K. Mohapatra, *Appl. Phys. Lett.* **1993**, *62*, 16.
40 A. Natansohn, P. Rochon, C. Barrett, A. Hay, *Chem. Mater.* **1995**, *7*, 1612–1615.
41 H. J. Coufal, D. Psaltis, G. T. Sincerbox, *Holographic data storage: With 12 tables*, Springer, Berlin **2000**.
42 I. Assaid, D. Bosc, I. Hardy, *J. Phys. Chem. B* **2004**, *108*, 2801–2806.
43 M. Shirai, W.-G. Ma, M. Tsunooka, *European Polymer Journal* **1993**, *29*, 913–918.
44 T. Griesser, T. Höfler, S. Temmel, W. Kern, G. Trimmel, *Chem. Mater.* **2007**, *19*, 3011–3017.
45 D. Stifter, H. Sitter, *Appl. Phys. Lett.* **1995**, *66*, 679.
46 A. Andreev, G. Matt, C. Brabec, Sitter H., D. Badt, Seyringer H., Sariciftci N.S., *Adv. Mater.* **2000**.
47 F. Schreiber, *Progress in Surface Science* **2000**, *65*, 151–257.
48 A. Ulman, *An introduction to ultrathin organic films: From Langmuir-Blodgett to self-assembly*, Academic Press, Boston **1991**.
49 W. A. Zisman, *Ind.& Eng. Chem.* **1969**.
50 J. Sagiv, *J. Am. Chem. Soc.* **1980**, *102*, 92–98.
51 L. Netzer, J. Sagiv, *J. Am. Chem. Soc.* **1983**, *105*, 674–676.
52 R. G. Nuzzo, D. L. Allara, *J. Am. Chem. Soc.* **1983**, *105*, 4481–4483.
53 G. M. Whitesides, P. E. Laibinis, *Langmuir* **1990**, *6*, 87–96.
54 J. C. Love, L. A. Estroff, J. K. Kriebel, R. G. Nuzzo, G. M. Whitesides, *Chem. Rev* **2005**, *105*, 1103–1170.
55 D. K. Schwartz, *Annu. Rev. Phys. Chem.* **2001**, *52*, 107–137.
56 J. D. Le Grange, J. L. Markham, C. R. Kurkjian, *Langmuir* **1993**, *9*, 1749–1753.
57 R. Banga, J. Yarwood, A. M. Morgan, B. Evans, J. Kells, *Langmuir* **1995**, *11*, 4393–4399.
58 D. Aswal, S. Lenfant, D. Guerin, J. Yakhmi, D. Vuillaume, *Analytica Chimica Acta* **2006**, *568*, 84–108.
59 S. Onclin, B. J. Ravoo, D. N. Reinhoudt, *Angew. Chem. Int. Ed* **2005**, *44*, 6282–6304.
60 B. Vercelli, G. Zotti, G. Schiavon, S. Zecchin, A. Berlin, *Langmuir* **2003**, *19*, 9351–9356.
61 S. Sun, G. J. Leggett, *Nano Lett.* **2007**, *7*, 3753–3758.
62 W. Gao, L. Dickinson, C. Grozinger, F. G. Morin, L. Reven, *Langmuir* **1996**, *12*, 6429–6435.
63 F. K. Huang, R. C. Horton, D. C. Myles, R. L. Garrell, *Langmuir* **1998**, *14*, 4802–4808.
64 S. W. Han, S. J. Lee, K. Kim, *Langmuir* **2001**, *17*, 6981–6987.
65 S. Flink, F. C. J. M. van Veggel, D. N. Reinhoudt, *J. Phys. Org. Chem.* **2001**, *14*, 407–415.
66 A. Lex, PhD Thesis, *Modification of Inorganic Surfaces with Photochemically and Chemically Reactive Thin Siloxane Layers*, Graz **2008**.
67 S. Onclin, B. J. Ravoo, D. N. Reinhoudt, *Angew. Chem.* **2005**, *117*, 6438–6462.
68 H. O. Finklea, L. R. Robinson, A. Blackburn, B. Richter, D. Allara, T. Bright, *Langmuir* **1986**, *2*, 239–244.
69 D. L. Allara, A. N. Parikh, F. Rondelez, *Langmuir* **1995**, *11*, 2357–2360.
70 P. Silberzan, L. Leger, D. Ausserre, J. J. Benattar, *Langmuir* **1991**, *7*, 1647–1651.

71 C. P. Tripp, M. L. Hair, *Langmuir* **1992**, *8*, 1120–1126.
72 C. P. Tripp, M. L. Hair, *Langmuir* **1995**, *11*, 1215–1219.
73 R. R. Rye, G. C. Nelson, M. T. Dugger, *Langmuir* **1997**, *13*, 2965–2972.
74 M. E. McGovern, K. M. R. Kallury, M. Thompson, *Langmuir* **1994**, *10*, 3607–3614.
75 Y. Wang, M. Lieberman, *Langmuir* **2003**, *19*, 1159–1167.
76 W. Bigelow, E. Glass, W. Zisman, *Journal of Colloid Science* **1947**, *2*, 563–591.
77 C. Carraro, O. W. Yauw, M. M. Sung, R. Maboudian, *J. Phys. Chem. B* **1998**, *102*, 4441–4445.
78 W. Barford, *Electronic and optical properties of conjugated polymers*, Clarendon Press, Oxford **2005**.
79 A. D. McNaught, A. Wilkinson, *Compendium of chemical terminology: IUPAC recommendations*, Blackwell Science, Oxford [England];, Malden, MA, USA **1997**.
80 R. Farchioni, G. Grosso, *Organic electronic materials: Conjugated polymers and low molecular weight organic solids*, Springer, Berlin;, New York **2001**.
81 H. Letheby, *J. Chem. Soc* **1862**, *15*, 161.
82 A. G. MacDiarmid, A. J. Epstein, *Faraday Discuss. Chem. Soc.* **1989**, *88*, 317.
83 H. K. Hall, A. B. Padias, H. W. Boone, *J. Polym. Sci. A Polym. Chem.* **2007**, *45*, 4751–4763.
84 P. Adams, P. Laughlin, A. Monkman, A. Kenwright, *Polymer* **1996**, *37*, 3411–3417.
85 M. G. Mikhael, A. B. Padias, H. K. Hall, *J. Polym. Sci. A Polym. Chem.* **1997**, *35*, 1673–1679.
86 C. H. McCoy, I. M. Lorkovic, M. S. Wrighton, *J. Am. Chem. Soc.* **1995**, *117*, 6934–6943.
87 M. Leclerc, J. Guay, L. H. Dao, *Macromolecules* **1989**, *22*, 649–653.
88 G. G. Wallace, G. M. Spinks, L. A. P. Kane-Maguire, P. R. Teasdale, *Conductive electroactive polymers: Intelligent materials systems*, CRC Press, Boca Raton ;, London ;, New York **op. 2009**.
89 G. Venugopal, X. Quan, G. E. Johnson, F. M. Houlihan, E. Chin, O. Nalamasu, *Chem. Mater.* **1995**, *7*, 271–276.
90 T. Griesser, S. V. Radl, T. Koepplmayr, A. Wolfberger, M. Edler, A. Pavitschitz, M. Kratzer, C. Teichert, T. Rath, G. Trimmel, G. Schwabegger, C. Simbrunner, H. Sitter, W. Kern, *J. Mater. Chem.* **2012**, *22*, 2922.
91 E. E. Havinga, *Adv. Mater.* **1996**, *8*, 453–454.
92 R. McCall, M. Roe, J. Ginder, T. Kusumoto, A. Epstein, G. Asturias, E. Scherr, A. MacDiarmid, *Synthetic Metals* **1989**, *29*, 433–438.
93 E. Kang, K. Neoh, K. Tan, *Synthetic Metals* **1995**, *68*, 141–144.
94 Z. Liu, J. H. Oh, M. E. Roberts, P. Wei, B. C. Paul, M. Okajima, Y. Nishi, Z. Bao, *Appl. Phys. Lett.* **2009**, *94*, 203301.
95 G. Gustafsson, Y. Cao, G. M. Treacy, F. Klavetter, N. Colaneri, A. J. Heeger, *Nature* **1992**, *357*, 477–479.
96 L. ZHAO, *Electrochimica Acta* **2009**, *55*, 491–497.
97 J. Huang, S. Virji, B. H. Weiller, R. B. Kaner, *J. Am. Chem. Soc.* **2003**, *125*, 314–315.
98 D. de Leeuw (Ed.), *International Electron Devices Meeting. IEDM Technical Digest*, IEEE **1997**.
99 M. Matters, D. de Leeuw, M. Vissenberg, C. Hart, P. Herwig, T. Geuns, C. Mutsaers, C. Drury, *Optical Materials* **1999**, *12*, 189–197.
100 M. Angelopoulos, *J. Vac. Sci. Technol. B* **1993**, *11*, 2794.
101 C. Slugovc, *Macromol. Rapid Commun.* **2004**, *25*, 1283–1297.
102 E. Reichmanis, B. C. Smith, R. Gooden, *J. Polym. Sci. Polym. Chem. Ed.* **1985**, *23*, 1–8.
103 V. N. Rajasekharan Pillai, *Synthesis* **1980**, *1980*, 1–26.
104 D. Belluc, P. Hrdlovic, *Chem. Rev.* **1967**, *67*, 599–609.
105 J. M. J. Frechet, T. G. Tessier, C. G. Willson, H. Ito, *Macromolecules* **1985**, *18*, 317–321.

106 G. Socrates, *Infrared and raman characteristic group frequencies: Tables and charts*, J. Wiley, Chichester **2001**.

107 Thomas Grießer, PhD Thesis, *Anwendung der Photo-Fries-Reaktion zur Oberflächenmodifizierung*, Graz **2008**.

108 Thomas Höfler, PhD Thesis, *Photoreactive polymers and surface layers based upon the Photo-Fries rearrangement*, Graz **2008**.

109 A. Tsumura, H. Koezuka, T. Ando, *Appl. Phys. Lett.* **1986**, *49*, 1210.

110 T. Someya, *Proceedings of the National Academy of Sciences* **2004**, *101*, 9966–9970.

111 B. Crone, A. Dodabalapur, Y.-Y. Lin, R. W. Filas, Z. Bao, A. LaDuca, R. Sarpeshkar, H. E. Katz, W. Li, *Nature* **2000**, *403*, 521–523.

112 D. Voss, *Nature* **2000**, *407*, 442–444.

113 S. Kobayashi, T. Nishikawa, T. Takenobu, S. Mori, T. Shimoda, T. Mitani, H. Shimotani, N. Yoshimoto, S. Ogawa, Y. Iwasa, *Nat Mater* **2004**, *3*, 317–322.

114 A. Salleo, M. L. Chabinyc, M. S. Yang, R. A. Street, *Appl. Phys. Lett.* **2002**, *81*, 4383.

115 B. H. Hamadani, D. A. Corley, J. W. Ciszek, J. M. Tour, D. Natelson, *Nano Lett.* **2006**, *6*, 1303–1306.

116 L.-L. Chua, J. Zaumseil, J.-F. Chang, E. C.-W. Ou, P. K.-H. Ho, H. Sirringhaus, R. H. Friend, *Nature* **2005**, *434*, 194–199.

117 G. Horowitz, *Adv. Mater.* **1998**, *10*, 365–377.

118 M. Marchl, A. W. Golubkov, M. Edler, T. Griesser, P. Pacher, A. Haase, B. Stadlober, M. R. Belegratis, G. Trimmel, E. Zojer, *Appl. Phys. Lett.* **2010**, *96*, 213303–213305.

119 A. Di Carlo, F. Piacenza, A. Bolognesi, B. Stadlober, H. Maresch, *Appl. Phys. Lett.* **2005**, *86*, 263501.

120 S. D. Wang, T. Miyadera, T. Minari, Y. Aoyagi, K. Tsukagoshi, *Appl. Phys. Lett.* **2008**, *93*, 43311.

121 S. Y. Yang, K. Shin, C. E. Park, *Adv. Funct. Mater.* **2005**, *15*, 1806–1814.

122 A. Wang, I. Kymissis, V. Bulovic, A. Akinwande (Eds.), IEEE **2004**.

123 A. Wang, I. Kymissis, V. Bulović, A. I. Akinwande, *Appl. Phys. Lett.* **2006**, *89*, 112109.

124 H. Sakai, K. Konno, H. Murata, *Appl. Phys. Lett.* **2009**, *94*, 73304.

125 M. Marchl, M. Edler, A. Haase, A. Fian, G. Trimmel, T. Griesser, B. Stadlober, E. Zojer, *Adv. Mater.* **2010**, *22*, 5361–5365.

126 Ulman Abraham, *Chem. Rev* **1996**, *96*.

127 R. K. Smith, P. A. Lewis, P. S. Weiss, *Progress in Surface Science* **2004**, *75*, 1–68.

128 K. A. Bush, P. F. Driscoll, E. R. Soto, C. R. Lambert, W. G. McGimpsey, G. D. Pins, *J. Biomed. Mater. Res* **2009**, *90*, 999–1009.

129 F. So, *Organic Electronics: Materials, Processing, Devices and Applications*, Taylor & Francis, **2010**.

130 K. P. Pernstich, S. Haas, D. Oberhoff, C. Goldmann, D. J. Gundlach, B. Batlogg, A. N. Rashid, G. Schitter, *J. Appl. Phys* **2004**, *96*, 6431.

131 D. Ryan, B. A. Parviz, V. Linder, V. Semetey, S. K. Sia, J. Su, M. Mrksich, G. M. Whitesides, *Langmuir* **2004**, *20*, 9080–9088.

132 A. P. Quist, E. Pavlovic, S. Oscarsson, *Anal Bioanal Chem* **2005**, *381*, 591–600.

133 J. Ji, J.-C. Yang, D. N. Larson, *Biosensors and Bioelectronics* **2009**, *24*, 2847–2852.

134 J.-F. Liu, S. Cruchon-Dupeyrat, J. C. Garno, J. Frommer, G.-Y. Liu, *Nano Lett* **2002**, *2*, 937–940.

135 M. Liu, N. A. Amro, G.-Y. Liu, *Annu. Rev. Phys. Chem* **2008**, *59*, 367–386.

136 S. Ryu, G. C. Schatz, *J. Am. Chem. Soc* **2006**, *128*, 11563–11573.

137 L. G. Rosa, J. Liang, *J. Phys.: Condens. Matter* **2009**, *21*, 483001.

138 L. G. Rosa, J. Jiang, O. V. Lima, J. Xiao, E. Utreras, P. Dowben, L. Tan, *Materials Letters* **2009**, *63*, 961–964.
139 D. S. Ginger, H. Zhang, C. A. Mirkin, *Angew. Chem. Int. Ed* **2004**, *43*, 30–45.
140 M. Montague, R. E. Ducker, K. S. L. Chong, R. J. Manning, F. J. M. Rutten, M. C. Davies, G. J. Leggett, *Langmuir* **2007**, *23*, 7328–7337.
141 P. M. Mendes, J. A. Preece, *Current Opinion in Colloid & Interface Science* **2004**, *9*, 236–248.
142 A. del Campo, D. Boos, H. W. Spiess, U. Jonas, *Angew. Chem. Int. Ed.* **2005**, *44*, 4707–4712.
143 K. Critchley, J. P. Jeyadevan, H. Fukushima, M. Ishida, T. Shimoda, R. J. Bushby, S. D. Evans, *Langmuir* **2005**, *21*, 4554–4561.
144 K. Critchley, L. Zhang, H. Fukushima, M. Ishida, T. Shimoda, R. J. Bushby, S. D. Evans, *J. Phys. Chem. B* **2006**, *110*, 17167–17174.
145 N. D. Gallant, K. A. Lavery, E. J. Amis, M. L. Becker, *Adv. Mater.* **2007**, *19*, 965–969.
146 P. Prompinit, A. S. Achalkumar, X. Han, R. J. Bushby, C. Wälti, S. D. Evans, *J. Phys. Chem. C* **2009**, *113*, 21642–21647.
147 U. Jonas, *Proceedings of the National Academy of Sciences* **2002**, *99*, 5034–5039.
148 R. Bennewitz, *Materials Today* **2005**, *8*, 42–48.
149 K. Yamaguchi, H. Nakayama, Futami T., T. Shimizu, *Journal of Photopolymer Science and Technology* **2008**, *21*, 519–524.
150 C. D. Wagner **2003**, http://srdata.nist.gov/xps/.
151 S. Stafström, J. Brédas, A. Epstein, H. Woo, D. Tanner, W. Huang, A. MacDiarmid, *Phys. Rev. Lett.* **1987**, *59*, 1464–1467.
152 K. Müllen, U. Scherf, *Organic Light Emitting Devices*, Wiley-VCH Verlag GmbH & Co. KGaA, Weinheim, FRG **2005**.
153 C. Tengstedt, A. Crispin, C. Hsu, C. Zhang, I. Parker, W. Salanek, M. Fahlman, *Organic Electronics* **2005**, *6*, 21–33.
154 I. D. Parker, *J. Appl. Phys.* **1994**, *75*, 1656.
155 R. H. Fowler, L. Nordheim, *Proceedings of the Royal Society A: Mathematical, Physical and Engineering Sciences* **1928**, *119*, 173–181.
156 H. E. Gottlieb, V. Kotlyar, A. Nudelman, *J. Org. Chem.* **1997**, *62*, 7512–7515.
157 L. Parratt, *Phys. Rev.* **1954**, *95*, 359–369.
158 L. Névot, P. Croce, *Rev. Phys. Appl. (Paris)* **1980**, *15*, 761–779.
159 F. Garbassi, M. Morra, E. Occhiello, *Polymer surfaces: From physics to technology*, Wiley, Chichester [England] **1998**.
160 D. K. Owens, R. C. Wendt, *J. Appl. Polym. Sci.* **1969**, *13*, 1741–1747.
161 T.-C. Lin, G. Seshadri, J. A. Kelber, *Applied Surface Science* **1997**, *119*, 83–92.
162 M. Laurin **2009**, http://www.texample.net/tikz/examples/principle-of-x-ray-photoelectron-spectroscopy-xps/.
163 S. Tougaard, *Applied Surface Science* **1996**, *100-101*, 1–10.
164 K. Oura, V. G. Lifšič, A. A. Saranin, A. V. Zotov, M. Katayama, *Surface science: An introduction*, Springer, Berlin ;, New York **2003**.
165 J. W. Watts, J. Wolstenholme, *An introduction to surface analysis by XPS and AES*, Wiley, Chichester **2003**.
166 Institut Rayonnement Matière de Saclay (IRAMIS), http://iramis.cea.fr/Phocea/Vie_des_labos/Ast/ast_sstechnique.php?id_ast=508.

167 M. Tolan, *X-ray scattering from soft-matter thin films: Materials science and basic research*, Springer, Berlin ;, New York **1999**.
168 A. Dane, A. Veldhuis, D. Boer, A. Leenaers, L. Buydens, *Physica B: Condensed Matter* **1998**, *253*, 254–268.
169 G. Binnig, C. F. Quate, *Phys. Rev. Lett.* **1986**, *56*, 930–933.
170 R. W. Carpick, M. C. R. Salmeron, *Chem. Rev* **1997**.
171 R. Wiesendanger, *Scanning probe microscopy and spectroscopy: Methods and applications*, Cambridge University Press, Cambridge **1994**.
172 G. J. Leggett, N. J. Brewer, K. S. L. Chong, *Phys. Chem. Chem. Phys.* **2005**, *7*, 1107.
173 M. Nonnenmacher, M. P. O'Boyle, H. K. Wickramasinghe, *Appl. Phys. Lett.* **1991**, *58*, 2921.
174 H. G. Tompkins, W. A. McGahan, *Spectroscopic ellipsometry and reflectometry: A user's guide*, Wiley, New York **1999**.
175 T. H. Christian Bernhard, http://academic.brooklyn.cuny.edu/physics/holden/ellipsometry.htm.
176 H. Fujiwara (Ed.), *Spectroscopic Ellipsometry*, John Wiley & Sons, Ltd, Chichester, UK **2007**.
177 P. Williams, *Annu. Rev. Mater. Sci.* **1985**, *15*, 517–548.
178 M. Kunishima, *Tetrahedron (Tetrahedron)* **1999**, *55*, 13159–13170.
179 M. Kunishima, C. Kawachi, K. Hioki, Terao K., Tani S., *Tetrahedron (Tetrahedron)* **2001**, *57*, 1551–1558.
180 C. D. Dimitrakopoulos, D. J. Mascaro, *IBM J. Res. & Dev.* **2001**, *45*, 11–27.